



Plains CO<sub>2</sub> Reduction (PCOR) Partnership  
Energy & Environmental Research Center (EERC)

# **BELL CREEK TEST SITE – 3-D SEISMIC AND CHARACTERIZATION REPORT**

## **Plains CO<sub>2</sub> Reduction (PCOR) Partnership Phase III Task 4 – Deliverable D96**

*Prepared for:*

Andrea M. Dunn

National Energy Technology Laboratory  
U.S. Department of Energy  
626 Cochrans Mill Road  
PO Box 10940  
Pittsburgh, PA 15236-0940

DOE Cooperative Agreement No. DE-FC26-05NT42592

*Prepared by:*

Shaughn A. Burnison  
Matthew E. Burton-Kelly  
Xiaofeng Zhang  
Charles D. Gorecki  
Edward N. Steadman  
John A. Harju

Energy & Environmental Research Center  
University of North Dakota  
15 North 23rd Street, Stop 9018  
Grand Forks, ND 58202-9018

## **EERC DISCLAIMER**

**LEGAL NOTICE** This research report was prepared by the Energy & Environmental Research Center (EERC), an agency of the University of North Dakota, as an account of work sponsored by the U.S. Department of Energy (DOE). Because of the research nature of the work performed, neither the EERC nor any of its employees makes any warranty, express or implied, or assumes any legal liability or responsibility for the accuracy, completeness, or usefulness of any information, apparatus, product, or process disclosed or represents that its use would not infringe privately owned rights. Reference herein to any specific commercial product, process, or service by trade name, trademark, manufacturer, or otherwise does not necessarily constitute or imply its endorsement or recommendation by the EERC.

## **ACKNOWLEDGMENTS**

This work was performed under the DOE National Energy Technology Laboratory under Award No. DE-FC26-05NT42592. The EERC would like to thank Denbury Onshore (Denbury) for providing necessary data to perform this work. Special thanks go to CGG and Hampson-Russell Software & Services for the use of their HRS-9 software suite to perform the analysis and interpretation of the data.

## **DOE DISCLAIMER**

This report was prepared as an account of work sponsored by an agency of the United States Government. Neither the United States Government, nor any agency thereof, nor any of their employees, makes any warranty, express or implied, or assumes any legal liability or responsibility for the accuracy, completeness, or usefulness of any information, apparatus, product, or process disclosed, or represents that its use would not infringe privately owned rights. Reference herein to any specific commercial product, process, or service by trade name, trademark, manufacturer, or otherwise does not necessarily constitute or imply its endorsement, recommendation, or favoring by the United States Government or any agency thereof. The views and opinions of authors expressed herein do not necessarily state or reflect those of the United States Government or any agency thereof.

## **NDIC DISCLAIMER**

This report was prepared by the EERC pursuant to an agreement partially funded by the Industrial Commission of North Dakota, and neither the EERC nor any of its subcontractors nor the North Dakota Industrial Commission nor any person acting on behalf of either:

- (A) Makes any warranty or representation, express or implied, with respect to the accuracy, completeness, or usefulness of the information contained in this report or that the use of any information, apparatus, method, or process disclosed in this report may not infringe privately owned rights; or

- (B) Assumes any liabilities with respect to the use of, or for damages resulting from the use of, any information, apparatus, method, or process disclosed in this report.

Reference herein to any specific commercial product, process, or service by trade name, trademark, manufacturer, or otherwise does not necessarily constitute or imply its endorsement, recommendation, or favoring by the North Dakota Industrial Commission. The views and opinions of authors expressed herein do not necessarily state or reflect those of the North Dakota Industrial Commission.

## TABLE OF CONTENTS

LIST OF FIGURES .....	iii
LIST OF TABLES .....	vii
EXECUTIVE SUMMARY .....	viii
INTRODUCTION .....	1
Background .....	1
Geologic Overview .....	3
Site Characterization .....	4
Purpose and Application .....	7
Scope of Work and Key Findings .....	7
SOURCE TESTING .....	9
SURFACE 3-D SEISMIC DATA ACQUISITION.....	12
SEISMIC DATA PROCESSING .....	18
DATA PRESENTATION.....	19
Well Database and Well Ties .....	22
Data Bandwidth and Vertical Resolution.....	25
Lateral Resolution .....	33
Horizon Picking.....	33
Mapping .....	36
Analysis of a Channel Feature Visible on the Amplitude Map.....	40
Analysis of Permeability Barrier Between Phases 1 and 2 .....	47
Analysis of Incised Valleys – Northern Valley.....	51
Analysis of Incised Valleys – Southern Valley.....	56
Updip Field Boundary .....	59
ELEMENTS OF STRUCTURAL INTERPRETATION .....	60
Polygonal Fault Systems .....	60
Basement Faulting.....	62
FUTURE WORK.....	63
Integrate Seismic with the Petrel Geocellular Reservoir Model .....	63
3-D VSP Integration.....	66
Computation of Geomechanical Properties.....	67
4-D Time-Lapse VSP and 4-D Time-Lapse Surface 3-D .....	67

Continued . . .



## **TABLE OF CONTENTS (continued)**

CONCLUSIONS.....	68
BIBLIOGRAPHY .....	69
DATA-PROCESSING DETAILS .....	Appendix A
WELL TIE AND CORRELATION PROCESS .....	Appendix B
DATA BANDWIDTH AND TEMPORAL RESOLUTION .....	Appendix C

## LIST OF FIGURES

1	The Bell Creek oil field in southeastern Montana lies near the northeastern corner of the PRB .....	2
2	Injection will occur in a staged approach over nine planned CO <sub>2</sub> development phases, designated as Phases 1 to 9, across the Bell Creek Field .....	3
3	Stratigraphic column for the Bell Creek area with lithology .....	5
4	Project elements of the Bell Creek CO <sub>2</sub> capture and sequestration project .....	6
5	Location map of source test line, source test configuration, and check-shot well .....	9
6	The migrated 2-D dynamite test line acquired in August 2011 .....	10
7	An I/O AHV-3 heavy vibrator (left) and an IVI Minivib Vibrator on a field road at Bell Creek during the December 2011 source testing .....	10
8	A 96-channel field record of a vibrator test shot.....	11
9	Source test spectra for four different vibrator and sweep configurations show the highly attenuative nature of Bell Creek near-surface geology .....	12
10	Baseline 3-D surface seismic survey outline superimposed on the field boundaries.....	13
11	Seismic contractor plot of the 40-square-mile 3-D surface seismic survey layout demonstrating production in progress nearing completion .....	14
12	Seismic crew members laying out receiver stations.....	15
13	GSR (geospace seismic recorder) recording unit with geophones planted in a 2-ft circle .....	16
14	Nodal recording units in a rack used for operational checks, programming, and data collection .....	17
15	Vibrator crew during Bell Creek survey .....	18
16	Bell Creek field phases and wells that fall within the farthest extent of inline and crossline 3-D data as indicated by the overlaid rectangle .....	19

Continued . . .

## LIST OF FIGURES (continued)

17	A gray-scale image of a time slice through the 3-D volume reveals the areal extent of data coverage within the survey boundary.....	20
18	A portion of Crossline 1220 showing data zeroed above 1 sec and below 1.3 sec .....	21
19	Time slice from 970 msec shows areal extent of data redactions for times less than 1 second and greater than 1.3 seconds .....	22
20	The well log data from 05-06 OW exhibit a strong synthetic-to-seismic tie with the seismic data .....	24
21	The EERC's naming convention and lithostratigraphy for the Bell Creek model modified from Molnar .....	25
22	Lower panel shows the amplitude spectrum computed over 40,293 traces in the central area of Phase 1 in a 500-msec window centered on the zone of interest .....	26
23	Demonstration of the limit of resolution of the embedded wavelet .....	27
24	Demonstration of the tuning thickness of the embedded wavelet.....	28
25	The P-wave acoustic impedance curve (sonic velocity $\times$ density) demonstrates that significant impedance changes occur at the Springen Ranch and Skull Creek boundaries which give rise to the Muddy Formation reflection .....	29
26	The relationship between the well logs, formation tops, and seismic reflection from the reservoir zone is shown .....	31
27	Seismic data showing color-coded amplitude varying spatially along the inline passing through Well 05-06 OW.....	32
28	Four picked horizons are shown on this inline.....	34
29	Areal view of the Muddy horizon .....	35
30	Map of Muddy Formation reflector amplitude created as described in the text .....	37
31	A sand isopach map developed by a geologist from well logs and an intimate understanding of the field.....	38

Continued . . .

## LIST OF FIGURES (continued)

32	The seismic amplitude map overlaid on the sand isopach map .....	39
33	Zoom to the area of the fluvial channel.....	40
34	Seismic Section A-A' with gamma ray and sonic p-wave velocity logs overlaying.....	41
35	Well logs for Channel Well 21-16 .....	42
36	Well 22-12, north of the channel, has significant Bell Creek sand development and a thick impedance contrast section .....	43
37	Northwest to southeast section.....	44
38	Well logs for 28-07 indicate the absence of clean sand as in 21-16 .....	44
39	Location map of Cross-Section Line C-C' across the permeability barrier between field Phases 1 and 2 .....	47
40	Crossline display showing the Cross-Section C-C' across the Phase 1–Phase 2 permeability barrier .....	48
41	Well within the barrier, 33-14X .....	49
42	Well 33-14 near the edge of the permeability barrier .....	50
43	Schematic modified from Molnar (1990) indicating location of drainage system and incised valley development at the Bell Creek Field area following a major drop in sea level not long after deposition of the Bell Creek sand.....	51
44	Overlay of the incised valley features indicated on Figure 43 after georeferencing.....	52
45	Location map of the northern incised valley .....	53
46	Cross-Section D-D' from southwest to northeast across northern incised valley .....	54
47	Closer look at Well 33-09 located in incised valley.....	55
48	Well 32-01 is located in a northern incised valley toward the west end of the field .....	55

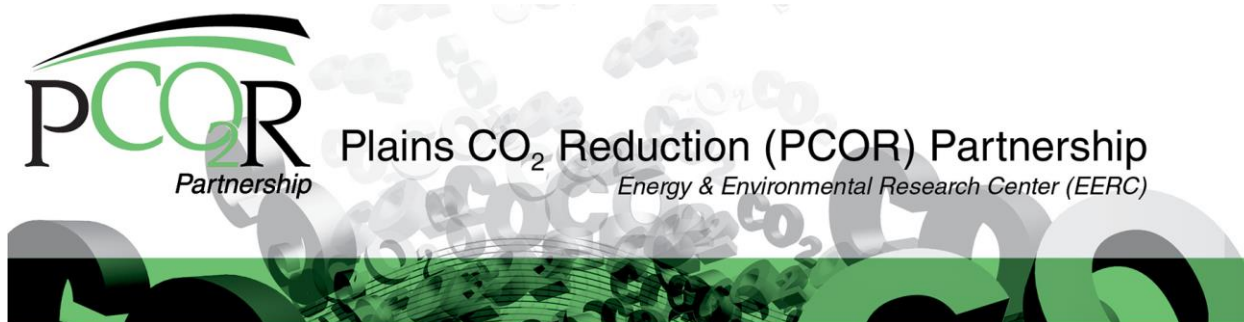
Continued . . .

## LIST OF FIGURES (continued)

49	Close-up view of southern incised valley low-amplitude expression with dendritic character .....	56
50	Inline Seismic Section E-E' across southern incised valley .....	57
51	Well 63-06 in the center of the incised valley exhibits a 6-foot coalbed response above the Bell Creek sand erosional surface .....	58
52	Well 62-02 located north of Well 63-06 farther up the incised valley .....	58
53	The updip field boundary occurs between Wells 09-02 and 42-09 as the Bell Creek sand thins .....	59
54	Seismic survey slice through the Belle Fourche Formation in the Bell Creek Field at 1048 msec or approximately 4285' depth.....	60
55	Cross-Section F-F' of PFS in the Belle Fourche Formation at Bell Creek.....	61
56	Indications of basement faulting visible on southwest–northeast Crossline 1177 may be part of the paleostructure referred to by Weimer and others (1988) and the cause of the topographic high seen at the reservoir level.....	63
57	Display from the current reservoir model showing the spatial distribution of clean sand in feet of thickness .....	64
58	Seismic amplitude map overlaid on the reservoir model showing clean sand.....	65
59	Location map and notional coverage of baseline 3-D VSPs acquired in May 2013.....	66
60	Time slice display from the 3-D VSPs at reservoir level showing well locations .....	67
61	An example cross section of PR computed over a portion of the reservoir area .....	68

## LIST OF TABLES

1	Acquisition Parameters .....	14
2	Analysis of High-Amplitude vs. Low-Amplitude Seismic Response at Wells.....	46



## **BELL CREEK TEST SITE – 3-D SEISMIC AND CHARACTERIZATION REPORT**

### **EXECUTIVE SUMMARY**

The Plains CO<sub>2</sub> Reduction (PCOR) Partnership, led by the Energy & Environmental Research Center (EERC), is working with Denbury Onshore (Denbury) to evaluate the effectiveness of large-scale injection of carbon dioxide (CO<sub>2</sub>) into the Bell Creek oil field for CO<sub>2</sub> enhanced oil recovery (EOR) and to study long-term incidental CO<sub>2</sub> storage. A technical team that includes Denbury, the EERC, and others are conducting activities to determine the baseline reservoir characteristics for development of a geologic model for predictive simulations and to serve as a comparison to time-lapse data as they are acquired. One of the activities was the acquisition and interpretation of a baseline three-dimensional (3-D) surface seismic survey acquired over a major portion of the field which is the subject of this report. The interpretation will be used to advance the field characterization effort. The geophysical data will be integrated with the EERC's geologic model to improve its accuracy. In the future, when paired with at least one subsequent 3-D surface seismic survey, the data difference will provide a direct indication of where the CO<sub>2</sub> has migrated within the reservoir and aid in monitoring, verification, and accounting goals.

A brief overview of the source testing, data acquisition, and processing is given. A seismic source configuration consisting of two heavy vibrators operated in tandem was chosen after a series of tests conducted in August and December of 2011. The data acquisition for the main survey occurred in August and September 2012. The data were processed by a contractor in Houston and delivered to Denbury early in 2013. The EERC received a stacked data set in April with redactions where Denbury did not have mineral rights or leases.

Seismic interpretation efforts began with making well ties to the data and identifying the Bell Creek reservoir reflector. The polarity of the dataset was established to be such that an increase in acoustic impedance (AI) would cause a negative deflection on the data. The reservoir is thin and of higher AI than the encasing shale layers, so with this polarity, it presents on the seismic data as a trough–peak combination representing the entering and exiting reflections at a two-way time of ~1150 msec at the 05-06 OW monitoring well location.

The origin of the reservoir reflection is due to a large increase in AI at the top of the Springen Ranch and a similar decrease in AI at the top of the Skull Creek. The measured thickness of the Springen Ranch-to-Skull Creek interval in the field varies from about 50 to 75 feet. Spectral analysis of data in the zone of interest reveals a bandwidth of 10–48 Hz, which together with the average interval velocity mathematically limits the vertical resolution of the seismic data at reservoir depth to just under 60 feet. Therefore, the reservoir is a thin-bed reflector with thickness near or below the limit of resolution. A reflector of this type would be expected to exhibit possible tuning effects, but they are not evident.

Tuning is an effect that occurs on thin beds when the top and bottom reflections interact to partially add in phase resulting in high reflection amplitudes. An important assumption is that the

interval is lithologically homogeneous. The tuning thickness for this data's bandwidth is 76 feet, so high amplitudes would be expected in thicker Springen Ranch-to-Skull Creek sections and lower amplitudes expected where the interval is thinner. The data exhibit the opposite character. This implies a nonhomogeneous interval where internal interactions due to lithology affect the composite reflection amplitude. The character of the Bell Creek sand meaningfully contributes to this effect.

The Bell Creek reservoir sand is a subset of the reflection interval. Typically 20 to 30 feet thick, its top and bottom cannot be directly resolved on the seismic data set as delivered. When the sand is thick and clean and juxtaposed against the harder, fine-grained components of the Springen Ranch at the top and the Rozet below, these impedance contrasts internal to the overall composite reflection appear to cause interference effects which result in a low-amplitude reflection. When the sand is thinner or fines upward with less AI contrast, less internal interference results, and the composite reflection maintains a higher amplitude. Because of this, a map of seismic amplitudes generated from the reservoir reflection differentiates between areas of 1) thick clean sand and 2) thinner clean sand or sand with a fine-grained component or shaley matrix. The effect is illustrated in cross sections paired with well logs and also by overlaying the map on existing isopach maps of sand, with good agreement.

Several geologic features are visible on the amplitude map and are briefly examined in cross section with the seismic data and well logs. These features include (Figure ES-1):

1. A fluvial channel feature in the northern part of the field, trending roughly north–south, has a higher amplitude than surrounding areas and is shown to be shale-filled and acts as a flow boundary.
2. A flow boundary between Phases 1 and 2 is also shown to be shale-filled and is a possible extension of the fluvial channel feature to the north.
3. A linear erosional valley trending northwest–southeast which predates the fluvial channel feature and serves as a flow boundary between Phases 1 and 3 and between Phases 2 and 4. The fill at the erosional surface is characterized by coal and bentonitic shales.
4. An erosional valley on the south end of the field which exhibits a dendritic outline. The fill at the erosional surface is characterized by coal and bentonitic shales.

Three structural aspects of the field are briefly explored:

1. Thinning of the Bell Creek sand which forms the updip boundary and trap to the southeast is not directly discernible on the seismic data.
2. Polygonal faulting is shown to be prevalent within the overlying Belle Fourche Formation. The faults are thought to originate from dewatering of thick bentonite layers at the bottom of the Belle Fourche and top of the Mowry. Faults do not extend below the top of the Mowry or above the Belle Fourche and likely do not impact the containment integrity of the reservoir.
3. A possible basement faulting system thought to control the southwest to northeast trend of the reservoir paleo-high was identified and is shown on a section.

Future work will include integrating the 3-D data and interpretation with the geocellular model and 3-D VSP data acquired in 2013 and 2014. Geomechanical properties will be computed across the field guided by the seismic data. Future time-lapse surface seismic data will use the baseline survey to generate difference displays to image and verify the progress of CO<sub>2</sub> that has been injected into the reservoir. Modeling performed by Denbury has shown that injected CO<sub>2</sub> will induce a detectable amplitude reduction on the reservoir reflection at the current bandwidth.



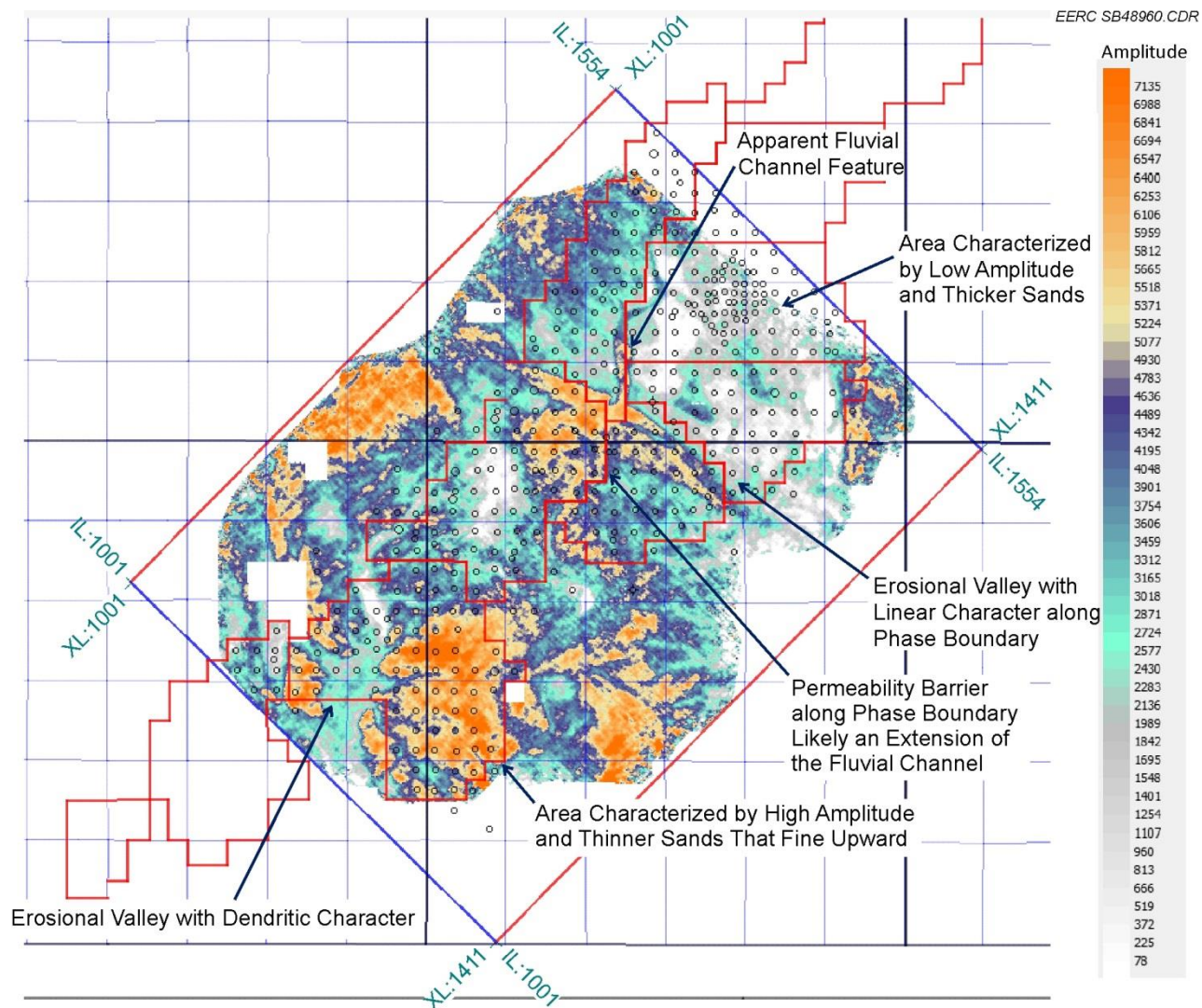
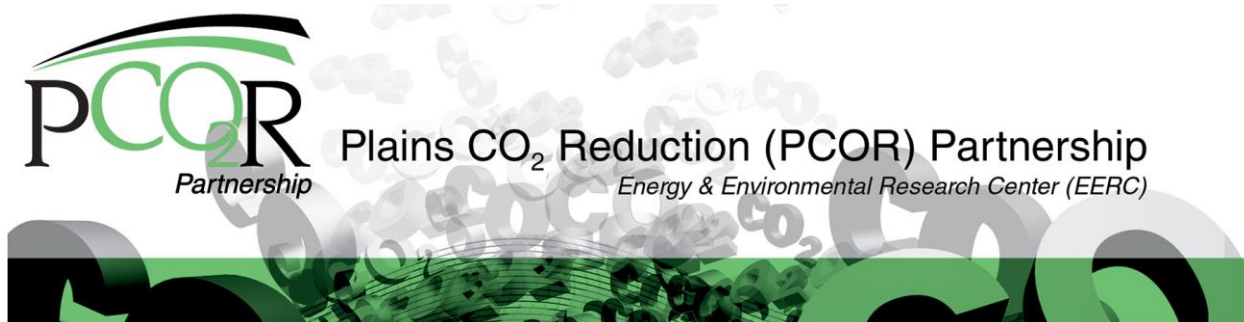


Figure ES-1. A map of Muddy Formation reflector amplitude, with the amplitude scale on the right. Warmer colors indicate higher amplitudes, and white indicates near-zero amplitude. The map shows township and section lines, field phase boundaries, and well locations. Several visible geologic features are denoted and examined in the text.



## **BELL CREEK TEST SITE – 3-D SEISMIC AND CHARACTERIZATION REPORT**

### **INTRODUCTION**

The Plains CO<sub>2</sub> Reduction (PCOR) Partnership, led by the Energy & Environmental Research Center (EERC), is working with Denbury Onshore (Denbury) to determine the effect of large-scale injection of carbon dioxide (CO<sub>2</sub>) into a deep clastic reservoir for the purpose of CO<sub>2</sub> enhanced oil recovery (EOR) and to monitor incidental CO<sub>2</sub> storage at the Bell Creek oil field, which is operated by Denbury Onshore LLC (Figure 1). A technical team that includes Denbury, the EERC, and others is conducting a variety of activities to determine, among other things, the baseline reservoir characteristics to develop a geologic model for predictive simulations and to serve as a comparison to time-lapse data as they are acquired. One of the activities was the acquisition and interpretation of a three-dimensional (3-D) surface seismic survey acquired over a major portion of the field in August 2012, which is the subject of this report. This baseline survey, especially when paired together with at least one subsequent 3-D surface seismic survey to be acquired in the future, may facilitate assessment of injection schemes and guide monitoring strategies by providing a direct indication of where the CO<sub>2</sub> has migrated within the reservoir and help to determine the ultimate fate of injected CO<sub>2</sub>. The baseline 3-D survey interpretation and data will be integrated with the EERC's geologic model to enhance its predictive capabilities.

As the field operator, Denbury will carry out the injection and production operations. The EERC will provide support for the site characterization, modeling and simulation, and risk assessment and will aid in the development of the monitoring, verification, and accounting (MVA) plan to address key technical subsurface risks related to the incidental CO<sub>2</sub> storage study. The baseline 3-D surface seismic survey plays a key role in these tasks. This document describes key aspects associated with the acquisition, processing, and interpretation of this survey and its integration with the EERC's characterization program and geologic model.

### **Background**

The Bell Creek oil field in southeastern Montana is an initially subnormally pressured reservoir with significant hydrocarbon accumulation that lies near the northeastern corner of the Powder River Basin (PRB) (Figure 1). Exploration and production activities for mineral and energy resources in the area over the last 55 years have yielded a significant amount of information about the geology of southeastern Montana and the northern PRB. Over the course of decades, oil and gas production through primary and secondary recovery (waterflood and polymer flood pilot

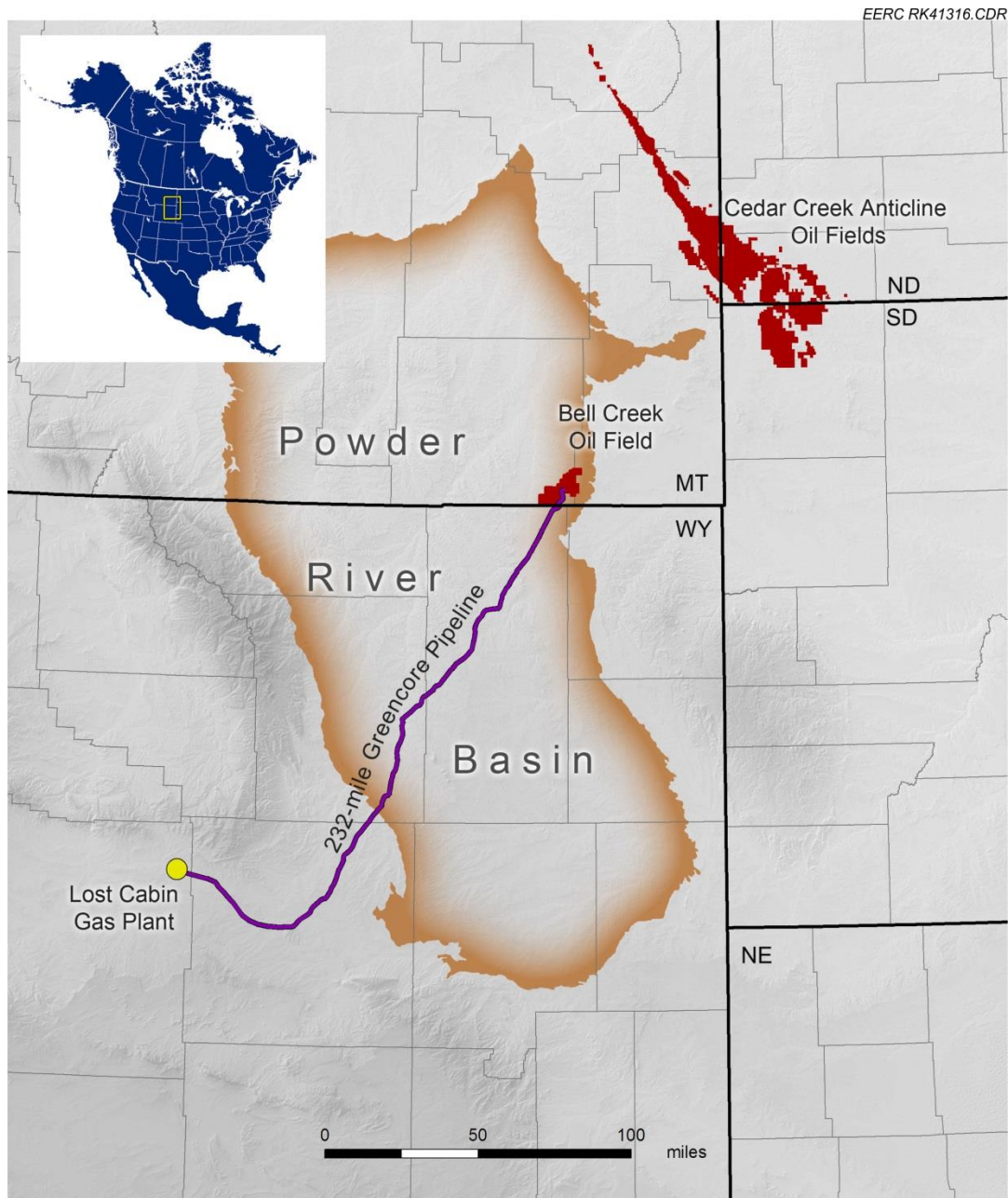


Figure 1. The Bell Creek oil field in southeastern Montana lies near the northeastern corner of the PRB. CO<sub>2</sub> will be delivered to the site via pipeline from the Lost Cabin Gas Plant.

tests) has resulted in production decline and has now led to the implementation of a CO<sub>2</sub> injection-based tertiary oil recovery project. CO<sub>2</sub> is sourced from the ConocoPhillips-operated Lost Cabin Gas Plant, where CO<sub>2</sub> is separated from the process stream during refinement of natural gas. The plant is located in Fremont County, Wyoming (Figure 1), and the Denbury-operated Greencore pipeline is delivering a target injection rate of around 50 million cubic feet of CO<sub>2</sub> a day to the Bell Creek oil field.



CO<sub>2</sub> is being injected into the oil-bearing sandstone reservoir in the Lower Cretaceous Muddy (Newcastle) Formation at a depth of approximately 4500 feet (1372 meters). Implementation is occurring in a staged approach (nine planned CO<sub>2</sub> development phases, designated as Phases 1 to 9) across the field (Figure 2). At full development, the activities at the Bell Creek oil field could inject up to 1 million tons of CO<sub>2</sub> annually, with as much as 14 million tons incidentally and permanently stored at the end of the EOR project.

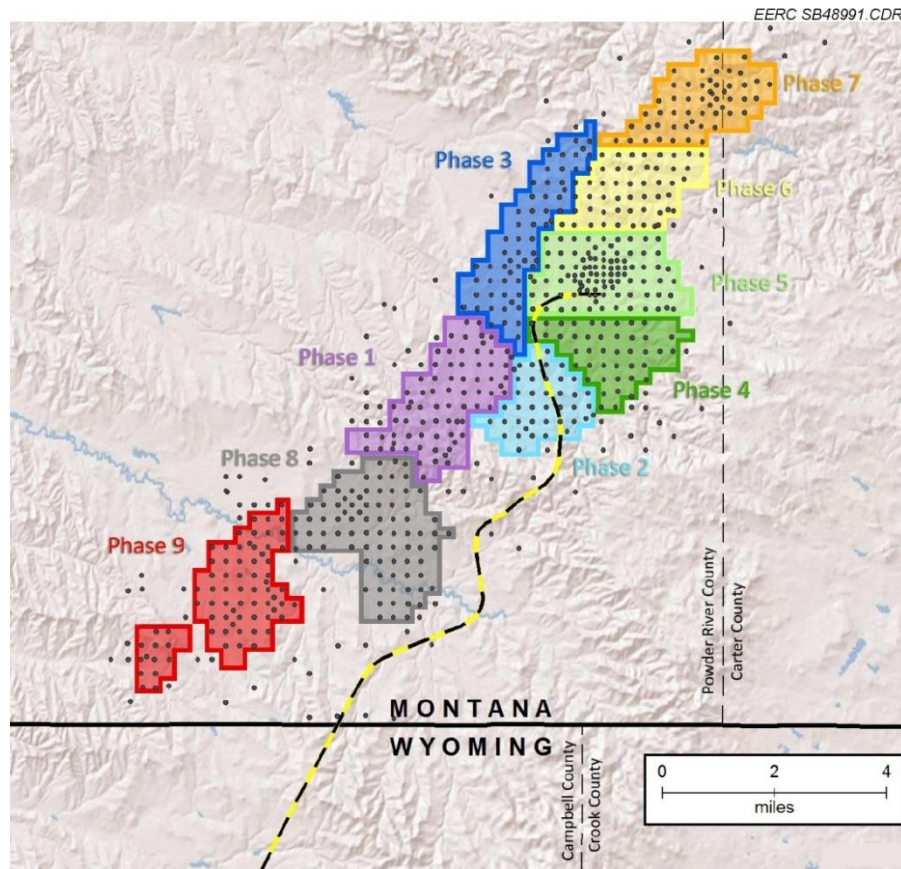


Figure 2. Injection will occur in a staged approach over nine planned CO<sub>2</sub> development phases, designated as Phases 1 to 9, across the Bell Creek Field.

### Geologic Overview

Within the Bell Creek oil field, the Muddy Formation is dominated by high-porosity (15%–35%), high-permeability (150–1175-mD) sandstones deposited in a near-shore marine environment. The initial reservoir pressure was 1200 psi at the time of discovery, which is significantly lower than the regional hydrostatic pressure regime (2100 psi at 4500 ft) (Saini and others, 2012). The oil field is located structurally on a shallow monocline with a 1°–2° dip to the northwest and with an axis trending southwest to northeast for a distance of approximately 20 miles. Stratigraphically, the Muddy Formation in the Bell Creek oil field features an updip facies change from sand to shale that serves as a trap.

The barrier-bar sand bodies of the Muddy Formation strike southwest to northeast and lie on a regional structural paleo-high that was controlled by movement along a northeast-trending system of basement fault blocks. After deposition, a major sea-level drop subaerially exposed the area, and a drainage system was incised by erosion into or through the Bell Creek sandstone. As the sea level rose, the drainage system filled with marine, estuarine, and tidal flat deposits (Weimer and others, 1988). As sea level continued to rise, the migrating shoreline moved over the coastal plain leaving a surface of erosion on the sand and valley fill deposits. Deltaic siltstone deposits overlap the sandstone, and fluvial channel cuts filled with shale compartmentalize the sand bodies in places. As the sea level continued to rise, the black marine shale of the Mowry was deposited. Several of these geologic features can be seen or inferred from the 3-D seismic data and are highlighted in this report.

The overlying Upper Cretaceous Mowry Formation shale is the primary seal, preventing fluid migration to overlying aquifers and to the surface. On top of the Mowry Formation is several thousand feet of low-permeability shale formations, including the Belle Fourche, Greenhorn, Niobrara, and Pierre shales, which will provide redundant layers of protection in the unlikely event that the primary seal fails to prevent upward fluid migrations (Figure 3).

### **Site Characterization**

The Bell Creek project provides a unique opportunity to develop methods to monitor and account for CO<sub>2</sub> incidentally stored in association with a complex, large-scale (>1 million tons/per year) CO<sub>2</sub> EOR operation. Detailed site characterization was conducted to provide a solid foundation for critical activities necessary to complete project objectives.

The EERC's site characterization activities serve as essential inputs into geocellular modeling activities (geologic, geomechanical, numerical, and predictive simulation) to determine 1) the capacity of the reservoir; 2) the mobility and fate of the CO<sub>2</sub> at near-, intermediate-, and long-term time frames; 3) potential storage efficiency of the reservoir; and 4) ability of the formation to permanently retain injected CO<sub>2</sub> and reservoir fluids. Characterization activities consist of collecting, evaluating, and interpreting data sets throughout the field such as 1) historic core analyses, outcrop analysis, and analyses of new characterization wells drilled in development Phases 1 and 2 of the Bell Creek oil field; 2) all available historic well logs; 3) all available well files which include data on drilling, completion, and stimulation/workover records; 4) geological and geophysical information including maps, cross sections, and geophysical surveys; and 5) a 75-square-mile lidar survey. Additional characterization work includes collection, interpretation, and integration of 1) modern high-resolution well logs in over 35 legacy wells and all recent redrills, 2) bottomhole pressure (BHP) survey data in over 156 wells, 3) continuous downhole pressure and temperature data, 4) additional modern core analysis on historic and newly acquired core, 5) two 3-D vertical seismic profiles (VSPs), and 6) a 40-square-mile 3-D seismic survey.

## Stratigraphic Column of the Bell Creek Area

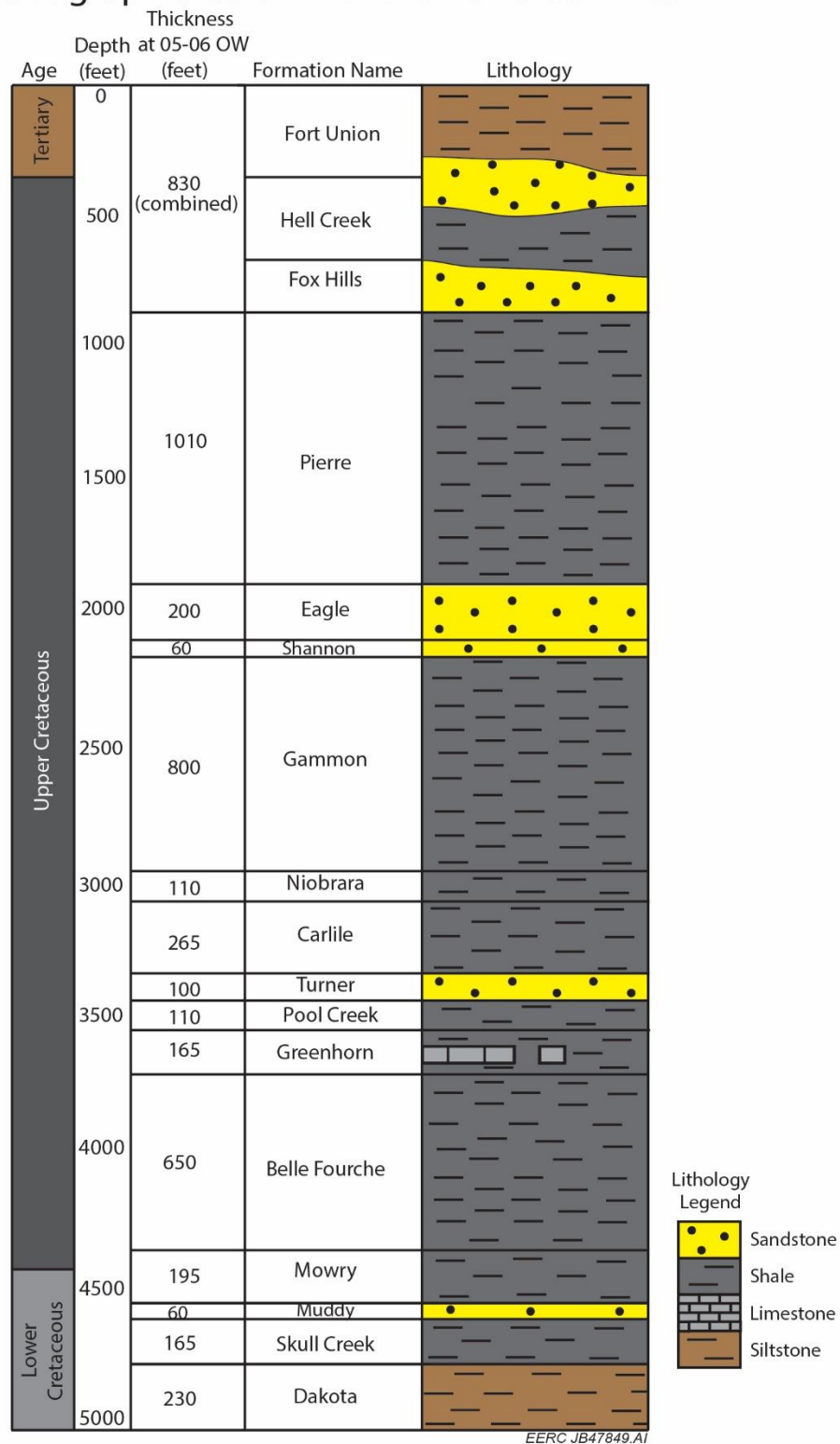


Figure 3. Stratigraphic column for the Bell Creek area with lithology.

The PCOR Partnership applies a philosophy of integrating site characterization, modeling and simulation, risk identification, and MVA strategies into an iterative, adaptive management approach (Figure 4). Elements of any of these activities play a role in the understanding and development of the others. The baseline 3-D surface seismic survey plays a meaningful role in each of the four elements by providing, among other benefits, 1) a measurement and image of physical properties throughout the geologic section on an 82.5-foot-square grid over the field that will aid geologic characterization, 2) a means of constraining the statistical modeling along geobody boundaries to improve model predictions, 3) a means of identifying faulting or leakage pathways within the reservoir and seal that feeds directly into the risk assessment, and 4) a means of directly indicating the locations of CO<sub>2</sub> accumulation when paired with a subsequent time-lapse survey as part of the MVA plan.

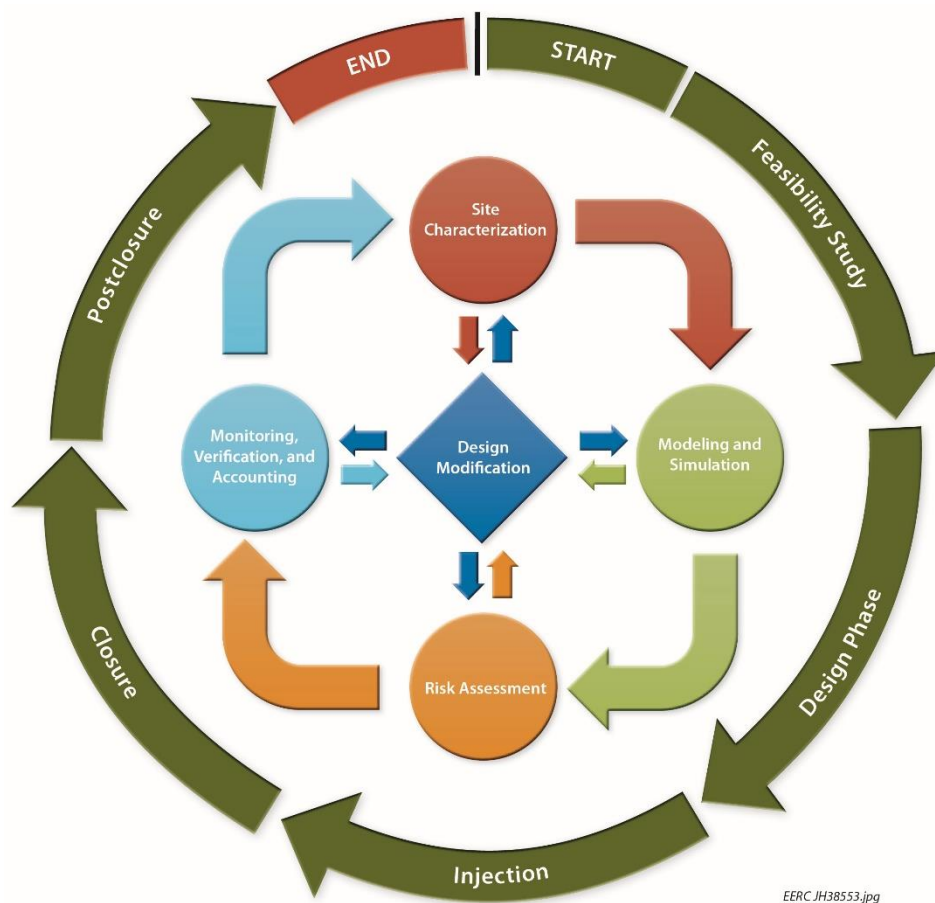


Figure 4. Project elements of the Bell Creek CO<sub>2</sub> capture and sequestration project. Each of these elements feeds into another, iteratively improving results and efficiency of evaluation.

## **Purpose and Application**

The 3-D surface seismic survey was acquired to serve several purposes for characterization and MVA of the Bell Creek project:

1. Aid in the structural interpretation of the Bell Creek Field.
2. Identify and map the distribution of lateral heterogeneities and flow boundaries within the field.
3. Combine well data with inverted seismic impedances to derive and map geologic facies.
4. Calculate and map the distribution of geomechanical properties.
5. Track the distribution and movement of CO<sub>2</sub> when paired with subsequent surveys.
6. Provide an indication of CO<sub>2</sub> sweep and storage efficiency.
7. Identify migration of CO<sub>2</sub> outside of the storage complex and geologic leakage pathways.
8. Account for the injected CO<sub>2</sub>.
9. Provide improvements to reservoir models and simulations.

## **Scope of Work and Key Findings**

This report documents the following:

1. The key aspects in acquiring the survey data are provided, with a brief overview of the source testing, data acquisition, and data processing.
2. An overview of the delivered processed data set is provided to show its context within the field.
3. The polarity of the data is established to be equivalent to that of an impulsive source like dynamite, where an increase in acoustic impedance causes a negative deflection on the data: a trough.
4. A brief analysis of the vertical resolution is given and shown to be about 59 feet.
5. The geologic source of the reservoir reflection is identified and shown to originate from the Springen Ranch-to-Skull Creek interval, which includes, but does not resolve, the actual Bell Creek reservoir sand within. However, the geologic characteristics of the sand interval are shown to influence the amplitude of the reflection.



6. Horizon picking on reflections and mapping using the Muddy horizon are used to generate an amplitude map of the reservoir which reveals known flow boundaries and matches very well with existing well-based interpretations of the field.
7. Seismic sections with well log overlays are used to illustrate five geobody boundaries and reveal the continuity and dimensions of:
  - a) An apparent shale-filled fluvial channel in the northern part of the field.
  - b) An extension of the shale-filled fluvial channel between Phases 1 and 2.
  - c) An erosional valley that predates the fluvial channel and crosses the field from northwest to southeast, has eroded the Bell Creek sand, and is characterized by valley fill containing coals and/or bentonite.
  - d) An erosional valley with dendritic features that cuts the field on the south and is characterized by eroded sand and valley fill containing coals and/or bentonite.
  - e) The updip stratigraphic trap, which is shown to be ambiguous and not directly identifiable.
8. Structural elements of the field are identified, including:
  - a) Well-imaged polygonal faulting confined to the Belle Fourche and very upper Mowry Formations that may be related to the dewatering of several thick bentonite layers.
  - b) A glimpse at a possible basement faulting system thought to control the southwest to northwest trend of the reservoir paleo-high.
9. A brief discussion of future work, including:
  - a) Integration of the 3-D data with the geocellular model. The seismic amplitude map is shown to correspond well with the model's computation of clean sand, providing support to the concept that clean sand correlates to low seismic amplitudes and higher amplitudes correlate with facies characterized by finer-grained material.
  - b) Integrating 3-D VSP data acquired in 2013 with the 3-D surface data.
  - c) Completion of geomechanical property computations using seismic data. A preliminary Poisson's Ratio plot is shown.
  - d) 4-D time-lapse VSP data are expected, and 4-D time lapse surface seismic may be acquired in 2014. Integration of those results will be a key future scope of work. The time-lapse data will be used to image and verify the progress of CO<sub>2</sub> that has been injected into the reservoir.

## SOURCE TESTING

During December 2011, tests were conducted at Bell Creek to choose between dynamite or vibrators as the source for the 3-D surface seismic survey. The geophysical services contractor was CGG Veritas. A 2-mile-long 96-channel receiver line was laid out running southwest–northeast adjacent to Well 32-12 near the western side of the Phase 1 area (Figure 5). During the source parameter testing, the contractor used the receiver layout to acquire a complete two-dimensional (2-D) test line with vibrators as the source to examine data quality after application of a modern data-processing sequence (Figure 6).

As part of the test, a check shot survey was performed by lowering a geophone sonde into the 32-12 well. By taking a measurement opposite the Muddy Formation, the time to the target formation was established. Comparisons between test records were made by focusing on the time window of interest around the target formation.

Two types of vibrators were tested: three 16,500-pound Mini-vibes made by Industrial Vehicles International and two 64,000-pound AHV-3 units made by I/O (now Inova) (Figure 7). Tests included the number of units sweeping together, different sweep frequency bandwidths,

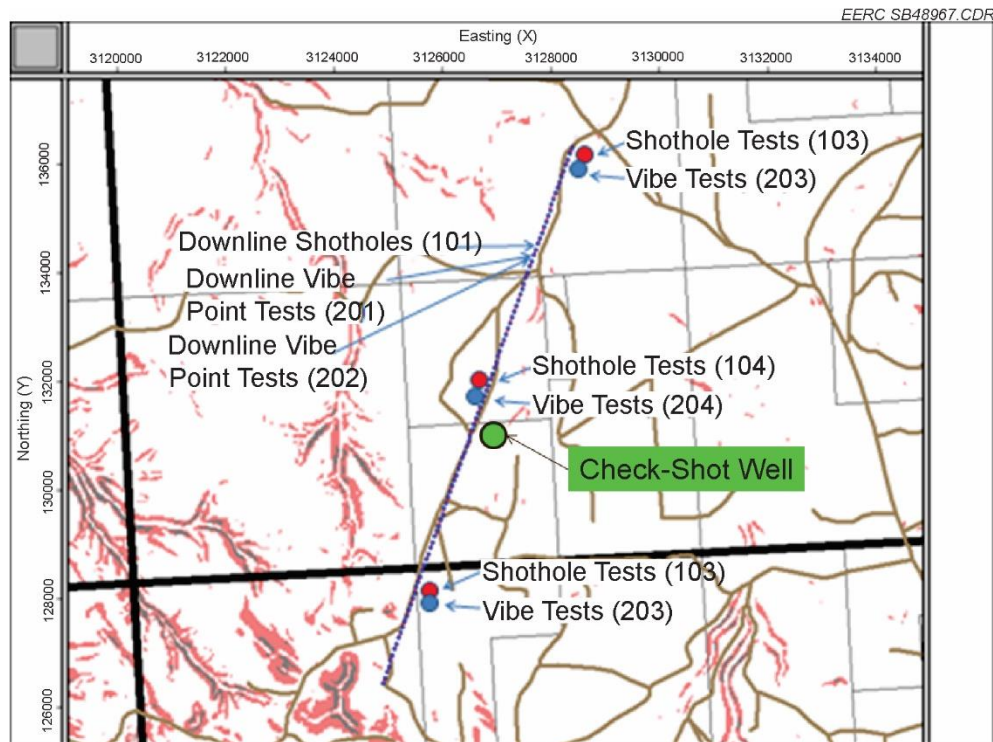


Figure 5. Location map of source test line, source test configuration, and check-shot well.

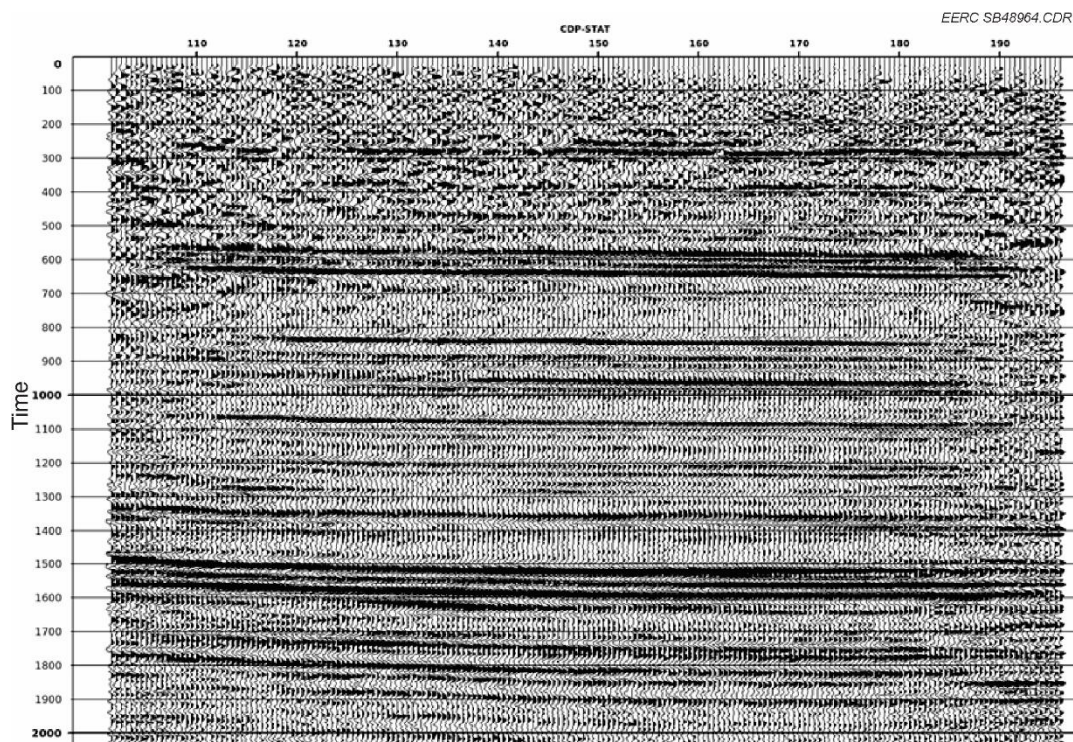


Figure 6. The migrated 2-D vibrator test line acquired in December 2011. Orientation is southwest–northeast, along the strike. The Muddy Formation reflection is the trough–peak split by the 1200-ms time line in the center part of the section.



Figure 7. An I/O AHV-3 heavy vibrator (left) and an IVI Minivib Vibrator on a field road at Bell Creek during the December 2011 source testing.



and sweep times. Dynamite charges of different sizes and shot depths were also tested. Shot records (Figure 8) and amplitude spectra (Figure 9) from each were compared over the target time window. Test results were evaluated with regard to data quality, economic factors, and logistical factors. A source configuration consisting of two large vibrators was chosen for the 3-D survey.

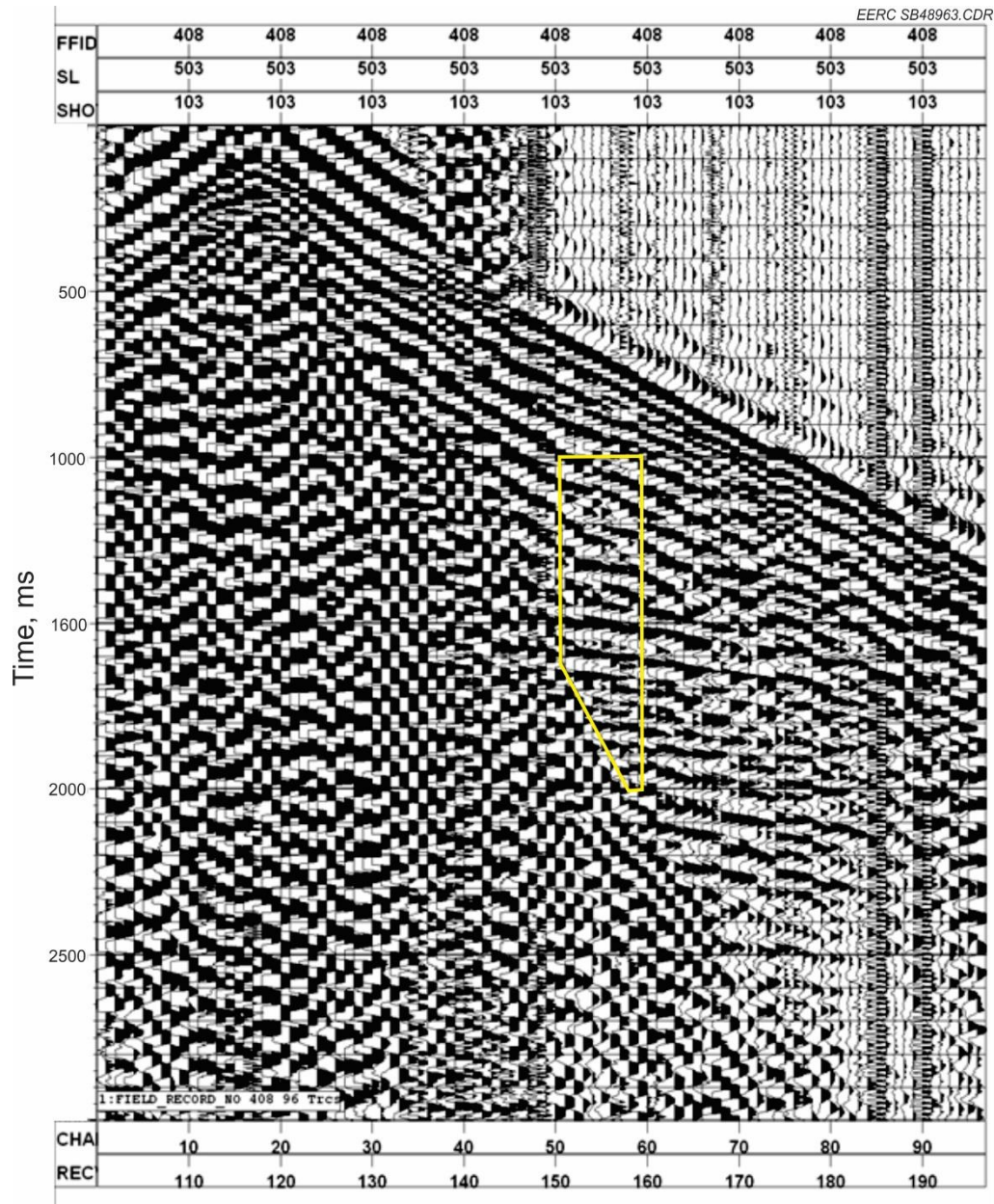


Figure 8. A 96-channel field record of a vibrator test shot. Ground roll noise is propagating diagonally across the record from early times on near offset traces to later times on far offsets. This type of noise is dependent on surface conditions. It can often be removed during processing, although the high amplitudes can sometimes overwhelm receivers near the shot point. The highlighted area shows data from the zone of interest.

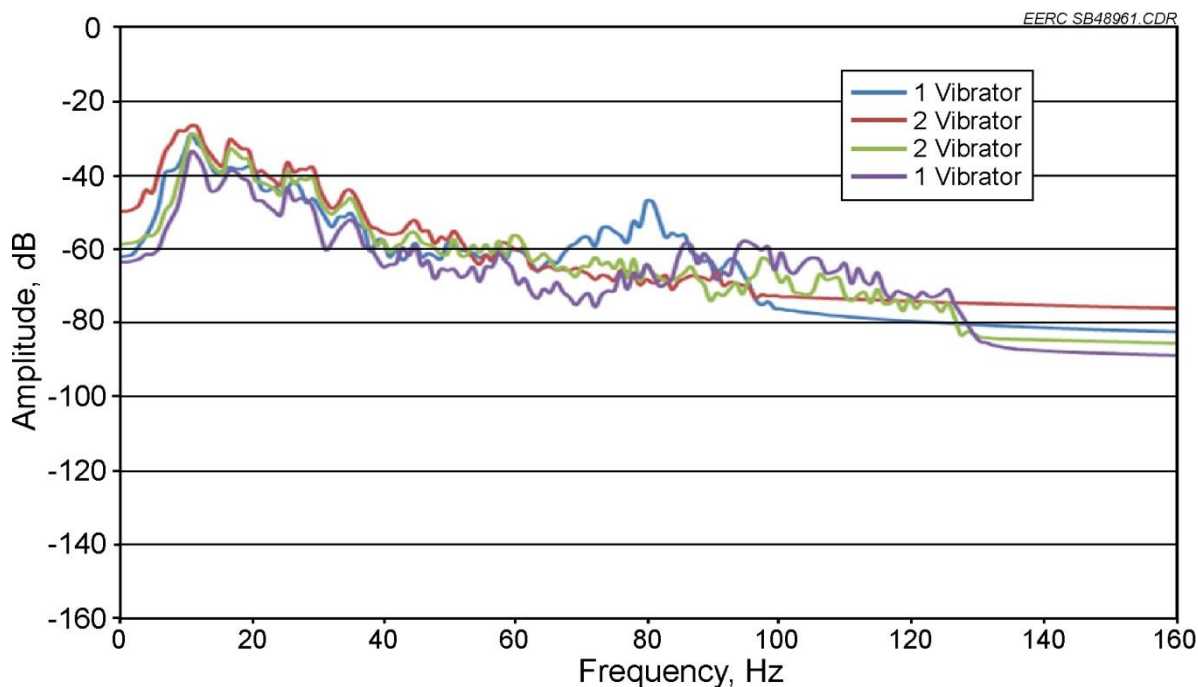


Figure 9. Source test spectra for four different vibrator and sweep configurations show the highly attenuative nature of Bell Creek near-surface geology. Signal attenuates rapidly, down 40 dB by 62 Hz, which is a decrease by a factor of about 100. Attenuation is usually a function of local conditions. Less is desirable as a limited bandwidth on the processed data presents resolution challenges during interpretation. Details of configurations and parameters have been masked as they are proprietary to Denbury.

### SURFACE 3-D SEISMIC DATA ACQUISITION

A 40-square-mile 3-D surface seismic survey was acquired over a significant portion of the Bell Creek Field during the 19-day period of August 20 through September 7. The geophysical services contractor was Dawson Geophysical Company. The survey boundary encompasses the central part of the field lengthwise along the geologic strike but omits coverage in Phases 6, 7, and 9. Significant coverage along dip outside the field boundaries was achieved with the intention of possibly identifying the field's stratigraphic edge during interpretation (Figure 10). A total of 5499 source points with 10,243 receiver stations were employed (Table 1). Source point and receiver locations are illustrated on a contractor plot with the layout design (Figure 11). Field acquisition parameters are listed in Table 1.

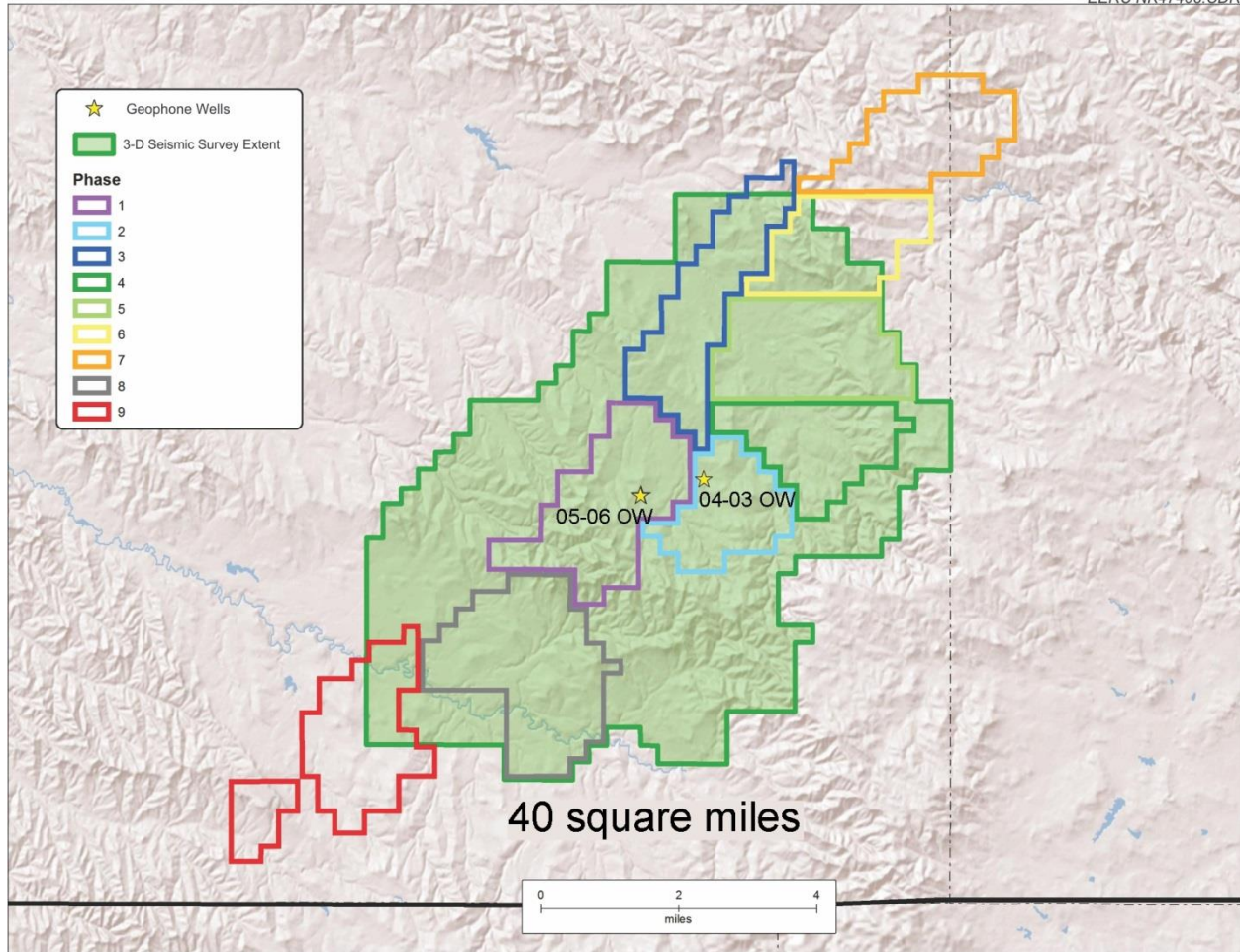


Figure 10. Baseline 3-D surface seismic survey outline superimposed on the field boundaries. Complete or significant coverage was obtained over Phases 1–5 and 8.



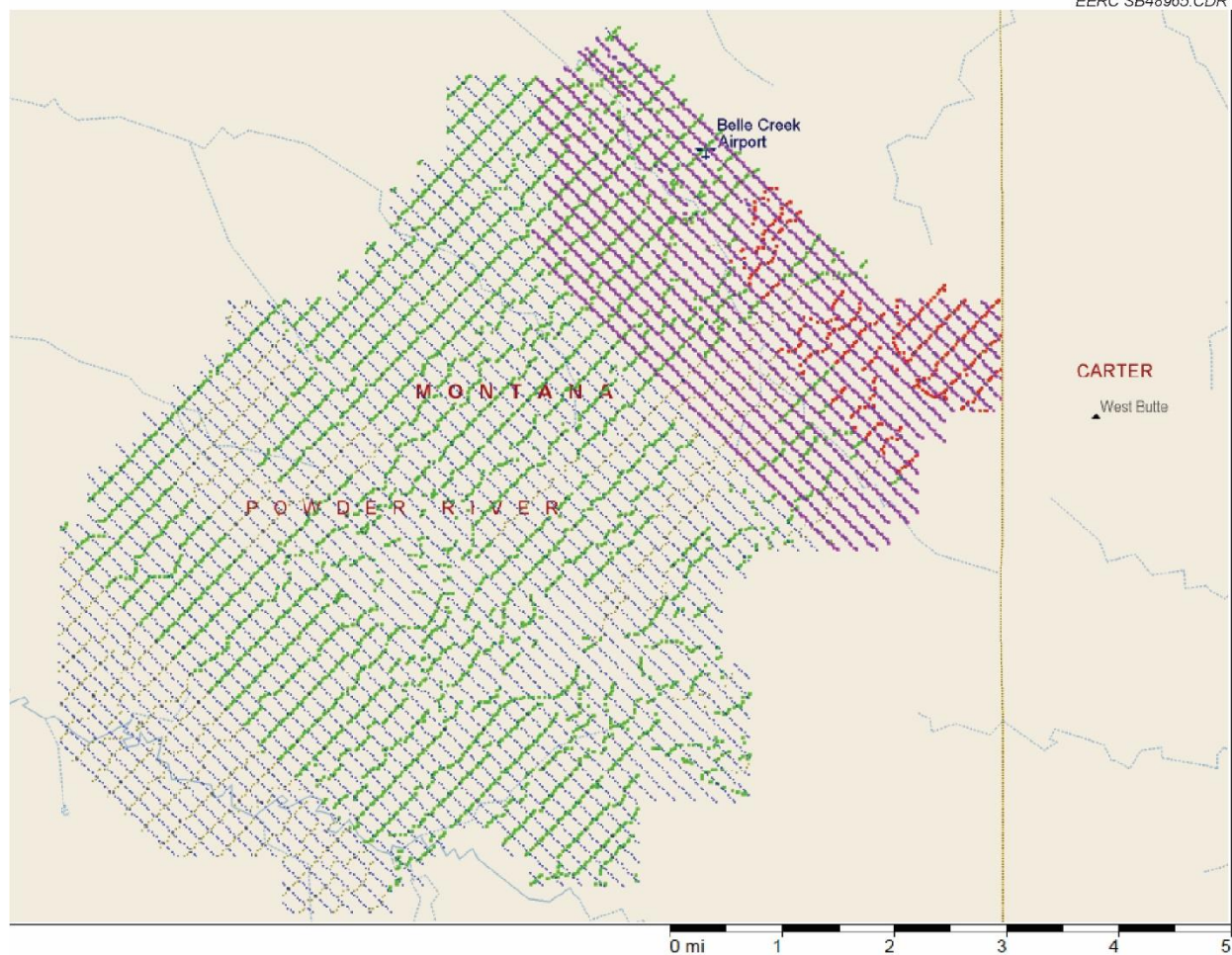


Figure 11. Seismic contractor plot of the 40-square-mile 3-D surface seismic survey layout demonstrating production in progress nearing completion. Northwest-southeast lines are receiver positions. Southwest-northeast lines are shot points. The 16 magenta lines are 2016 live receivers. Red lines are a day's shotpoints. Green lines are shotpoints previously acquired.

**Table 1. Acquisition Parameters**

Energy Source	Two 64,000-lb I.V.I. Birdwagon vibrators
Source Interval	165 feet
Total Source Points	5499
Recording Instrument	OYO-Geospace GSR nodes
Group Interval	165 feet
Geophone Pattern	Six phones per trace in a 2-ft circle
Active Spread	16 lines, 126 stations each
Active Stations	2016
Total Receiver Stations	10,243
Sweep Parameters	Proprietary
Record Length	4.2 seconds
Sample Interval	1 millisecond

The survey was acquired using autonomous receiver nodes; each receiver station is self-contained with a solid-state battery-powered recording unit. Each unit is wired with six geophones recording into the same channel. When laid out, the geophones are planted in a 2-foot circle (Figures 12 and 13). When in the field, the units record data continuously to internal memory. After the survey is completed, the data memory is dumped, and individual shot records are sorted from the data based on GPS (global positioning system) time coding (Figure 14).

The energy source was two 64,000-lb I.V.I. Birdwagon vibrators operating in unison at each of the 5499 shot points (Figure 15). Sweep parameters are proprietary to Denbury.



Figure 12. Seismic crew members laying out receiver stations.





Figure 13. GSR (geospace seismic recorder) recording unit with geophones planted in a 2-ft circle.



Figure 14. Nodal recording units in a rack used for operational checks, programming, and data collection.





Figure 15. Vibrator crew during Bell Creek survey. Two units shook together at each shotpoint. The third unit is a spare.

## SEISMIC DATA PROCESSING

After acquisition, the 3-D surface seismic data was processed by Geotrace, Inc., during the fall and winter of 2011 and 2012. The processing steps were as follows. A more detailed explanation of the steps are provided in Appendix A.

- Reformat data for processing.
- Define geometry and edit
- Noise attenuation/FK filter
- Spherical divergence spreading correction
- Surface consistent gain
- Surface consistent deconvolution
- Noise attenuation/wavelet transform filter
- Refraction statics
- Initial velocity analysis
- Surface consistent residual statics
- Second velocity analysis every 1 square mile
- Surface consistent residual statics (second pass)
- Migration velocity analysis every 0.5 square mile
- Ray trace prestack time migration
- CMP stack
- Filter
- Scale traces

Processed data were output to data files in SEG-Y format for transfer to the client.

## DATA PRESENTATION

The processed baseline 3-D surface seismic data were received by the EERC in April 2013. Interpretation and analysis activities began by loading the SEG-Y formatted stacked data into Hampson–Russell HRS-9, a graphical package of sophisticated display and analytical tools.

The orientation of the processed survey overlaid on the field is shown in Figure 16. The irregular survey boundary of the acquisition area is replaced by a simple rectangle which defines the limits of the processed inlines and crosslines. There are 554 inlines (1001–1554) spaced 82.5 feet apart along the dip of the field (northwest to southeast). There are 411 crosslines (1001–1411) spaced 82.5 feet apart along the strike of the field (southwest to northeast). Well locations that fall within the coverage area are shown.

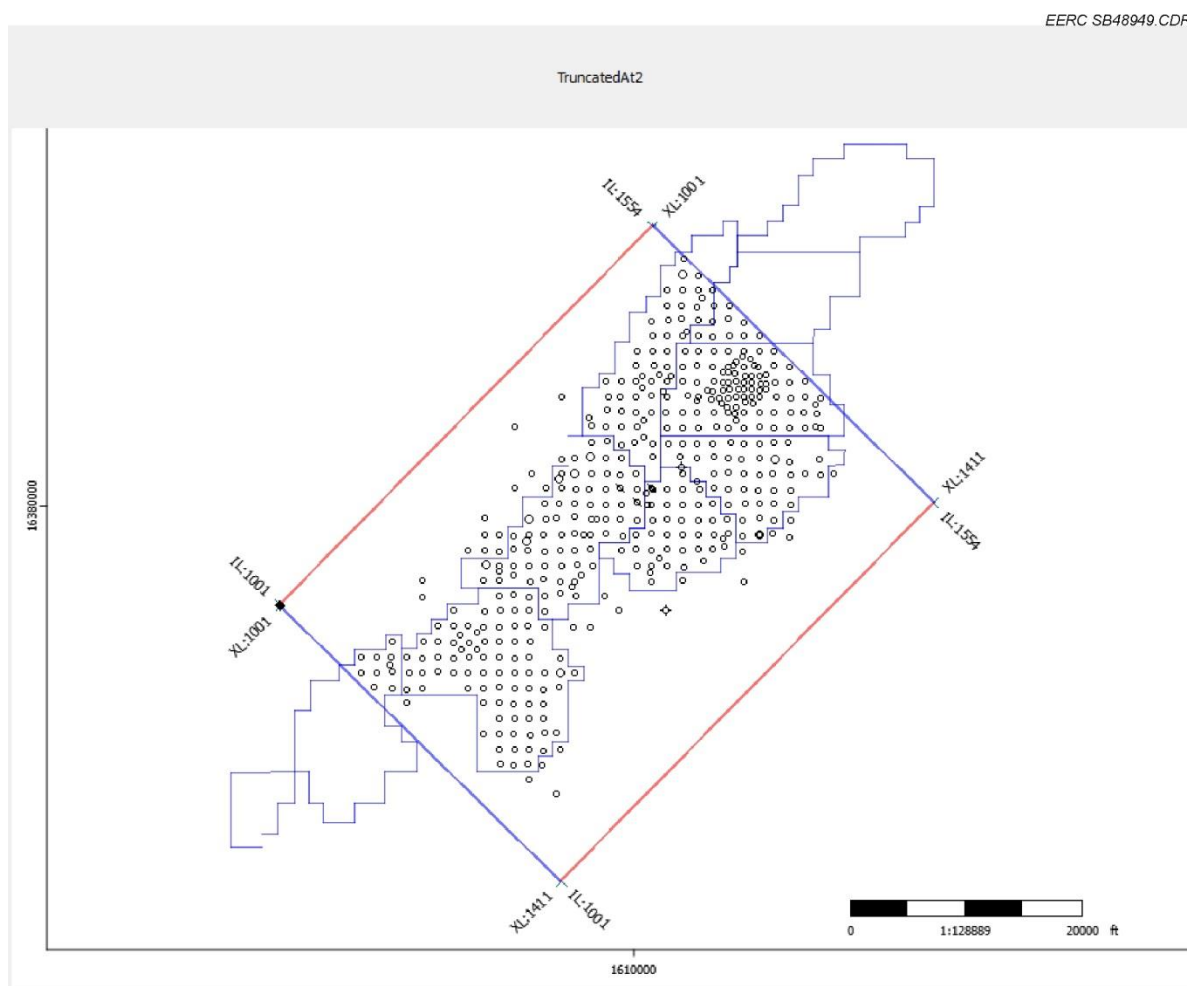


Figure 16. Bell Creek field phases and wells that fall within the farthest extent of inline and crossline 3-D data as indicated by the overlaid rectangle. Inlines (IL) are oriented northwest to southeast along dip and number from 1001 to 1554. Crosslines (XL) are oriented southwest to northeast along strike and number from 1001 to 1411. Spacing between adjacent lines in both directions is 82.5 feet.

The field geometry was not a perfect rectangle, so the boundary is not filled entirely with data. Figure 17 shows a gray-scale time slice through the data volume and how it fits within the boundary. The solid light gray around the edges of the volume indicates where there are no data. Four small geometric areas within the data are also void. The field operator does not have rights to those data based on the mineral leases and seismic permit. Significant portions of data above and below the geologic zone of interest have also been cut for the same reasons. See Figures 18 and 19.

The horizontal time slice in Figure 17 is from 1010 msec. The geologic layers it cuts through are visible as stripes of differing amplitude akin to a contour map. The geologic dip is to the northwest, with older units on the southeast. The dark black unit between Crosslines 1210 and 1350 represents a strong reflector within the Belle Fourche Formation overlying the Mowry Formation. It shows signs of polygonal faulting.

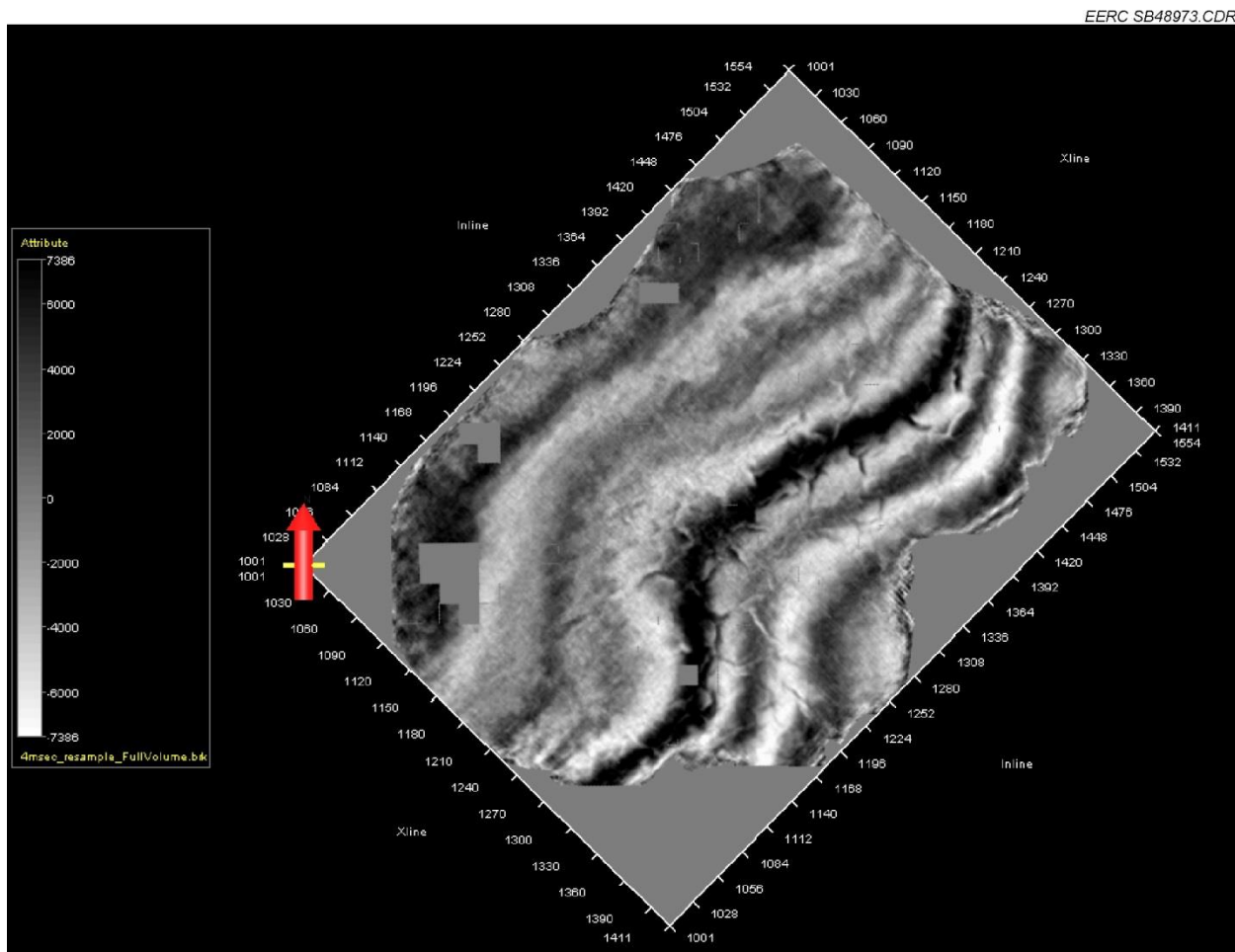


Figure 17. A gray-scale image of a time slice through the 3-D volume reveals the areal extent of data coverage within the survey boundary. The scaled attribute is reflection amplitude. The time slice is from 1010 msec. Geologic layers are dipping down to the northwest, so the horizontal slice cuts through successively younger units from southeast to northwest.

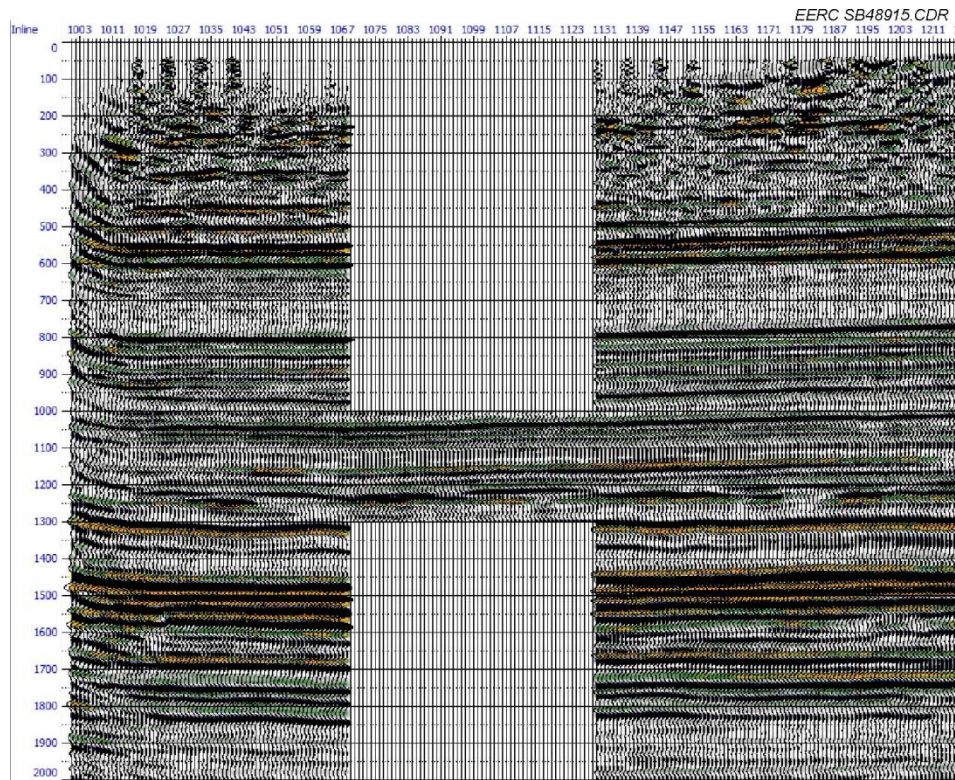


Figure 18. A portion of Crossline 1220 showing data zeroed above 1 sec and below 1.3 sec. The field operator does not have rights to those data based on the mineral leases and seismic permit. The reservoir reflector is visible at approximately 1.15 sec (1150 msec).



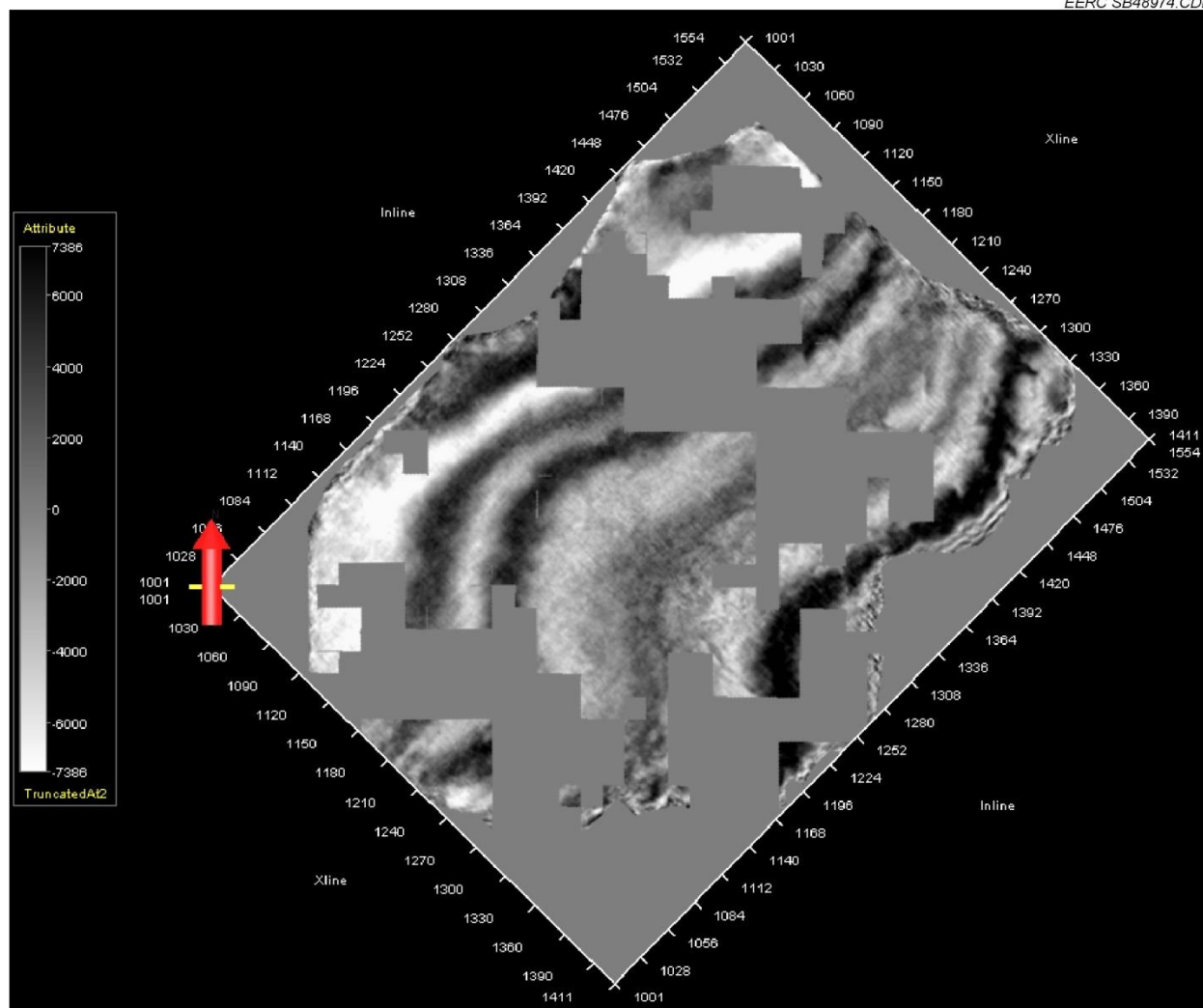


Figure 19. Time slice from 970 msec shows areal extent of data redactions for times less than 1 second and greater than 1.3 seconds. The redactions had little practical impact on the interpretation efforts.

### Well Database and Well Ties

For interpretation work, well data and seismic data are used together. A well database was constructed by importing the locations of 337 wells within the survey boundary area. Well logs were loaded from digital LAS (log ASCII standard) files as needed and tied to the seismic data.

Tying to well logs is an important initial step because it is through this process that geologic layers of interest, including the reservoir, are identified on the seismic data. This is especially important at Bell Creek, where the reservoir is relatively thin and variable as it may be difficult to locate otherwise. Another important characteristic determined with ties is the polarity of the data—whether a positive “peak” on a seismic trace corresponds to an increase in acoustic impedance or a decrease.

A tie is made by matching the character of a synthetic seismogram derived from the sonic log with the character of seismic traces located near the well. Because the physical volumes of rock measured by the sonic and seismic are not exactly the same, ambiguity sometimes exists. As subsequent interpretation steps depend on getting this one correct, the details are of great interest to the interpretation geophysicist and are included in Appendix B.

The tie with Well 05-06 OW that resulted in the maximum computed correlation coefficient after the minimum amount of adjustment to the sonic log is shown in Figure 20. The wavelet, shown above the blue synthetic and red repeated seismic trace, is reversed in polarity from the zero-degree default, with an additional 28 degrees of phase that makes it look a little lopsided. This polarity implies that a peak on the seismic data represents a decrease in acoustic impedance. The Muddy Formation reflector is identifiable on the log at 1150 ms (left axis scale) or 4500 feet (right axis scale) by the gamma ray and sonic response. It is represented by a trough–peak combination on the seismic section.

There are inevitable imperfections in synthetic-to-seismic ties. An apparent mismatch on Figure 20 is the Niobrara reflection at about 800 ms. The cause is unknown but may be attributed to the different scale of measurements between logs and seismic as described above. Events below the Niobrara tie very well, and the relationships shown are verified on other wells.



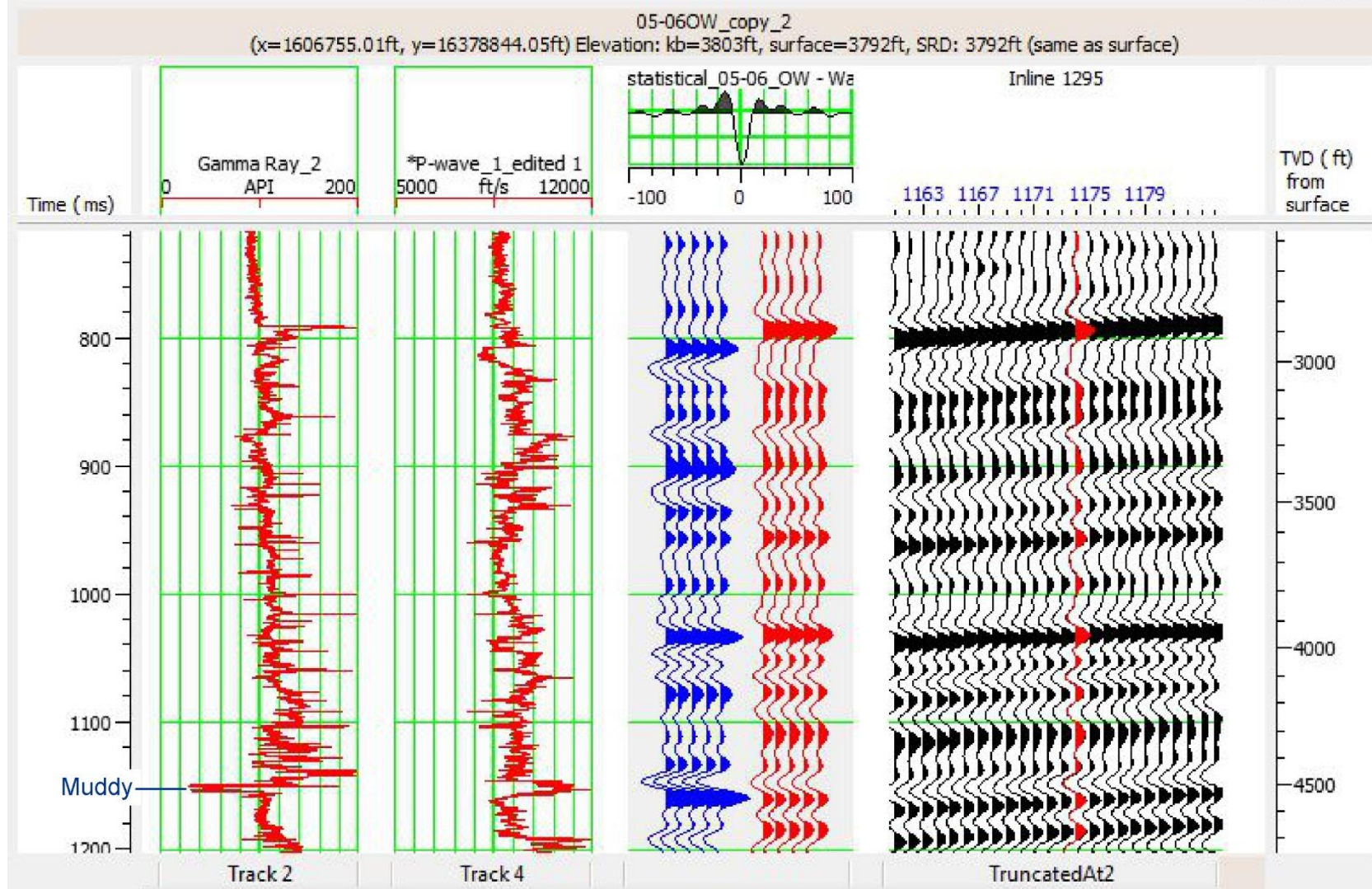


Figure 20. The well log data from 05-06 OW (left two columns) exhibit a strong synthetic-to-seismic tie with the seismic data (right two columns). Muddy Formation reflector is the large event at 1150 ms (left axis) or 4500 feet (right axis) and is represented by a trough-peak combination on the seismic data.

## Data Bandwidth and Vertical Resolution

The geologic target zone of interest at Bell Creek is the Muddy Formation and especially the Bell Creek sandstone, the Bell Creek sand, within it that makes up the reservoir. The Muddy Formation includes the sequence of formations from Shell Creek through the Rozet (Figure 21). It is about 4500 feet in depth and varies from 70 to 90 feet in thickness. The Bell Creek sand within is typically between 20 and 30 feet thick. To resolve formations of this thickness requires both an acoustic impedance contrast at the layer boundaries great enough to generate an interpretable reflection and a frequency bandwidth sufficient to produce a wavelet sharp enough to avoid interference from the lower interface reflection.

The bandwidth of the data can be seen on an amplitude spectrum. Figure 22 shows one in the lower panel that was computed over a data window in time and space that includes the zone of interest in the neighborhood of the 05-06 OW monitor well. Bandwidth is the range of frequencies that are above the noise level, from 10 to about 48 Hz. The data have a low-cut filter applied which explains the rolloff at 10 Hz. There was no high-cut filter applied, but frequencies drop steeply at 48 Hz to the noise level.

The upper panel of Figure 22 shows the wavelet derived from the amplitude spectrum of the data. Phase information is lost in the process, so it is displayed as zero phase. Mathematically, it is the same as the wavelet on the seismic data, and we can use it to investigate resolution.

EERC SB48950.CDR

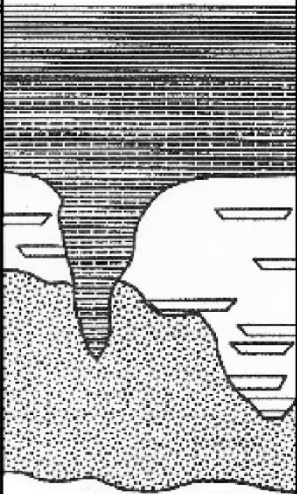

This Study	Lithostratigraphy
Mowry Shale	
Shell Creek	
Springen Ranch	
Coastal Plain Sequence	
Bell Creek Sandstone	
Rozet Sequence	
Skull Creek Shale	

Figure 21. The EERC's naming convention and lithostratigraphy for the Bell Creek model modified from Molnar (1990). Coastal Plain sequence is often thin and not easily picked, so it is not shown on the following figures.

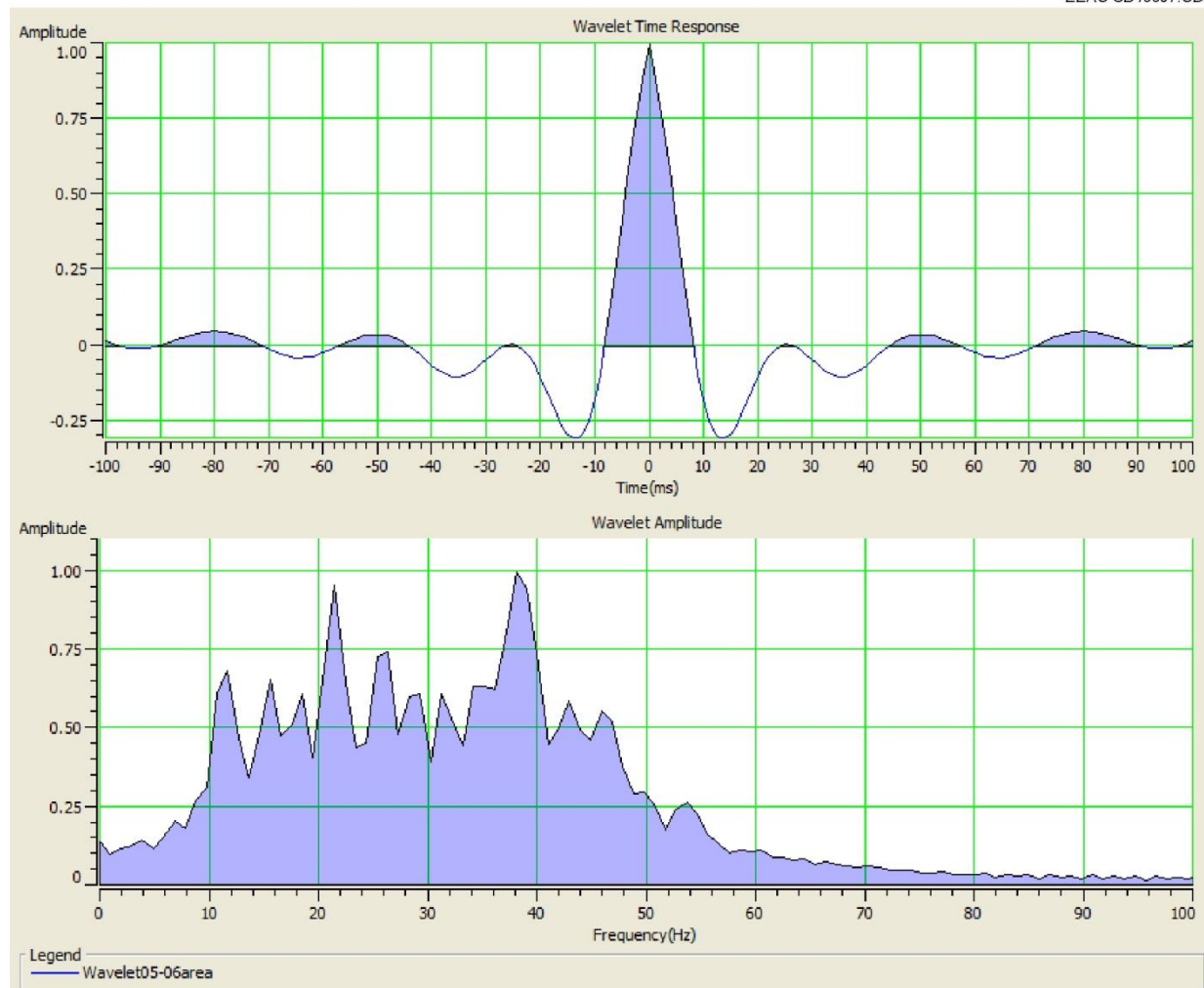


Figure 22. Lower panel shows the amplitude spectrum computed over 40,293 traces in the central area of Phase 1 in a 500-msec window centered on the zone of interest. Useful bandwidth is about 10–48 Hz. The upper panel shows the wavelet derived from the amplitude spectrum. Tuning thickness for this wavelet is 14 ms. The maximum resolution is 11 ms, meaning any bed with a two-way time thickness less than 11 ms will not be resolvable.

The wavelet has a time thickness which determines the limit of its ability to resolve a thin bed such as the Muddy Formation. This wavelet has a resolution limit of 11 ms. To illustrate this, Figure 23 shows the wavelet and a reversed version in gray separated by 5 ms to represent the simplistic model of a bed 5 ms thick. The waveform in blue is a superposition of the two waveforms. The superposition is what would be seen on the seismic section. Indeed, it looks like the Muddy reflection on Figure 20. Note that the peak-to-peak interval of the superposition is 11 ms, not the actual value of 5 ms. For bed thickness intervals less than 11 ms, the peak-to-peak interval would remain about 11 ms; only the amplitude would change. Thickness intervals greater than 11 ms will be resolved accurately in theory. As a practical matter, resolution at the theoretical limit on real data is not always possible.

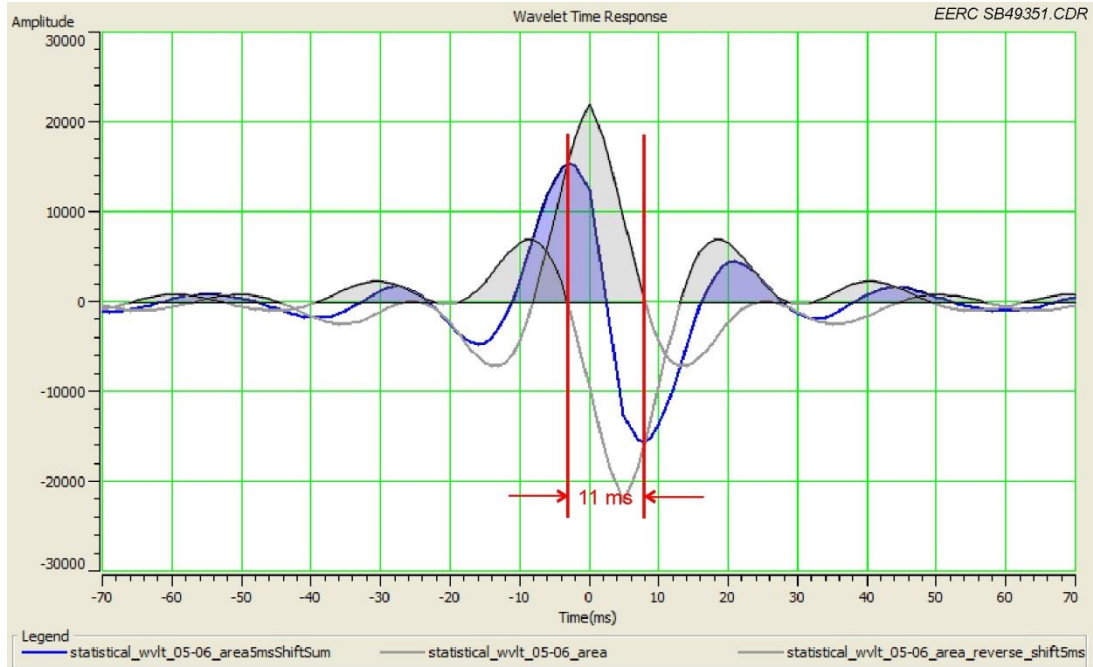


Figure 23. Demonstration of the limit of resolution of the embedded wavelet. Two wavelets in gray are shown 5 ms apart and reversed from each other to represent the entering and exiting reflections on a bed 5 ms thick. The blue wavelet is the sum—the superposition—of the other two. The superposition is what would be seen on a seismic section. The peak-to-peak interval on the blue wavelet is 11 ms even though the two gray wavelets are only 5 ms apart. The peak-to-peak interval would remain at ~11 ms for any wavelet interval less than 11 ms. Only the amplitude will vary.

The tuning thickness for the wavelet is 14 ms. That is the interval in which the overlapping waveforms add constructively to sum to the highest possible amplitude. Figure 24 shows the result at the tuning thickness. The vertical scales for both Figures 23 and 24 are the same to allow direct comparison.

The vertical scale for wells and geology is depth, not time. The vertical scale on a seismic section is two-way travel time (twt), the time it takes for sonic waves to travel to the subsurface layers and back. Two-way travel time is related to depth by the velocity:  $\text{Depth} = \text{Velocity} \times \text{twt}/2$ . If the 11-ms resolution limit described above occurred in a homogeneous layer that had an interval velocity of 10,800 ft/s, which is about the average Muddy velocity, the resolution limit in terms of feet would be  $(10,800 \text{ ft/s} \times 0.011 \text{ s})/2 = 59.4 \text{ feet thick}$ .



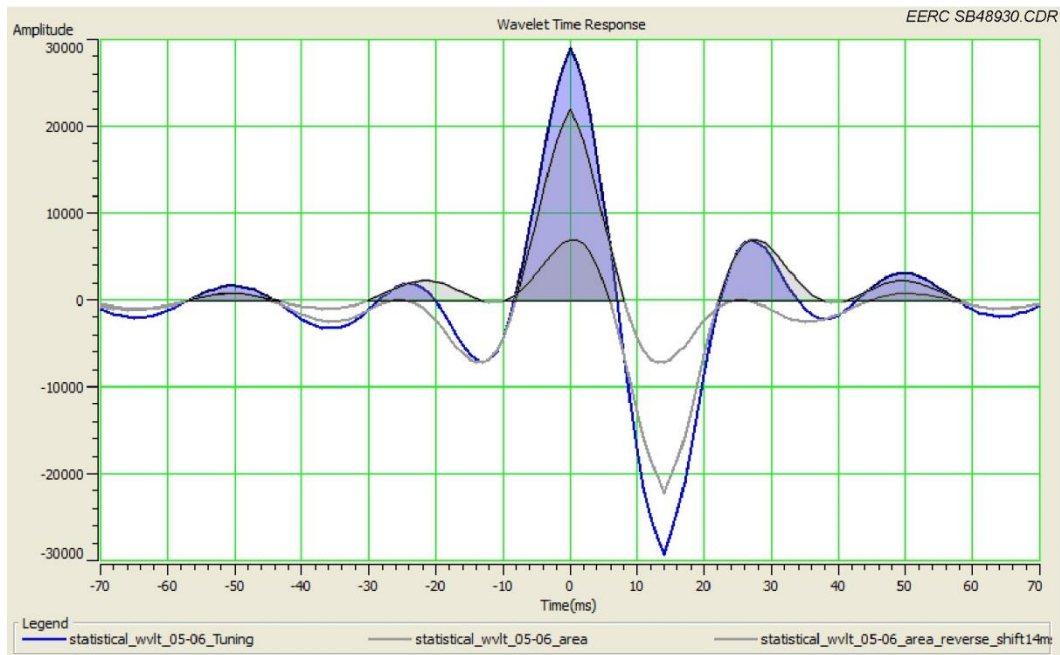


Figure 24. Demonstration of the tuning thickness of the embedded wavelet. Two wavelets in gray are shown 14 ms apart and reversed from each other to represent the entering and exiting reflections on a bed 14 ms thick. The blue wavelet represents the superposition of the other two. The 14-ms interval results in the maximum amplitude as the wavelets sum constructively.

The same calculation for the tuning thickness in feet would be  $(10,800 \text{ ft/s} \times 0.014 \text{ s})/2 = 75.6$  feet thick. An interval of this thickness could be expected to produce the maximum amplitude reflection, again assuming a homogeneous layer. For the actual, inhomogeneous case, contributions from lithology changes within the layer will contribute to the actual amplitude.

To generate a reflection, there must be an acoustic impedance contrast. Acoustic impedance is defined as the product of velocity and density. It can be easily calculated at a well using the sonic p-wave velocity and the bulk density log. Using Well 05-06 OW, Figure 25 shows the computed impedance log in the center. The gamma ray log is plotted on the left to provide lithology identification, and the seismic data within the depth window are plotted on the right with the red waveform indicating the well location. Lithologic tops have been marked with the naming convention used in the EERC's geologic model (Figure 21).

The acoustic impedance log varies at the resolution level of the well logs, but the eye can detect three different average levels within the window that relate to the lithology. From the top of the Springen Ranch through the Rozet, the impedance value is more than 20% greater than the Shell Creek and Mowry above and that of the Skull Creek below. This impedance contrast gives rise to the waveform shown. The polarity of the seismic data is such that an increase in impedance is represented by a trough or negative deflection. A decrease is represented by a peak or positive deflection. The zone of increased impedance in 05-06 OW is 65 feet thick and occurs over a depth range of 4485 to 4550 feet (right vertical axis). This corresponds to a twt interval of

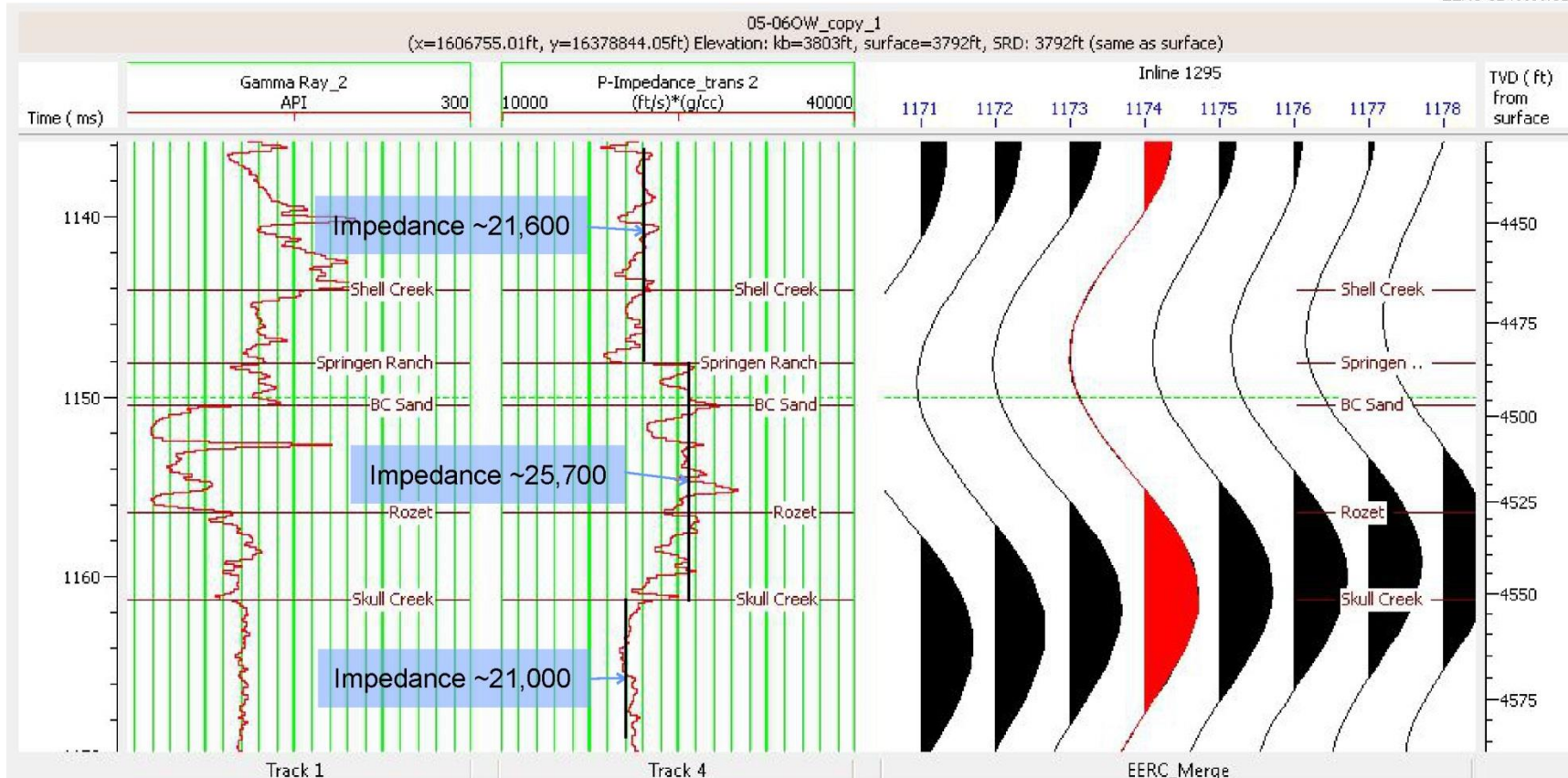


Figure 25. The P-wave acoustic impedance curve (sonic velocity  $\times$  density) demonstrates that significant impedance changes occur at the Springen Ranch and Skull Creek boundaries which give rise to the Muddy Formation reflection. Bell Creek sand boundaries also exhibit impedance contrasts within this interval but are below the resolution of the wavelet. Note that the two-way time through the impedance contrast is 13 to 14 msec. This is near the limit of resolution of the embedded wavelet and the tuning thickness.

13–14 ms from 1148 to 1162 ms (left vertical axis) which is close to the limit of vertical resolution and tuning as determined above. The relationship of the seismic reflection to the well logs and geology is clearly displayed.

The clean Bell Creek sand within this interval totals about 30 feet which puts it below the 59-foot vertical limit of resolution of this data set as calculated above. The implication is that mapping the sand thickness directly may not be possible with the seismic data in its current state. The time thickness of the sand is shown as 6 ms (Figure 25 left axis), so roughly twice the current bandwidth would be needed to resolve it. The source bandwidth used comes close to what is needed, although attenuation of high frequencies appeared to be a challenge in the field. If high frequencies were preserved on the field data, a data-processing effort that specifically sought to preserve bandwidth in the zone of interest may result in additional vertical resolution.

The impedance contrasts between the Bell Creek sand and the Springen Ranch above, and the Rozet below, are visible on the impedance log in Figure 25 and exhibit notable deviations from the marked average level. These impedance contrasts could cause interference effects that impact the overall reflection amplitude. In a later section it is shown that the Muddy Formation reflection amplitude appears to be related to the character of the Bell Creek sand.

The tuning thickness concept described above assumes a homogeneous or isotropic interval between impedance contrasts. The logs on Figure 25 show that the Springen Ranch-to-Skull Creek interval is clearly not geologically isotropic. It is shown later that when the interval thickness approaches the tuning thickness, the Muddy Formation reflection actually decreases in amplitude instead of increasing as would be expected from tuning. Geological anisotropy within the reflection interval may render the tuning concept inapplicable for this thin-bed reflector.

Another representation of well logs and geology juxtaposed with the seismic is in Figure 26. The logs from left to right are the gamma ray, resistivity, and sonic p-wave velocity from the 05-06 OW well. As before, the seismic data are on the right, with the red waveform indicating the well location. For this display, the phase of the seismic data has been rotated 90 degrees to transform the natural thin-bed, trough–peak combination of the Muddy to a more intuitive centered peak. The peak encompasses the entire Springen Ranch-to-Skull Creek interval. As the appearance is more intuitive and easier to identify, subsequent figures will use phase-shifted data.

The ability to resolve different geologic features as seen on the logs within the peak is not something that can be done directly. The peak does have attributes that may be exploited to glean information, such as amplitude. The reflection is a composite response of the geologic characteristics occurring within it, and these characteristics may influence whether the amplitude is high or low in an area. Also, as shown above, the thickness of the high impedance interval may affect amplitude, with higher values expected where the thickness approaches the tuning thickness of 75 feet and less for thinner layers. The power of this attribute is seen when mapping and while interpreting along section lines. An example is shown in Figure 27 which overlays logs on the seismic data. Lateral variations in the amplitude of the Muddy reflection are clearly visible, and efforts to fully understand this effect are ongoing. Some experiments using complex attributes such as instantaneous frequency, instantaneous phase, and others have been attempted with mixed results, and additional efforts are planned.

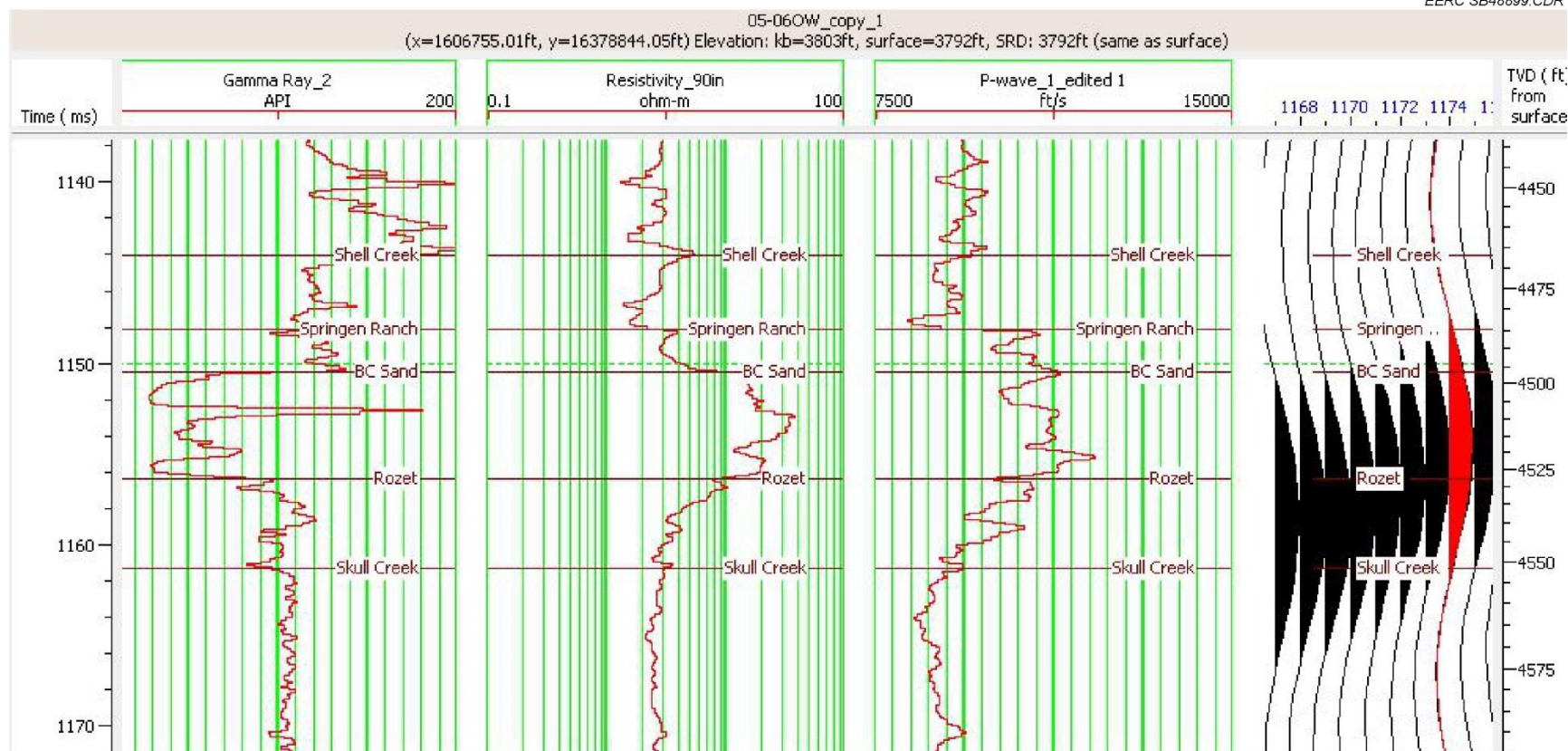


Figure 26. The relationship between the well logs, formation tops, and seismic reflection from the reservoir zone is shown. The seismic data have been phase-shifted +90 degrees to convert the trough-peak, thin-bed response to a single peak-centered response. The red-filled peak represents the well location. The reflection encompasses a “greater Muddy,” which includes the Springen Ranch through Skull Creek Formations.



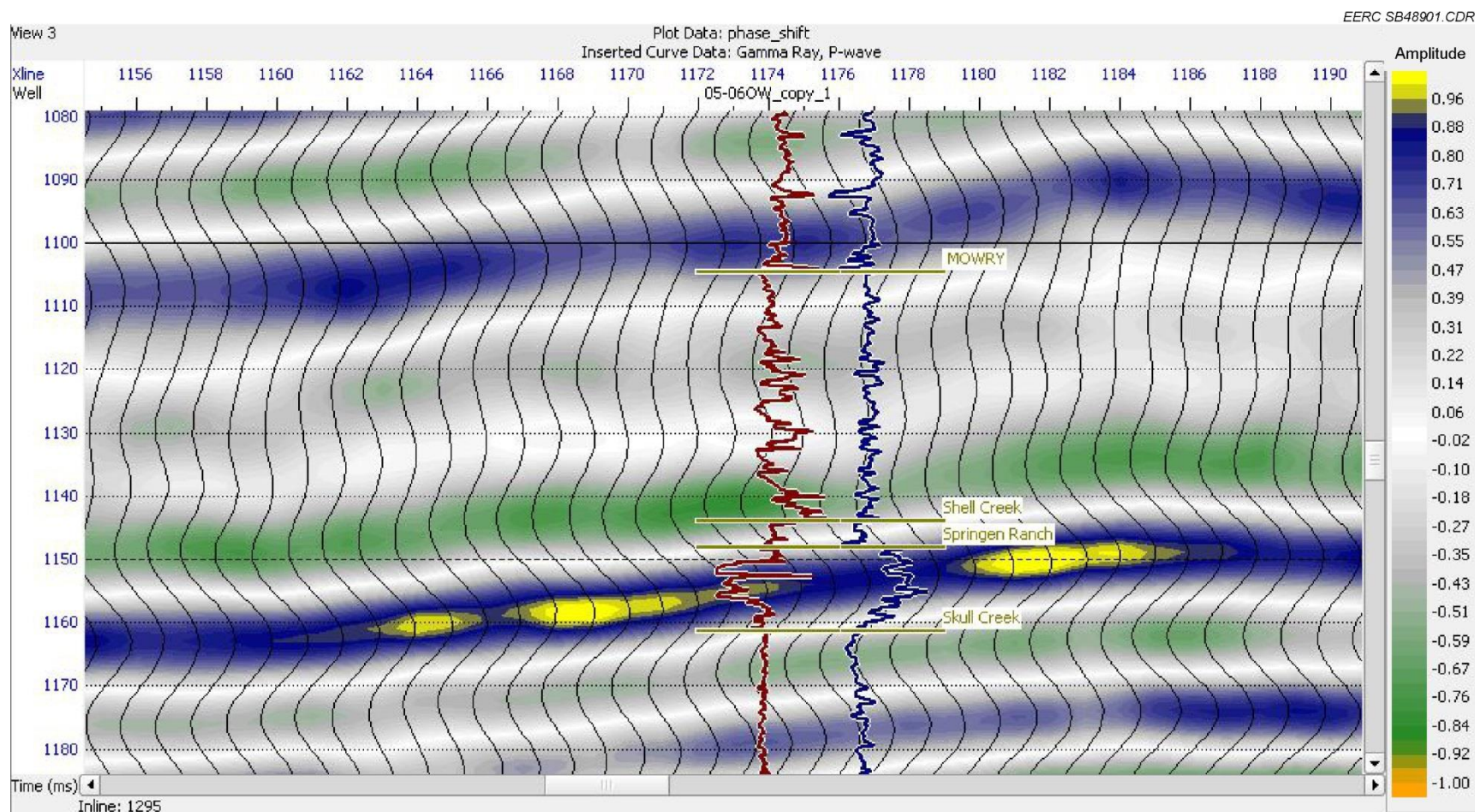


Figure 27. Seismic data showing color-coded amplitude varying spatially along the inline passing through Well 05-06 OW. Seismic data have been phase-rotated 90 degrees so that the Muddy Formation corresponds to the blue and yellow peak, with yellow representing the highest amplitude. Gamma ray (GR) and sonic p-wave velocity are overlaid with formation tops shown. GR trace overlays the well location. P-wave is slightly offset for clarity.

The key points are that vertical resolution of the wavelet on the data is about 59 feet; the reflection from the Muddy encompasses the Springen Ranch-to-Skull Creek interval because that is the source of the greatest acoustic impedance contrast; and the Bell Creek sand within this interval is below the resolution limit but may impact the amplitude of the reflection.

### **Lateral Resolution**

Spatially, the seismic data traces are 82.5 feet apart in both the x and y directions. This is a significantly finer sampling interval than the current quarter-mile well spacing. Even though the trace data lack the fine vertical resolution of well logs, the ability to track events away from and between wells is very powerful.

### **Horizon Picking**

Picking and viewing horizons are powerful ways to get a visual understanding of the data, to create maps, and to analyze intervals. Five horizons were picked and visualized (Figure 28):

1. The Niobrara reflection.
2. A strong reflector about 120 ms above the Muddy in the Belle Fourche Formation, referred to as Horizon 1.
3. The Muddy reflector.
4. A steady reflector ~30 ms immediately below the Muddy, referred to as Leg\_Below\_BCSand\_all. This is probably the top of the Fall River Formation.
5. The Mowry top.

Horizons were chosen because they had strong, consistent reflections. The exceptions are the Mowry and the Muddy, which are the focus of our interest. Their reflection character is variable and required great care to pick.

The Muddy horizon is shown in Figure 29 in map view. The scale bar shows the twt associated with the picked reflector. The color coding provides the appearance of a contour map, but the contours in this case are two-way reflection time.

Horizons are picked using a combination of hand picking and constrained autopicking. An intelligent autopicker is used to fill in between the hand-picked lines. Extremes near the edge are indicative of edge effects and can be ignored.



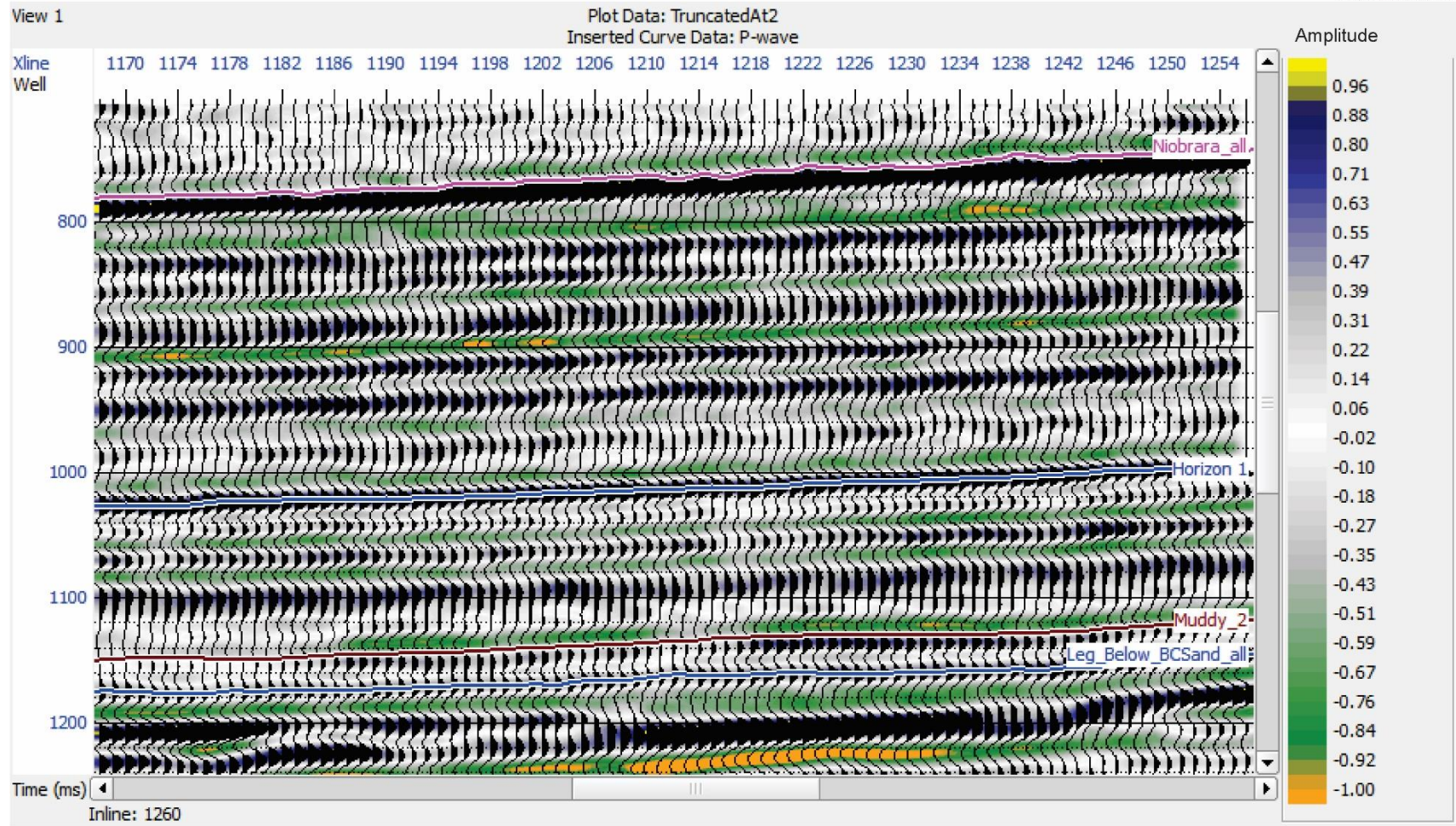


Figure 28. Four picked horizons are shown on this inline. From the top: the Niobrara, Horizon 1, the Muddy, and the leg below the Bell Creek sand.

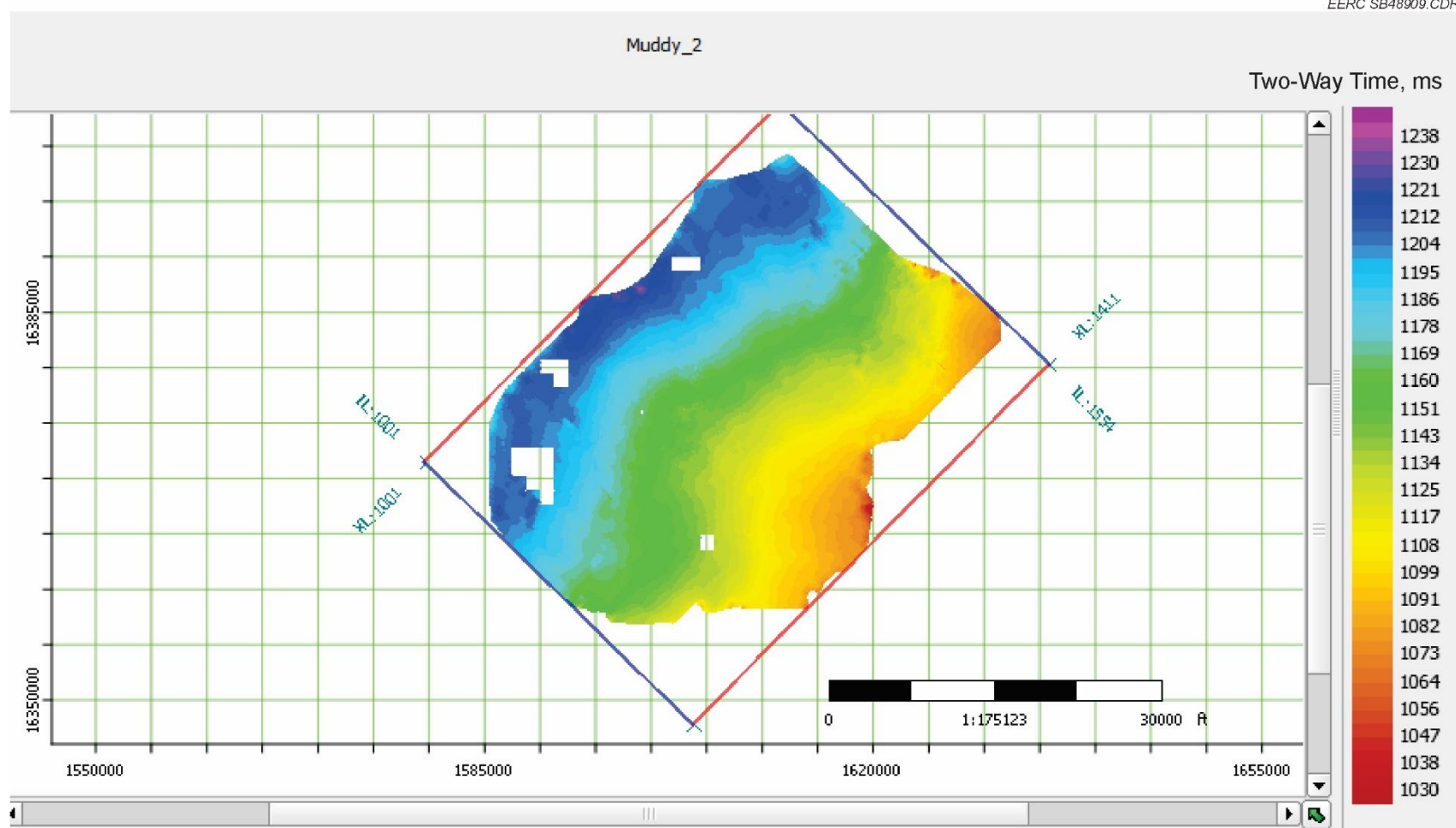


Figure 29. Areal view of the Muddy horizon. Color code is reflection time in milliseconds. Dip is to the northwest. Extreme values on the edge are mispicks due to edge effects and should be ignored.

## Mapping

In the previous section on vertical resolution, it was noted that the Muddy Formation reflection originates from the impedance anomalies associated with the top of the Springen Ranch and the top of the Skull Creek. It was also noted that the amplitude reflection varied from place to place. The source of amplitude variation could be tuning due to the thickness of the Springen Ranch-to-Skull Creek sequence approaching 76 feet or to the geologic makeup of the units within the sequence.

To better see the spatial variation of amplitude, a map of the Muddy Formation reflector amplitude was generated by summing the sample amplitudes within a 12-ms window centered on the Muddy reflector. The data set phase was first rotated by 90 degrees, as in Figure 27. This changed the character of the Muddy reflector from a trough–peak doublet of negative and positive values to a single positive peak. Sample amplitudes in the time window extending 6 ms above to 6 ms below the horizon pick on each trace were summed to get the amplitude at that location. The result is shown in Figure 30 with well locations and geographic location boundaries overlaid. Warmer colors indicate higher amplitudes; white and cooler colors are indicative of lower amplitudes.

The map clearly shows several geologic features. To the north, a channel feature traces along several phase boundaries. Another feature with a dendritic drainage type appearance is apparent in the southern portion of the map, and there are several areas of high amplitude, including one in the center of the field with an edge that parallels the southeast to northwest phase boundaries.

To see if other physical features and a relationship to sand character could be identified, the seismically derived amplitude map was compared to a geologic interpretation based on well logs. A net Muddy sand isopach map (effectively, a map of clean sand) is shown in Figure 31. On this map, hotter colors indicate thicker sand. Channel features within the field are prominent. When the amplitude map is overlain (Figure 32), several physical features are highlighted with a great degree of agreement. Where the clean sand is shown to be thickest on the isopach maps, the seismic amplitudes are generally the lowest. This is an important relationship. The following three sections show in greater detail three geologic features visible on the amplitude map.



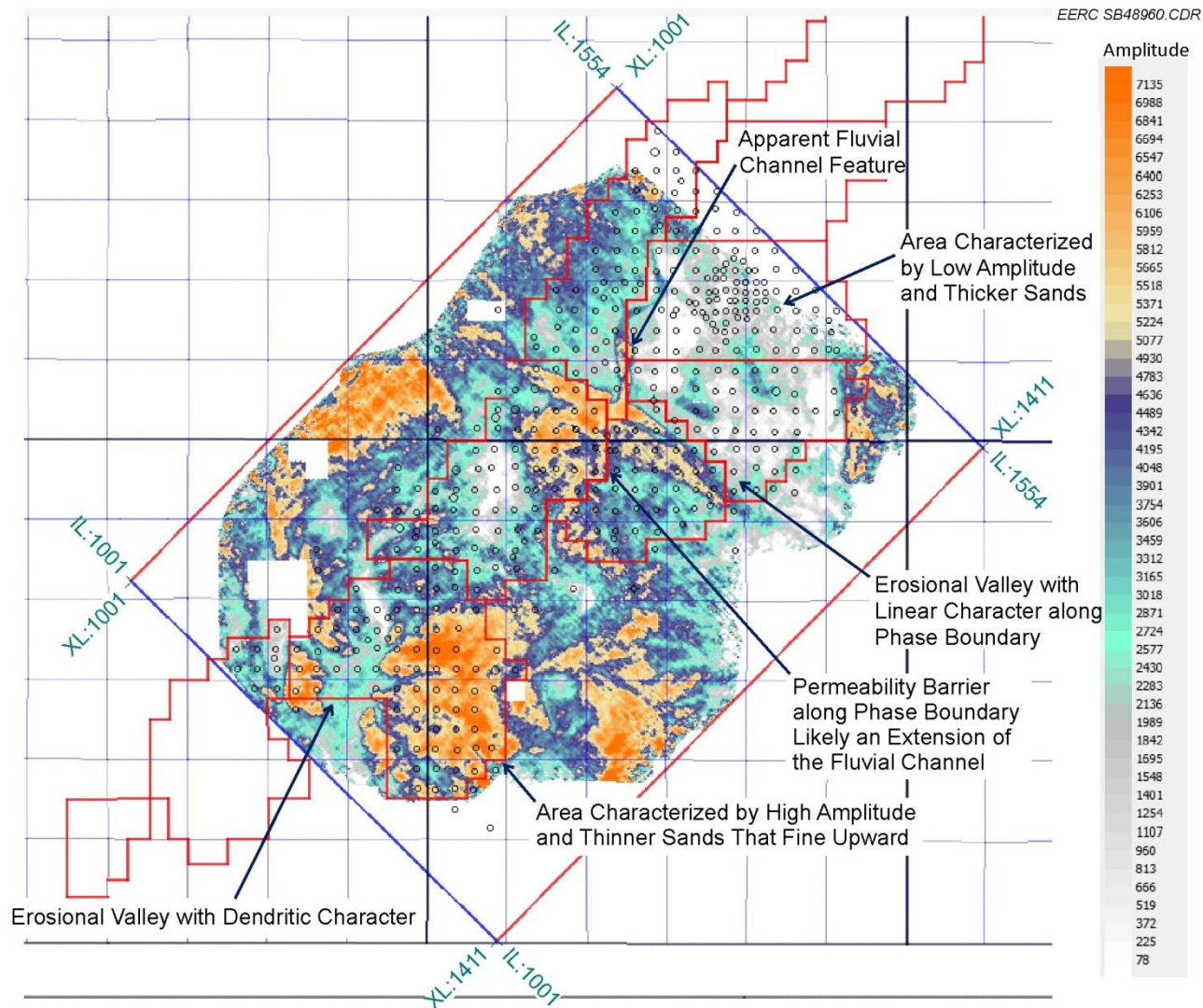


Figure 30. Map of Muddy Formation reflector amplitude created as described in the text. Amplitude scale is on the right, with warmer colors indicating higher amplitudes, and white indicating near-zero amplitude. Map shows township and section lines, phase boundaries, and well locations. Some phase boundaries parallel amplitude contrasts which may represent lithologic changes.

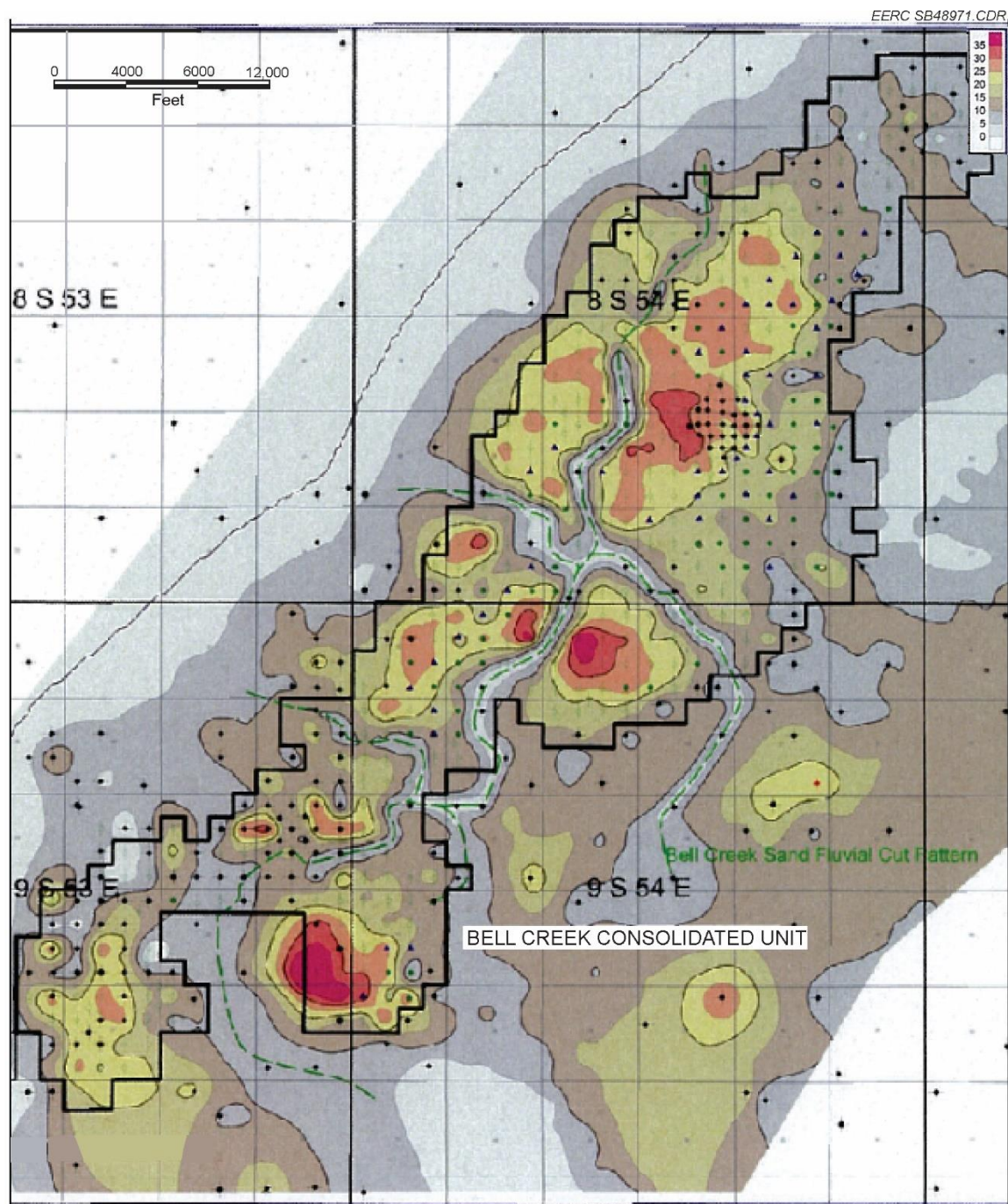


Figure 31. A sand isopach map developed by a geologist from well logs and an intimate understanding of the field. Hotter colors indicate thicker sand. Channel features within the field are obvious (modified from Sutherland [2011]).



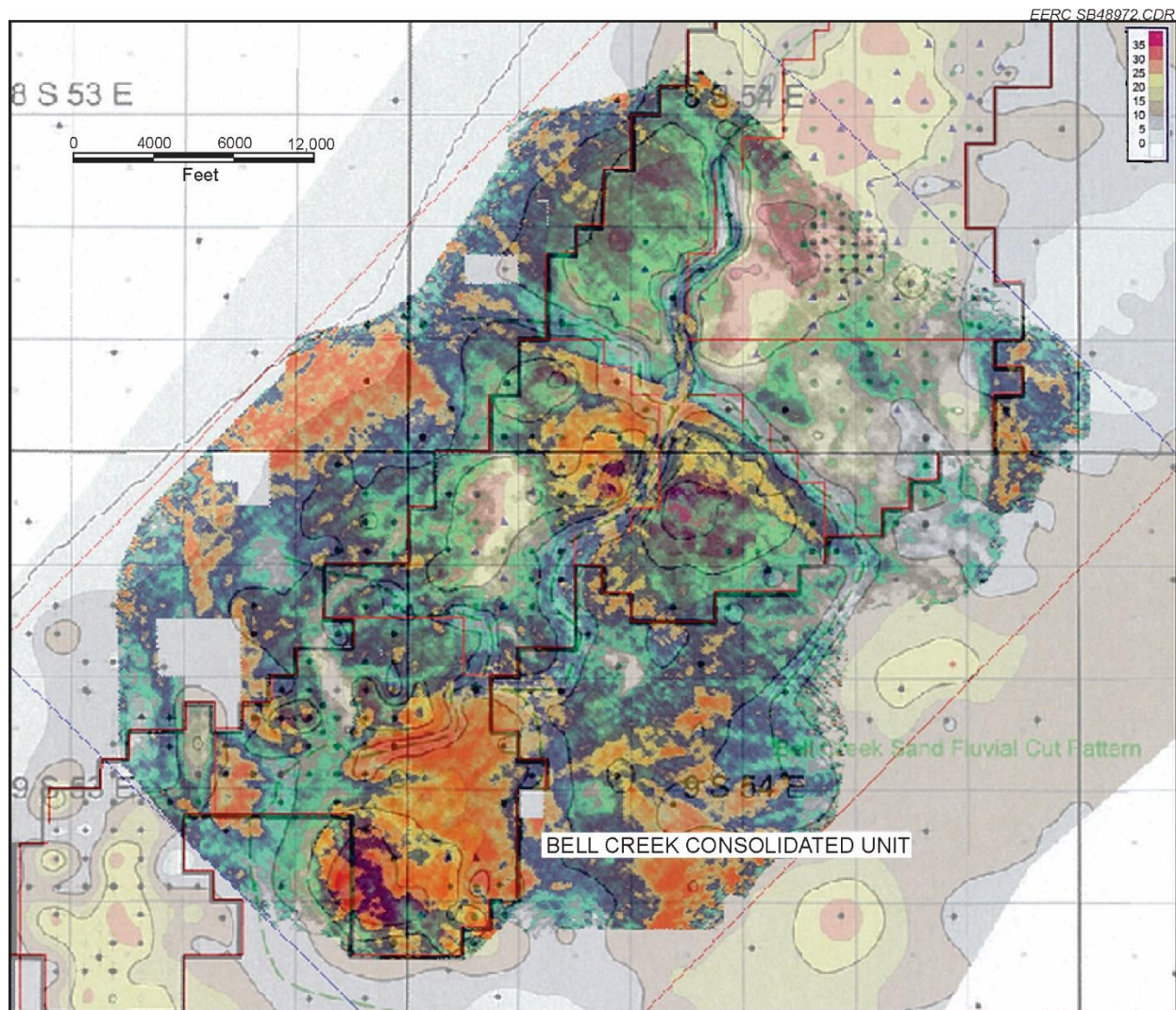


Figure 32. The seismic amplitude map overlaid on the sand isopach map. The physical features on both maps agree. Where sand was shown to be thickest, amplitude is generally the lowest.

### Analysis of a Channel Feature Visible on the Amplitude Map

Field development phase boundaries in many cases represent permeability barriers known to occur at the reservoir level. It is notable that some phase boundaries parallel amplitude contrasts on the seismic amplitude map. This is true of the higher amplitude feature along the boundary of the northern phases that has the appearance of a fluvial channel. A few wells have pierced this feature. A closer look at wells which have reveals that the clean Bell Creek sand has been eroded and replaced with some finer-grained material as indicated on the spontaneous potential (SP) or GR, but only partially so, leaving a gap in the section. This is illustrated in Figures 33–38. Figure 33 is a zoomed-in view of an area in the northern portion of the field along the phase boundary featuring the fluvial channel and shows the location of two cross sections: Line A-A' to the north and Line B-B' to the south.

Line A-A' follows a crossline through three wells: 21-16 in the channel and 28-02 and 22-12 on either side. Figure 34 is the seismic section with gamma ray and sonic p-wave velocity logs overlaying the data at the well locations. The background colors represent amplitude: darker colors indicate higher values; lighter colors are lower values with white representing zero. The wells on either side of the channel have well-developed sands and encompassing Springen-to-Skull Creek intervals visible on the sonics. Also notable is that they are in low-amplitude seismic areas.

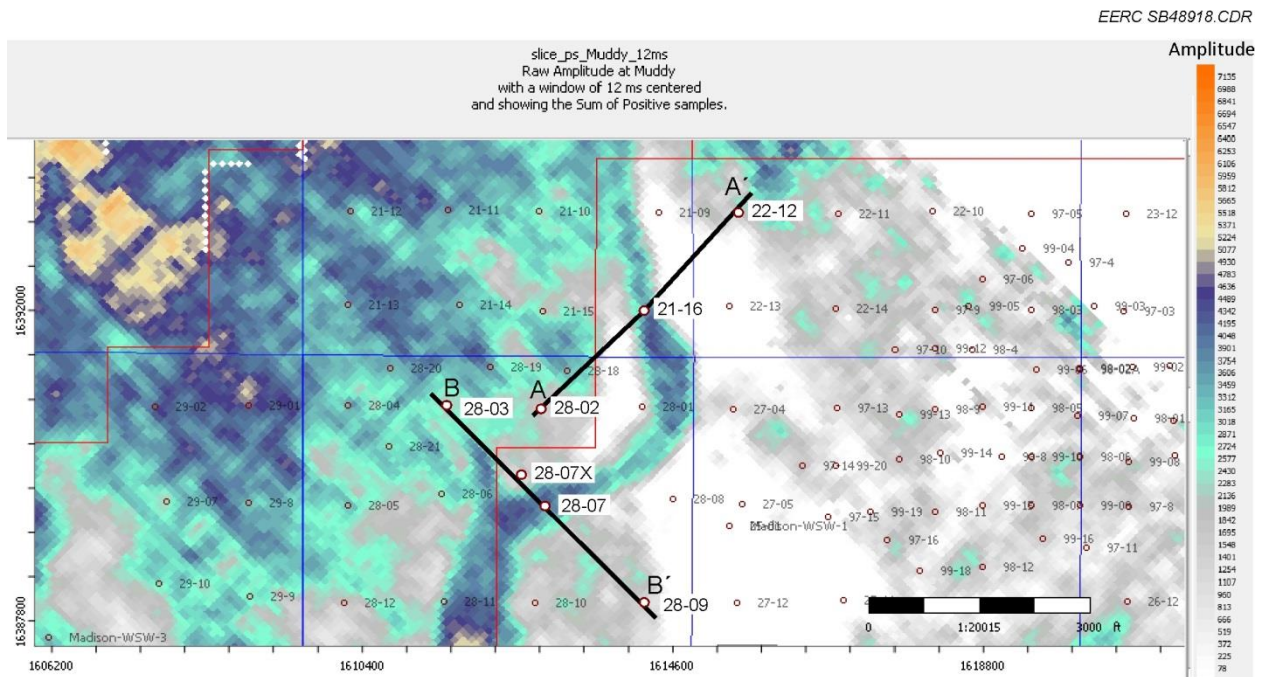


Figure 33. Zoom to the area of the fluvial channel. Location of two cross sections shown: Line A-A' to the north and Line B-B' to the south.



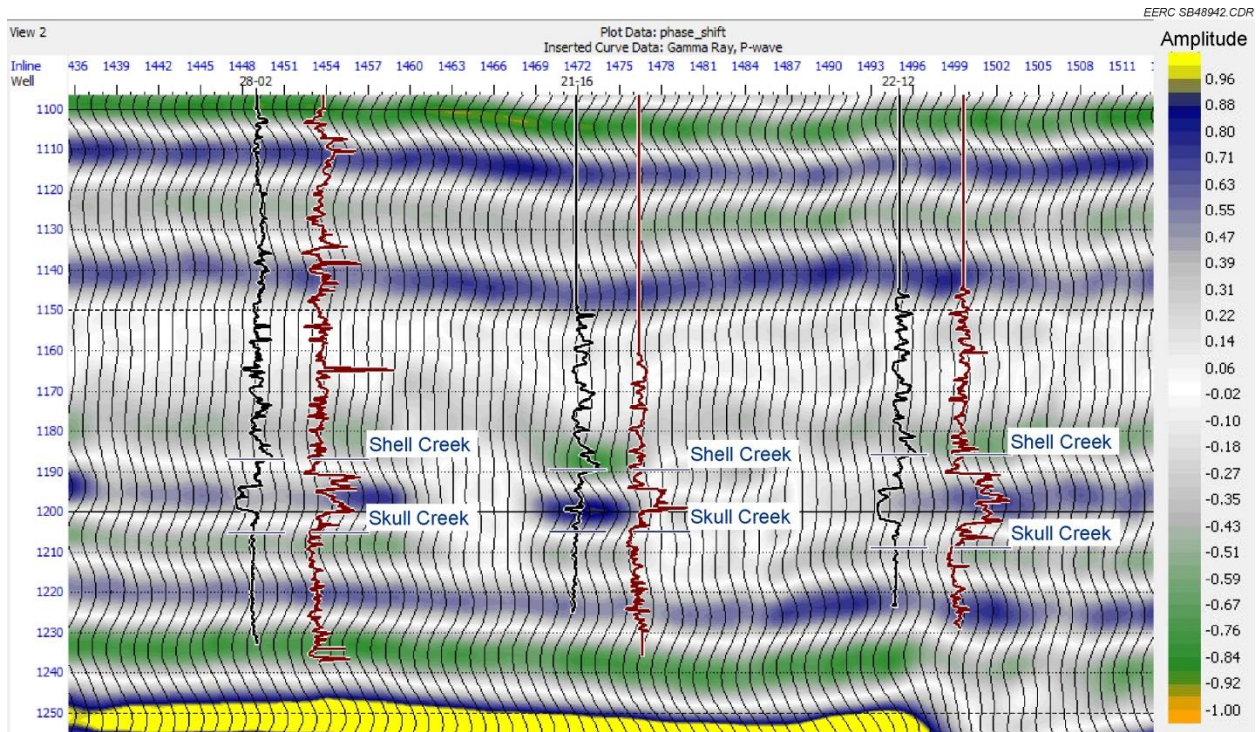


Figure 34. Seismic Section A-A' with gamma ray and sonic p-wave velocity logs overlaying. Background colors represent amplitude: darker colors are higher values; lighter colors are lower values; white is zero. Wells on either side of the channel have well-developed sands and are in low seismic amplitude areas. Channel Well 21-16 is in the higher-amplitude area of the channel geobody, as indicated by the darker blue background. Only a thin sand layer exists in this well at what correlates with the base of the Bell Creek sand.

The channel well, 21-16, is in the higher amplitude area of the channel geobody, as indicated by the darker blue background. The logs show a thin sand of 5 feet present. The character of the sand and its base correlates well with the base of the Bell Creek sand in adjacent wells, so it may be an erosional surface. Above it, the sonic log indicates a sand matrix with the lower velocities of a dirty sand for about 6 feet before appearance of the normal Springen Ranch to Shell Creek log character. Figure 35 provides a closer look at the well logs for 21-16, with the thin sand near the middle of the sequence. When compared with the adjacent wells, it appears that the Bell Creek sand has not just been eroded and replaced by reworked or different material, but a portion of the section below the Springen Ranch, up to 20 feet thick, is missing compared to Well 28-02. The Springen-to-Skull Creek interval is 51 feet thick and from the resolution discussion, this would suggest a lower-amplitude event, but the opposite is true. The high-amplitude response may be due to the predominance of fine-grained material within the interval combined with the absence of a clean sand interval at this location.



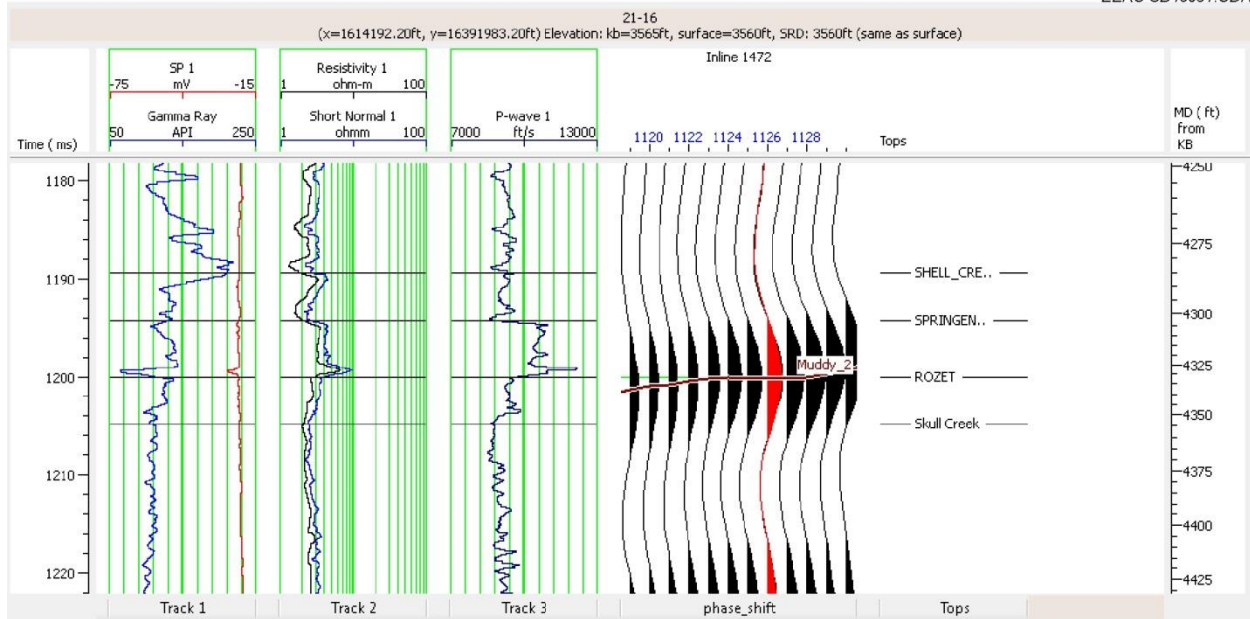


Figure 35. Well logs for Channel Well 21-16. A stringer of Bell Creek sand is near the middle of the sequence. Above it is a thin layer of finer-grained material 5 feet thick which rapidly transitions to a normal Springen Ranch–Shell Creek sequence. Up to 20 feet of section appears to be missing. The Springen-to-Skull Creek interval is 51 feet thick which would suggest a lower-amplitude event, but the opposite is true. The high-amplitude response may be due to the predominance of fine-grained material combined with the absence of a clean sand interval.

Well 22-12 (see Figure 36) is to the northeast of Well 21-16 and out of the channel. It has a Springen Ranch-to-Skull Creek interval 70 feet thick. This is near the thickness where tuning would occur, so it may be expected to exhibit a high seismic reflection amplitude if the interval lithology was homogeneous. However, the seismic reflection amplitude is low, possibly associated with the presence of a thick clean Bell Creek sand as shown on the well logs at this location.

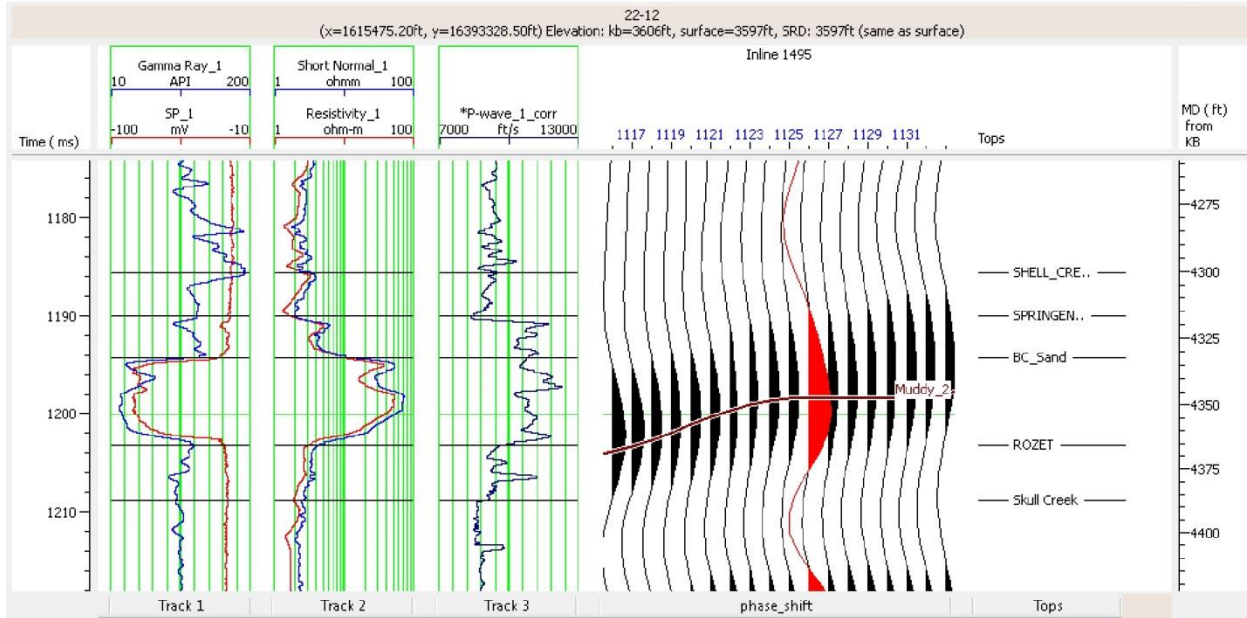


Figure 36. Well 22-12, north of the channel, has significant Bell Creek sand development and a thick impedance contrast section, but the reflection amplitude on the seismic data is low for this location, likely due to internal interference due to the presence of a thick clean sand interval.

Line B-B' follows an inline through three wells: 28-07 in the channel and 28-03 and 28-09 outside of the channel. Figure 37 shows the northwest to southeast section. Colors represent amplitudes as described above. SP logs are overlaid on the data to show, as before, that this confirming example shows the wells outside the channel have well-developed clean sands; the well in the channel has none. The relationship with amplitude holds for this section as well: a high-amplitude channel has no sand; low-amplitude flanks have well-developed sands. At Well 28-07, the well logs indicate the absence of a clean sand (Figure 38), as in Well 21-16. The section appears to immediately transition to a complete Springen Ranch–Shell Creek sequence, indicating a missing section up to 20 feet thick compared to the nearest offset well, 28-07X. The interval of high-impedance contrast as indicated by the sonic is 51 feet thick: thin, but still producing a high-amplitude reflection.

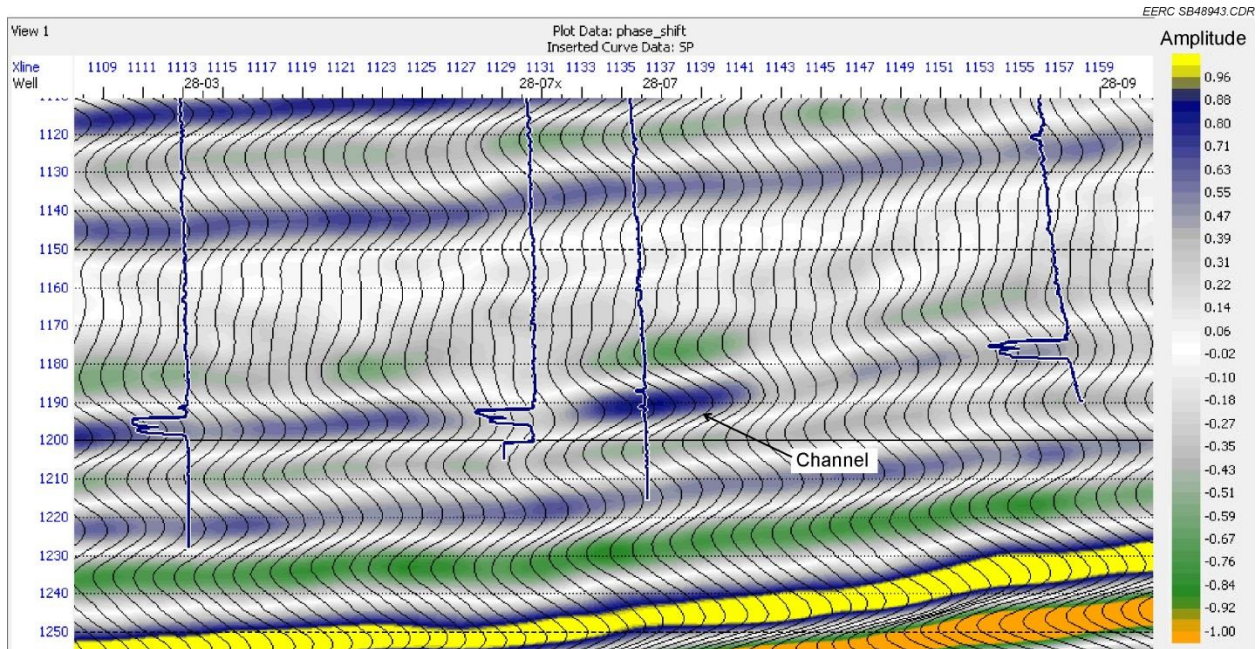


Figure 37. Northwest to southeast section. Confirming example. Colors represent amplitudes as described in Figure 34 above. SP logs are overlaid, well-developed clean sands on low-amplitude channel flanks are shown, and no sand is within the high-amplitude channel.

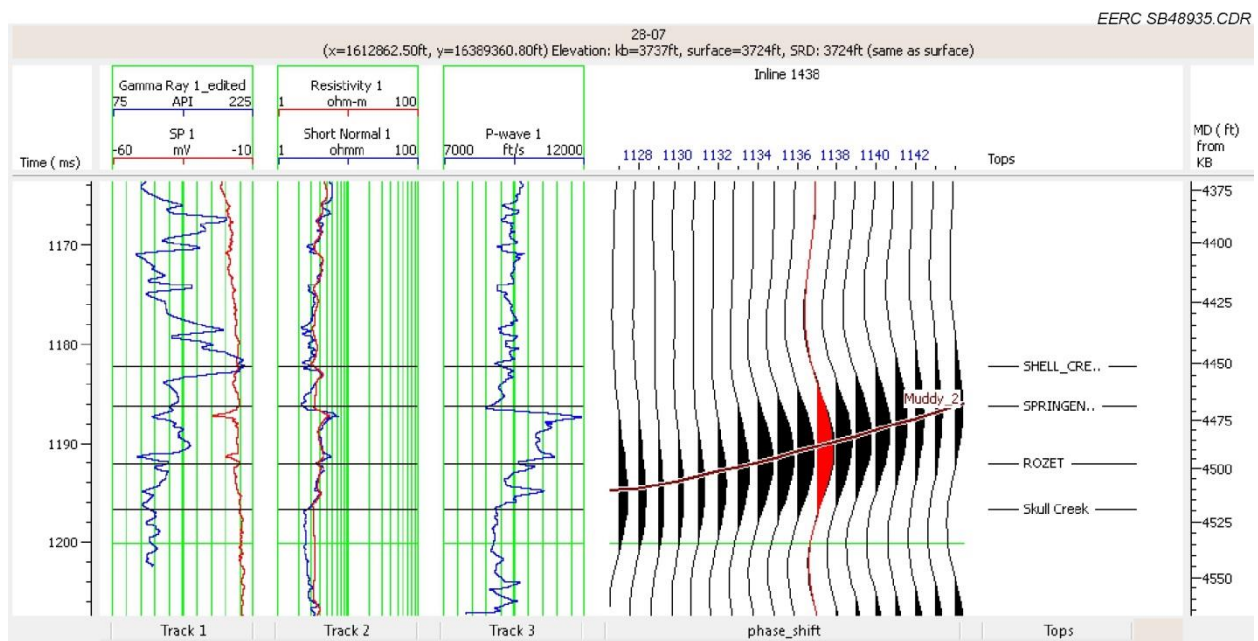


Figure 38. Well logs for 28-07 indicate the absence of clean sand as in 21-16. Both wells were drilled into an apparent channel. The Springen-to-Skull Creek interval is again 51 feet and produces a high-amplitude reflection.

The analysis of this feature suggests several key concepts:

1. That amplitude is more an indication of the geologic content of the interval and not its physical thickness. Tuning does not seem to be a factor. Instead, higher amplitudes may indicate thin or missing Bell Creek sand.
2. The Springen Ranch or Coastal Plain interval incorporates finer-grained material with the silica matrix that the sonic log indicates being a major component of the impedance contrast interval. Drillers' logs show this material to be very hard to drill through in contrast to the softer, clean Bell Creek sand. That hardness may contribute to a higher-amplitude reflection.
3. Wells with thick, clean, Bell Creek sands seem to correspond to low-reflection-amplitude areas, even when they have a Coastal Plain–Springen Ranch layer above. Reflection effects at the sand boundaries (like those shown in Figure 25) may introduce destructive interference within the composite reflection from the high-impedance zone, resulting in low amplitude.

In short, a critical factor for amplitude seems to be the presence of thick, clean sands—or lack of them.

A tentative confirmation of this conclusion may be found in Table 2. It shows a rough comparison of nine wells from high-amplitude areas with nine wells in low-amplitude areas. Wells were chosen arbitrarily based on their reflection amplitude on the amplitude map. The average sonic transit time is an estimated value over the high-impedance interval. The wells in high-amplitude areas tend to be siltier, have thinner clean sands, and have a thinner high-impedance zone averaging 55 feet. Wells in low-amplitude areas tend to have thicker clean sands and an impedance zone averaging 64 feet. The two-way transit times are below the level of tuning and at or below the apparent level of resolution for all samples. These results are general but suggest a confirmation that the presence of siltiness contributes to a higher amplitude and that thicker, cleaner sands contribute to lower-amplitude reflections. A closer look at this effect with a more sophisticated modeling approach may provide additional insight.

**Table 2. Analysis of High-Amplitude vs. Low-Amplitude Seismic Response at Wells**

Well	API	Muddy Seismic Response	Impedance Zone Thickness, ft	Sonic avg., μs/ft	Vel., ft/s	2-Way Transit Time, ms	Bell Creek Sand Characteristics from Logs
3312	21427	hi-amp	50	90	11,111	9.0	thin 15' sand
3208	21269	hi-amp	52	93	10,811	9.6	10' clean, else dirty sand
3215	21272	hi-amp	58	90	11,111	10.4	Two 10' lobes, some shaliness
503	21363	hi-amp	62	90	11,111	11.2	30' gross, dirty, hard streak in middle lobe
1806	21578	hi-amp	46	92	10,870	8.5	25' of dirty sand
1812	21316	hi-amp	50	90	11,111	9.0	30' very dirty sand; no sonic log, sonic velocity estimated
1907	21653	hi-amp	55	90	11,111	9.9	10' clean lobe, otherwise dirty; no sonic log, sonic velocity estimated
804	21417	hi-amp	56	95	10,526	10.6	19' 3-lobe sand, less clean, and 2' hard streak within the Muddy
304	21783	hi-amp	65	95	10,526	12.4	23' 2-lobe sand fining up, no sonic log, sonic velocity estimated
			55	92	10,921	10.1	Mean Values
2712	21013	lo-amp	56	95	10,526	10.6	28' clean sand
2713	21005	lo-amp	66	95	10,526	12.5	25' clean sand
3301	21003	lo-amp	62	95	10,526	11.8	28' clean sand
5609	21449	lo-amp	68	95	10,526	12.9	20' clean sand, 3' bentonite/coal on top
3514	21414	lo-amp	62	105	9,524	13.0	20' clean sand
3116R	22432	lo-amp	68	94	10,638	12.8	22' clean sand, 10' bentonite/coal on top
5702	21404	lo-amp	65	95	10,526	12.4	25' clean sand
816	22000	lo-amp	60	95	10,526	11.4	23' clean sand with shale break
313	21703	lo-amp	67	95	10,526	12.7	23' clean sand with shale break, no sonic log, sonic velocity estimated
			64	96	10,427	12.2	Mean Values

**Comments:**

Sands in high-amplitude areas are thinner, have a higher fine-grained component.

Sands in low-amplitude areas are thicker and cleaner.

Impedance zones for all wells shown are thinner than the tuning thickness, especially the higher-amplitude sands. Tuning effects do not appear to be relevant.

Inspection of gathers for high-amplitude areas exhibit constructive addition across offsets.

Inspection of gathers for low-amplitude areas (areas with thick sands) exhibit destructive addition across offsets.



## Analysis of Permeability Barrier Between Phases 1 and 2

The Phase 1–Phase 2 boundary is known to have a permeability barrier. Cross Section C-C' follows a seismic crossline obliquely across the Phase 1–Phase 2 boundary (Figure 39). Well 33-14X falls within the permeability barrier. Wells 33-14 to the northeast is near the edge of the barrier, and 04-04 to the southwest is outside of the barrier. The seismic amplitude map expression of the barrier is indistinct, but the location falls along a line that could be an extension to the south of the fluvial channel feature in the north. If so, a character similar to that of other wells in the fluvial channel may be expected on the logs.

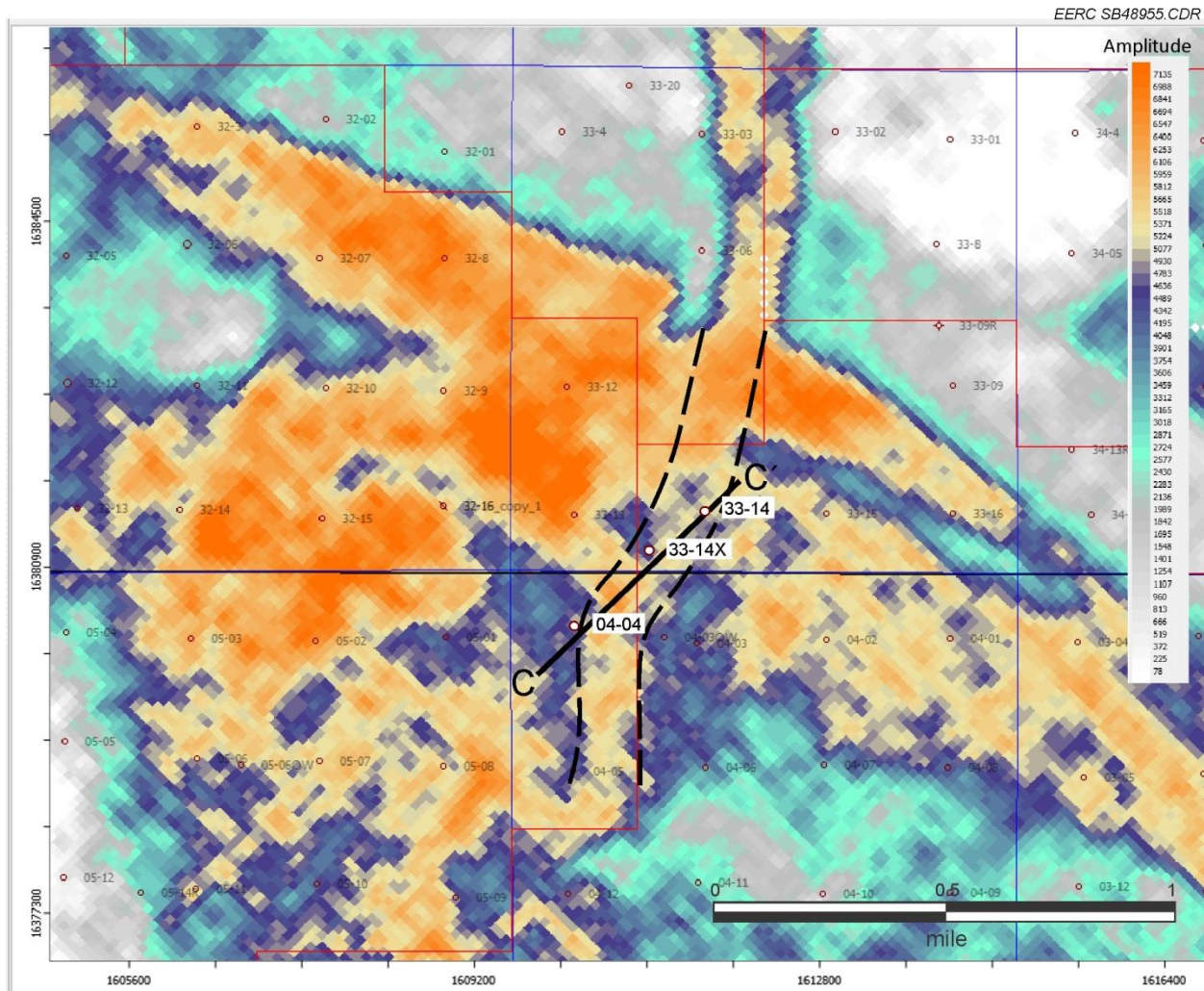


Figure 39. Location map of Cross-Section Line C-C' across the permeability barrier between field Phases 1 and 2. The seismic expression of the geobody is indistinct but may be an extension of the fluvial body to the north. Well 33-14X is directly in the barrier; 33-14 is on the eastern edge; 04-04 is not in the barrier.

The Cross-Section C-C' (Figure 40) shows that Well 04-04 has a fully formed two-lobe Bell Creek sand. Well 33-14 on the other side appears to exhibit an erosional truncation of the sand which suggests the well lies partially within the barrier. 33-14X is fully within the barrier and appears to have no clean sand at all. The sonic log shown for 33-14X is a transform computed from the resistivity log. As no sand was encountered during drilling, a sonic or density was not run. A pseudo-sonic log derived from the resistivity was used to generate a synthetic seismogram to tie the well to the seismic section. The two wells within the permeability barrier have high-amplitude reservoir reflections. The amplitude near Well 04-04 is less so, but still relatively high. As previously discussed, high amplitudes may be related to siltier material or a thinner Bell Creek sand. A closer look at Well 04-04 reveals that, at 14 feet, its bottom lobe is about 10 feet thinner than the thickest sands around the channel to the north, and the sonic log indicates some hard material in the upper lobe.

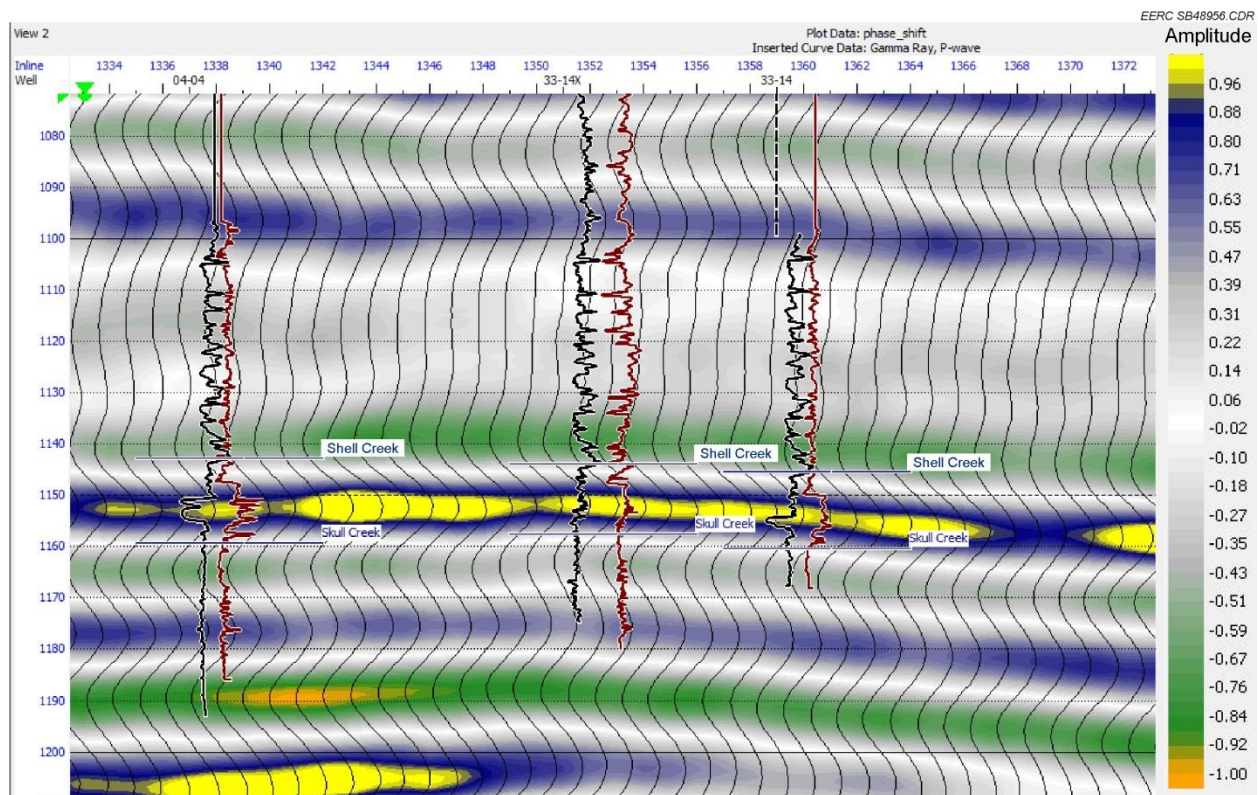


Figure 40. Crossline display showing the Cross-Section C-C' across the Phase 1–Phase 2 permeability barrier. Logs displayed are gamma ray in black, sonic p-wave velocity in red. Background colors on seismic indicate amplitude, with yellow having the highest amplitude and white the lowest. Well 04-04 exhibits a two-lobe sand with a relatively high-amplitude character. 33-14X has no visible sand; silty material exists where sand would be expected. 33-14 has Bell Creek sand with an erosional truncation. There is no distinct seismic expression of a geobody on the section. Note: P-wave for 33-14X is a transform of the resistivity log.



For clarity, the barrier well, 33-14X, is shown in Figure 41. The Springen Ranch and Skull Creek interval is 53 feet at this location, and the tops can be picked from the resistivity log. Events within the interval are difficult to determine. The interval is filled entirely with fine-grained material which may contribute to the high-amplitude reflection.

At Well 33-14, the Springen Ranch-to-Skull Creek interval is 55 feet thick (Figure 42). An erosional surface on the Bell Creek sand is evident on the well logs. The section, with a short pause amounting to 2 or 3 feet of material, transitions into Springen Ranch, suggesting a missing section similar to the wells in the fluvial channel feature to the north. The sand, at 11 feet, is not thick enough to dampen the high amplitude of the reflection.

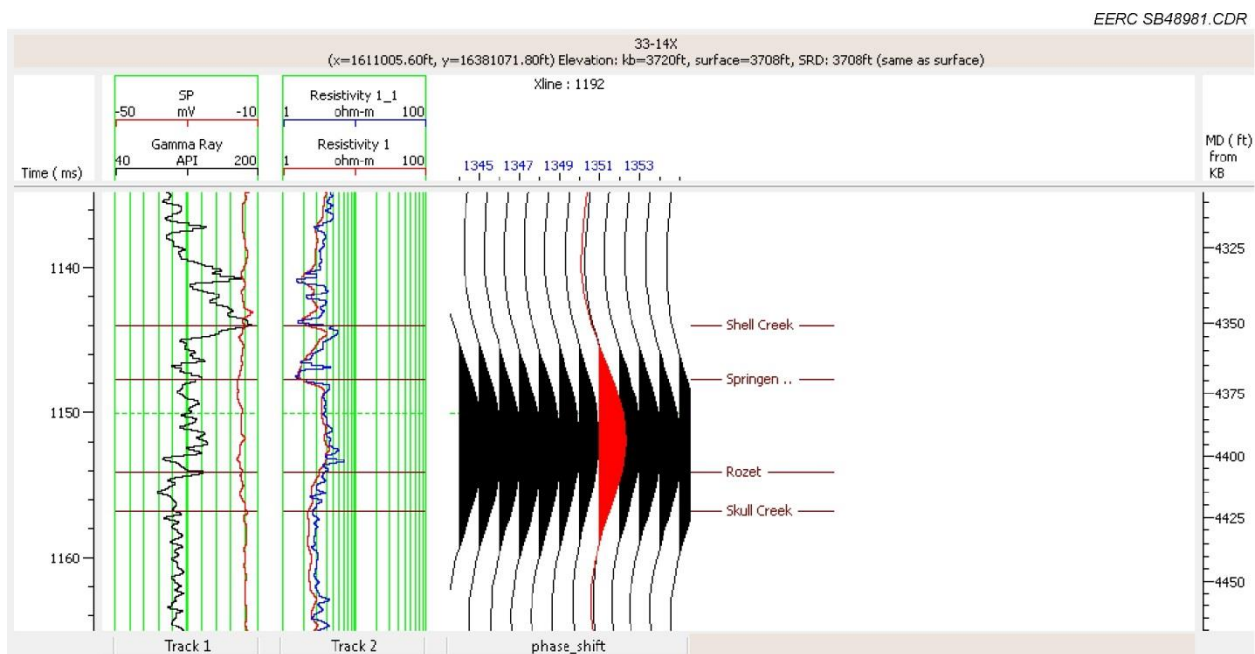


Figure 41. Well within the barrier, 33-14X. The Springen Ranch-to-Skull Creek interval is 53 feet. Tops were picked from the resistivity log character. Events within the interval are ambiguous. The interval is filled with fine-grained material which may contribute to the high-amplitude reflection.

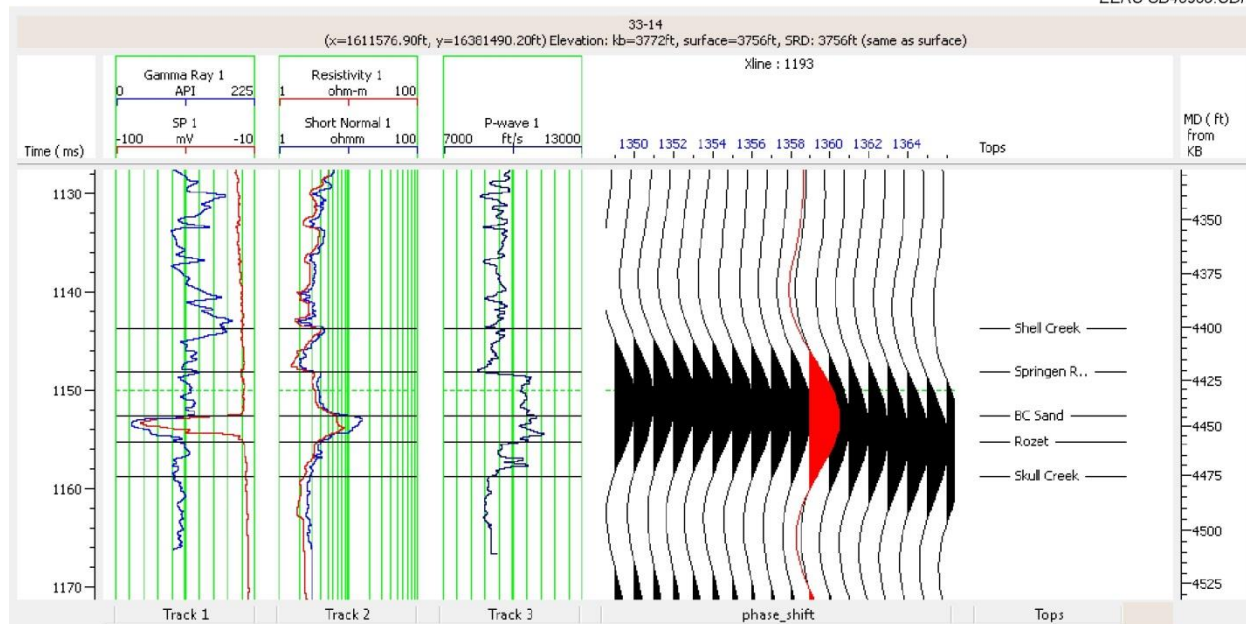


Figure 42. Well 33-14 near the edge of the permeability barrier. An erosional truncation of the Bell Creek sand is evident. Two or three feet of fill material above it immediately transitions into Springen Ranch, suggesting a missing section similar to the wells in the fluvial channel feature to the north. The sand, at 11 feet, is not thick enough to dampen the high amplitude of the reflection from this location.

## Analysis of Incised Valleys – Northern Valley

Weimer and others (1988) provide a depositional history of the Bell Creek area. They posit that after deposition of the Bell Creek sand, the area was subaerially exposed by a major drop in sea level. A drainage system of incised erosional valleys developed (Figure 43), in places eroding through the Bell Creek sandstone. As the area around Bell Creek was topographically high because of uplift along basement faults, there was a drainage divide, with drainage off the field area initially to the southeast before turning south and southwest. As sea level subsequently rose, the incised valleys were filled with sediments: initially freshwater fluvial deposits and then lower-energy brackish to marine estuarine and tidal flat deposits. Coals and bentonites associated with this type of depositional environment are sometimes seen at the erosional surface on the well logs of wells which have penetrated the incised valleys.

When the rough schematic in Figure 43 is overlaid on the Bell Creek Field and the seismic amplitude map, two incised valleys appear to traverse the field corresponding to two distinct and generally low amplitude features (Figure 44). The incised valley that appears to cross the northern part of the field corresponds very well to a northwest–southeast-trending field phase boundary known to be a permeability barrier. The southern feature has a dendritic character and looks like a drainage system.

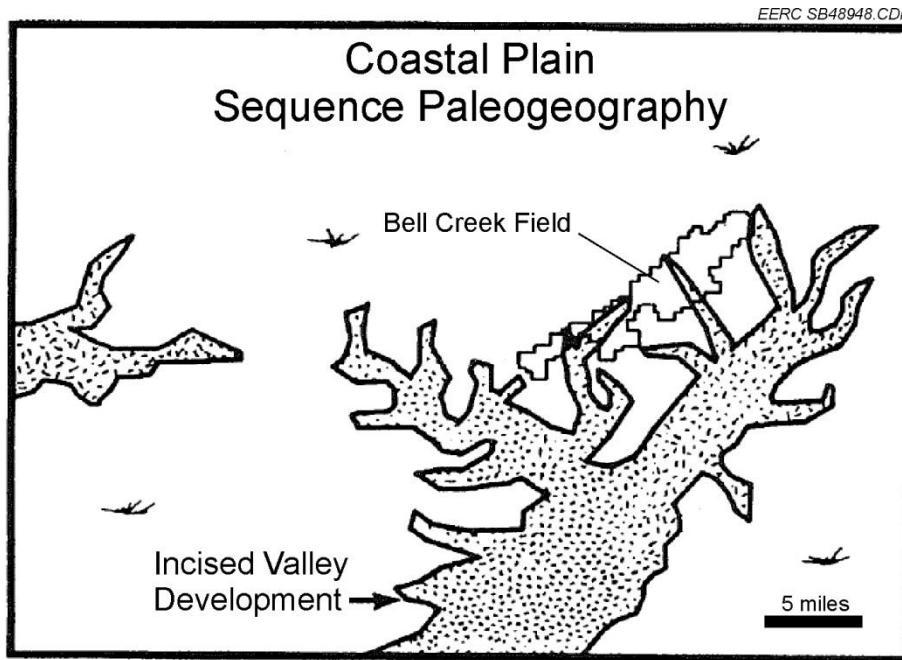


Figure 43. Schematic modified from Molnar (1990) indicating location of drainage system and incised valley development at the Bell Creek Field area following a major drop in sea level not long after deposition of the Bell Creek sand. A rough location of incised valleys within the field is indicated.



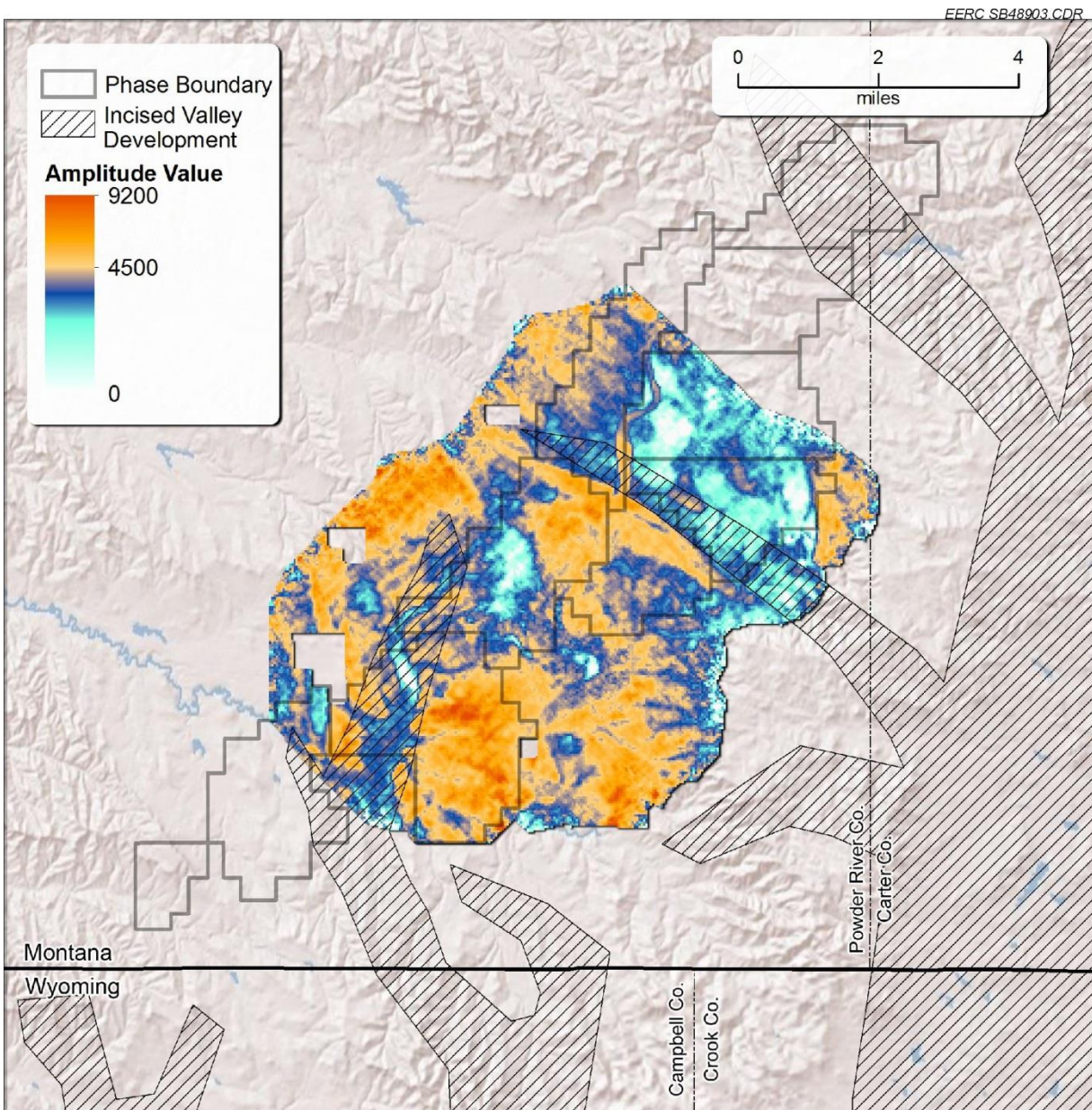


Figure 44. Overlay of the incised valley features indicated on Figure 43 after georeferencing. Implied valleys correspond nicely with two low-amplitude features on the Muddy Formation seismic amplitude map.





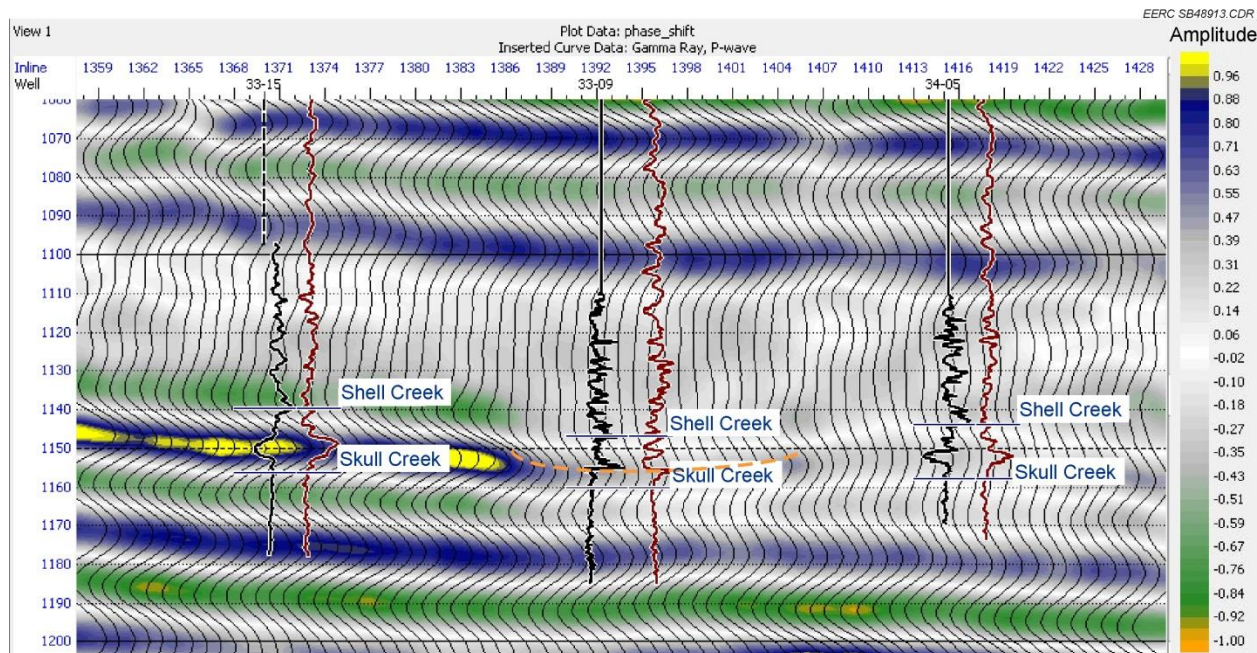


Figure 46. Cross-Section D-D' from southwest to northeast across northern incised valley. Well 33-09 exhibits a truncated sand because of erosion. The high-amplitude event to the southwest of 33-09 probably coincides with the valley boundary. Boundary to the northeast is not as clear but may be indicated by amplitude near inline 1404 and structure implied by a topographic radius of curvature centered about the 33-09's GR trace.

A closer view of 33-09 is in Figure 47. Above the erosional surface of the Bell Creek sand, the GR is reading very high and the density low, which likely indicate a coal bed or mix of coal up to 12 feet thick. This has been labeled as valley fill. The character of the Springen Ranch and Shell Creek are visible on the resistivity log and GR above the valley fill material.

Evidence of the erosional valley presence extends all the way to the western edge of the field. Well 32-01 near the western edge of the field and within the incised valley is shown in Figure 48 and exhibits similar character to Well 33-09. There appears to be thin beds of coal on the bottom and the top of the valley fill material. Well 32-01 has a sonic log, and it is clear from the sonic character that the acoustic impedance suffers a significant reversal within the Springen Ranch-to-Skull Creek sequence that generates the reservoir reflection. It is likely that this sharp reversal introduces destructive interference effects in the composite reflection from this event which results in its low-amplitude character. This obviously complicates the interpreter's task of discriminating between areas impacted by erosion with subsequent coal deposition from areas of thick, clean sand deposition, as their general amplitude character is similar.



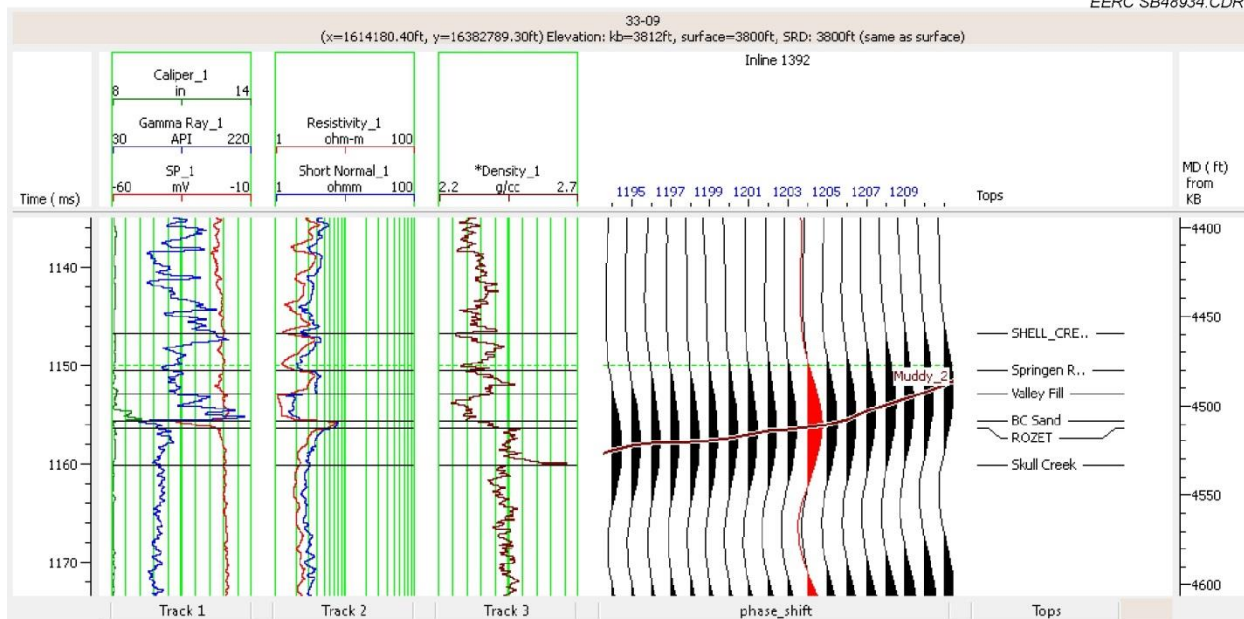


Figure 47. Closer look at Well 33-09 located in incised valley. Erosional surface on top of truncated Bell Creek sand is clear on well logs. Highly radioactive, low-density material on the erosional surface is likely a coal and up to 12 feet thick.

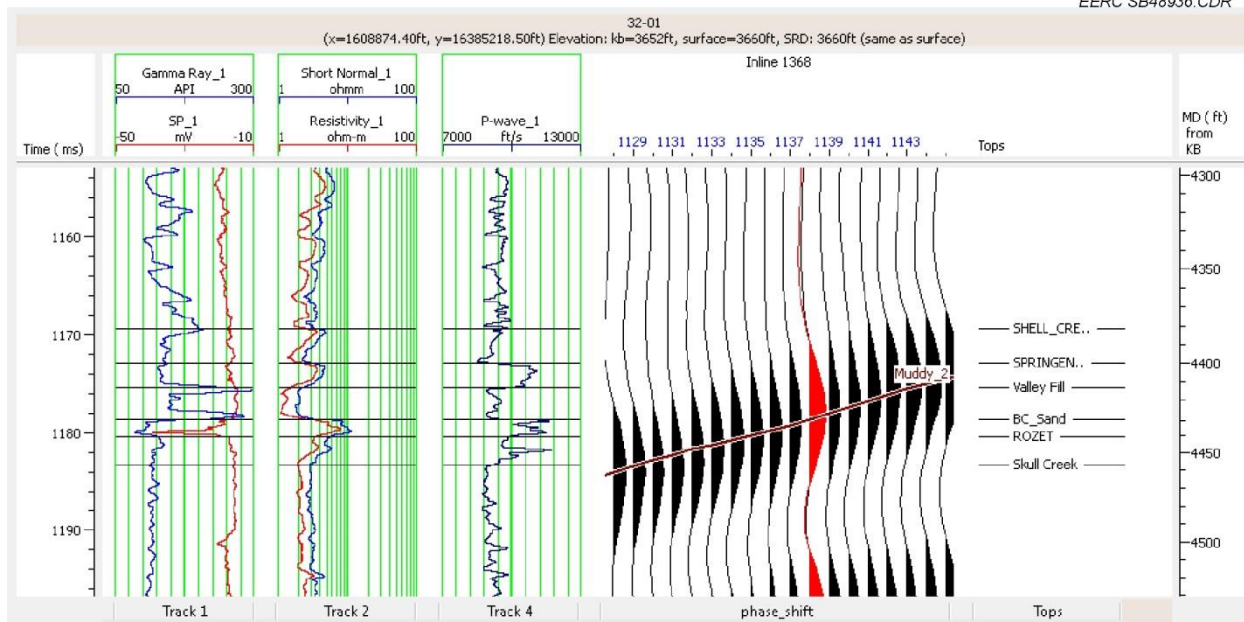


Figure 48. Well 32-01 is located in a northern incised valley toward the west end of the field. Erosional surface on top of truncated Bell Creek sand is clear on well logs. Highly radioactive, low-density material on the erosional surface is likely a thin coal, with another one at the top of the valley fill material. Valley fill is topped by normal Springen Ranch and Shell Creek Formations.

## Analysis of Incised Valleys – Southern Valley

The southern incised valley has a dendritic character and looks like a drainage system. The Cross-Section E-E' in Figure 49 falls along an inline and exhibits five wells. To remove the regional dip which would hide the topographic relationship, this section has been flattened on the Muddy reflection. The wells were tied to the flattened horizon. A consequence is that the Springen Ranch top lines up horizontally as if the wells were hung on that horizon. Well 63-06 is in the center of the valley at a topographic low and exhibits a coal bed response 6 feet thick, as evidenced by the high GR response together with a low sonic reading. Wells on either side appear topographically higher and exhibit thinner coal responses. The wells on either edge exhibit little to no coal response.

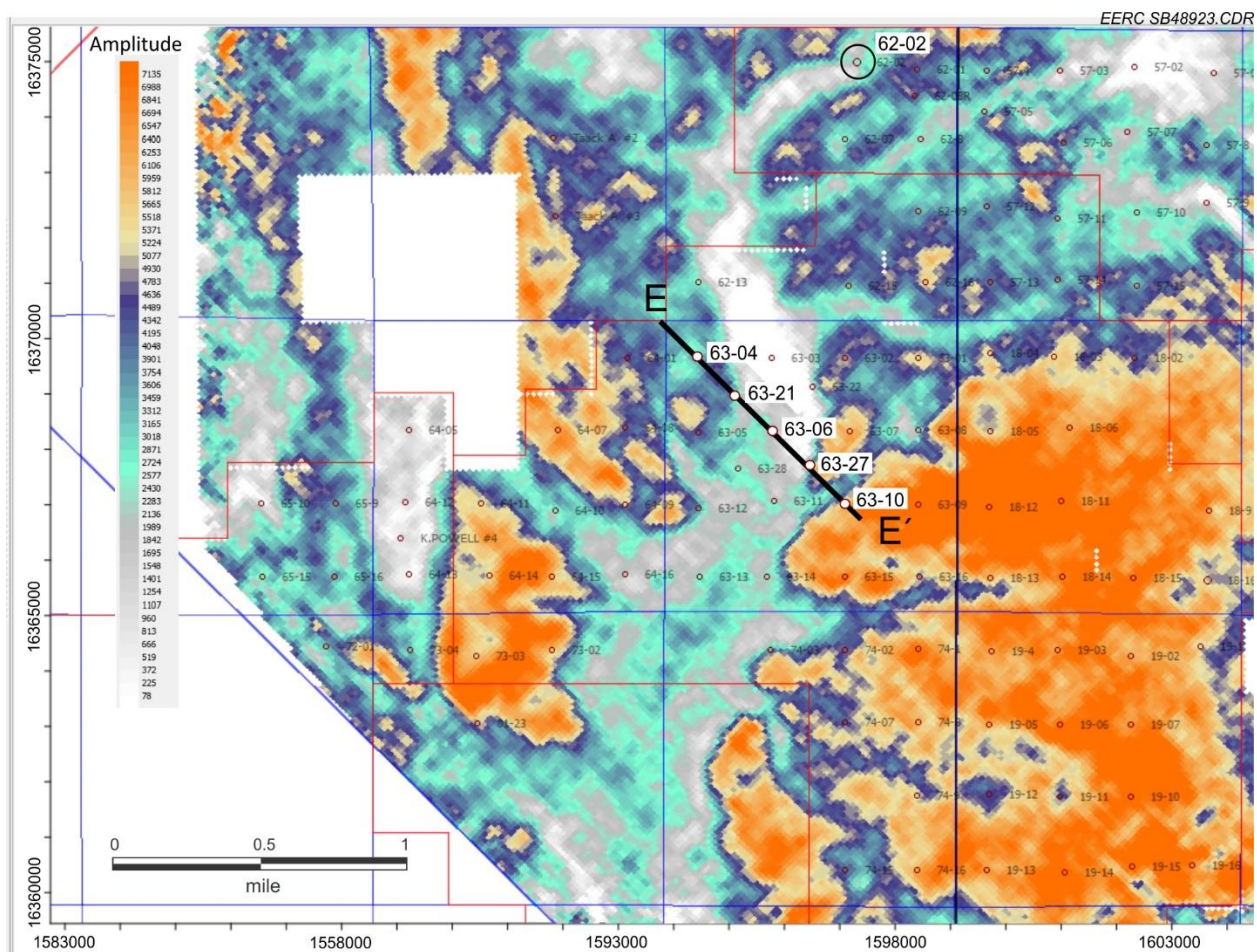


Figure 49. Close-up view of southern incised valley low-amplitude expression with dendritic character. Line E-E' indicates the seismic cross-section location for Figure 50.



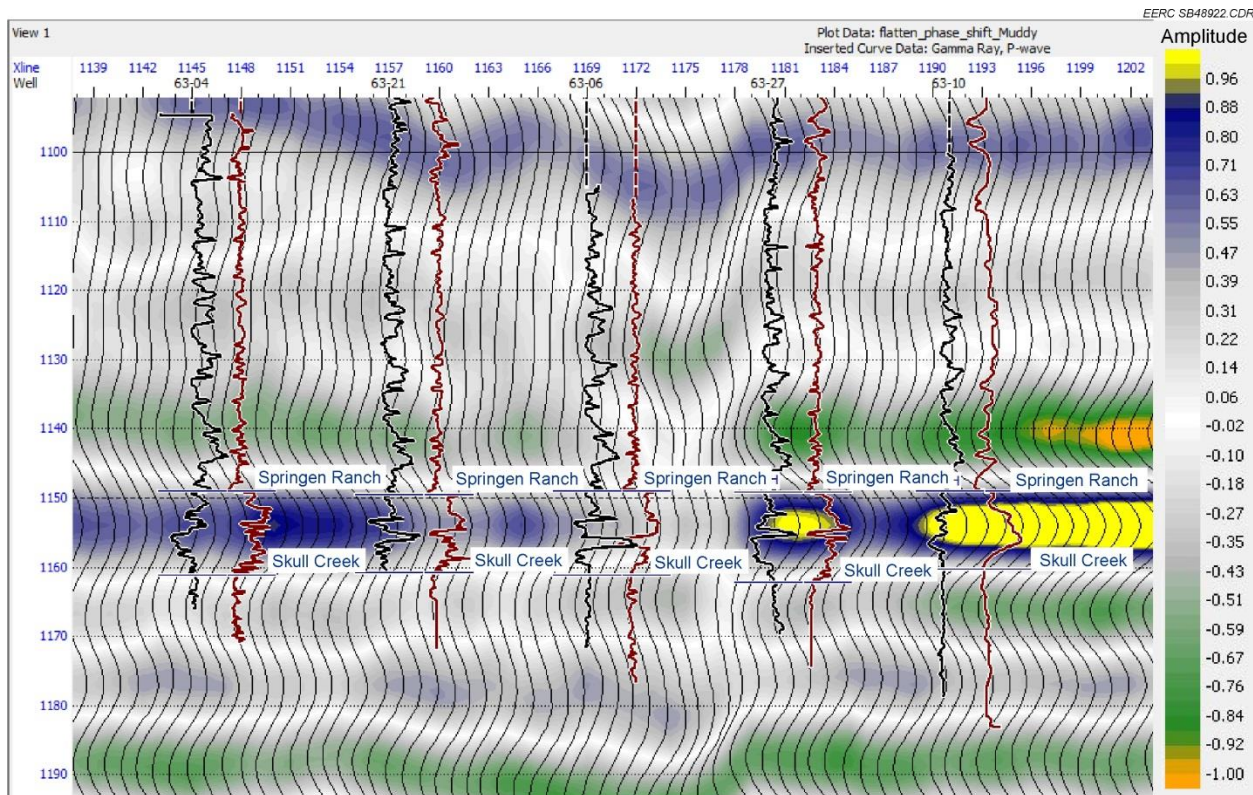


Figure 50. Inline Seismic Section E-E' across southern incised valley. Seismic data have been flattened on the Muddy horizon to remove regional dip. Gamma ray and sonic p-wave well logs are, in effect, hung on the Springen Ranch. A coal bed response that reaches 6 feet thick in the center of the valley and at the topographic low is visible in 63-06 and neighboring wells and is absent or nearly gone on bounding wells. Center of the valley also has low amplitude as with the valley to the north. The sonic curve on well 63-10 is a transform computed from the short normal log as no sonic was run on that well.

The log character of the erosional surface and the apparent 6-foot coal bed is clear in Well 63-06 and corresponds with the erosional valley character to the north (Figure 51). It is clear from the sonic character that the acoustic impedance suffers a significant reversal within the Springen Ranch-to-Skull Creek sequence. As with the north valley, it is likely that this sharp reversal introduces destructive interference effects in the composite reflection from this event which results in its low-amplitude character.

Farther up the dendritic channel is Well 62-02. The erosional surface on the Bell Creek sand and the coal deposition character is preserved there as well and visible on the GR log, although it is thinner than in Well 63-06 (Figure 52). The sonic log does not indicate a drop in interval velocity as drastic as that in 63-06, but there is a drop in velocity and choppy character within the sequence which may contribute to the low-seismic-amplitude character at this location.

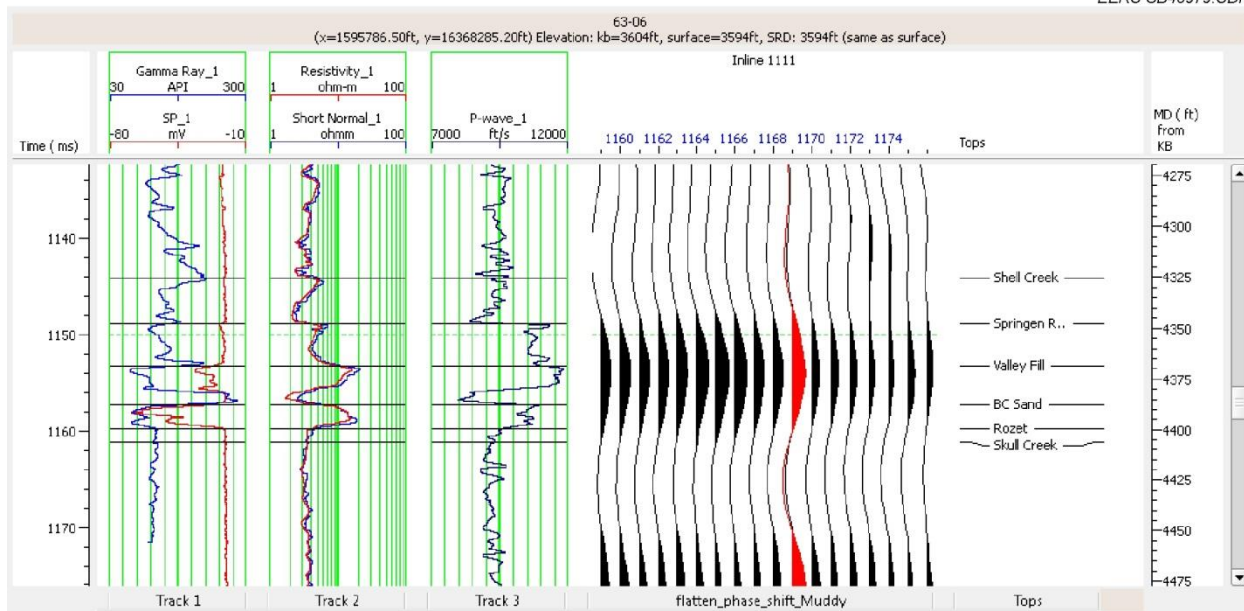


Figure 51. Well 63-06 in the center of the incised valley exhibits a 6-foot coalbed response above the Bell Creek sand erosional surface. The apparent coal and additional material covering it are labeled valley fill, which is then topped by the normal Springen Ranch and Shell Creek units.

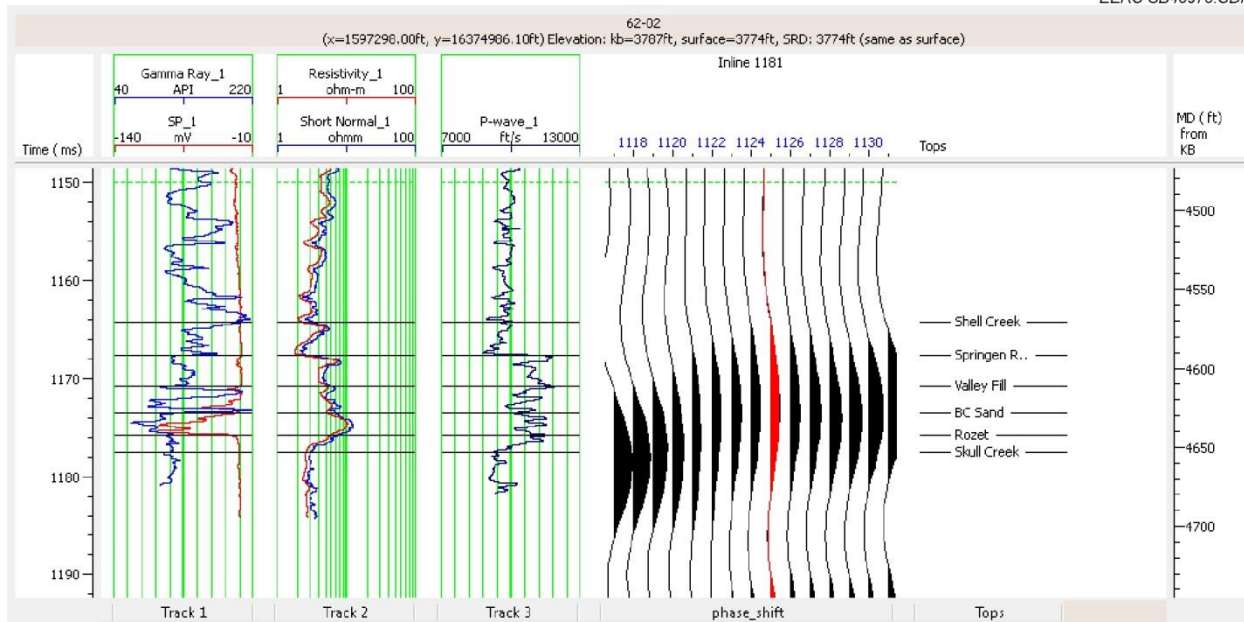


Figure 52. Well 62-02 located north of Well 63-06 farther up the incised valley. The erosional surface on the Bell Creek sand and the coal deposition character are preserved but are thinner than in Well 63-06, and the sonic interval velocity drop is less drastic.



## Updip Field Boundary

Of interest is whether the field boundary to the southeast, which manifests as an updip permeability barrier, is visible on the seismic. This topic has not been fully investigated, but initial indications are that it does not appear to be discernible. One inline section at the field margin near the middle of the field is shown as an example (Figure 53).

As above, the Muddy horizon is displayed as a peak. The dark red line tracks the Muddy horizon and runs across the display. Two wells are shown, 09-02 and 42-09, with GR and sonic p-wave curves overlaying the seismic. The geographic boundary of the field is halfway between the wells at Crossline 1271. The Bell Creek sand does exist in 42-09 but has thinned relative to that in 09-02. The thinning is not discernible on the seismic section between the wells, nor is there any significant indication of change to the right of 42-09 as the picked horizon continues updip. Similar ambiguous character exists on other inlines at the field edge.

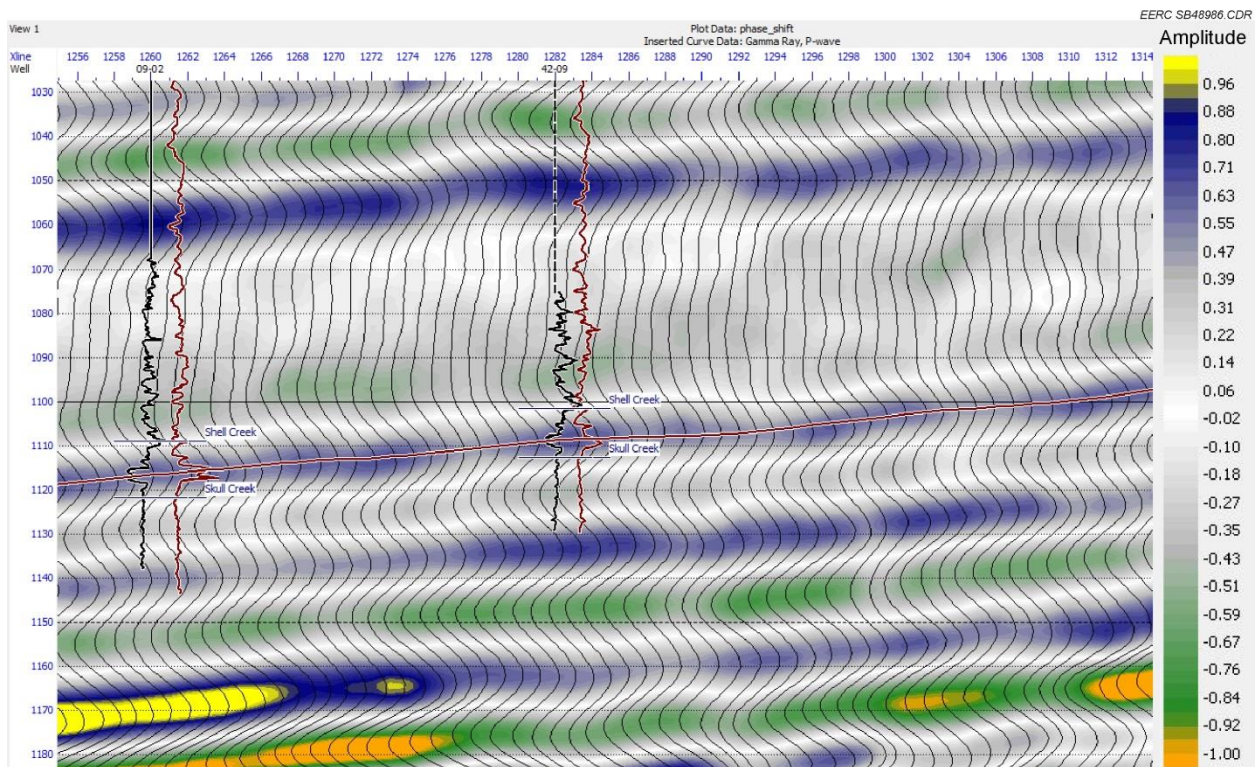


Figure 53. The updip field boundary occurs between Wells 09-02 and 42-09 as the Bell Creek sand thins, but there are no unambiguous changes in the seismic amplitude response such that the field edge could be picked based on the seismic data.

## ELEMENTS OF STRUCTURAL INTERPRETATION

### Polygonal Fault Systems

A polygonal fault system appears over a thickness of around 420 feet (127 m) in the Belle Fourche Formation, above the Muddy and Mowry Formations (Figure 54). The throw of these faults is about 27 feet (8 m) (Figure 55), but the faults appear to terminate in the Mowry Formation and do not extend into the Bell Creek sands.

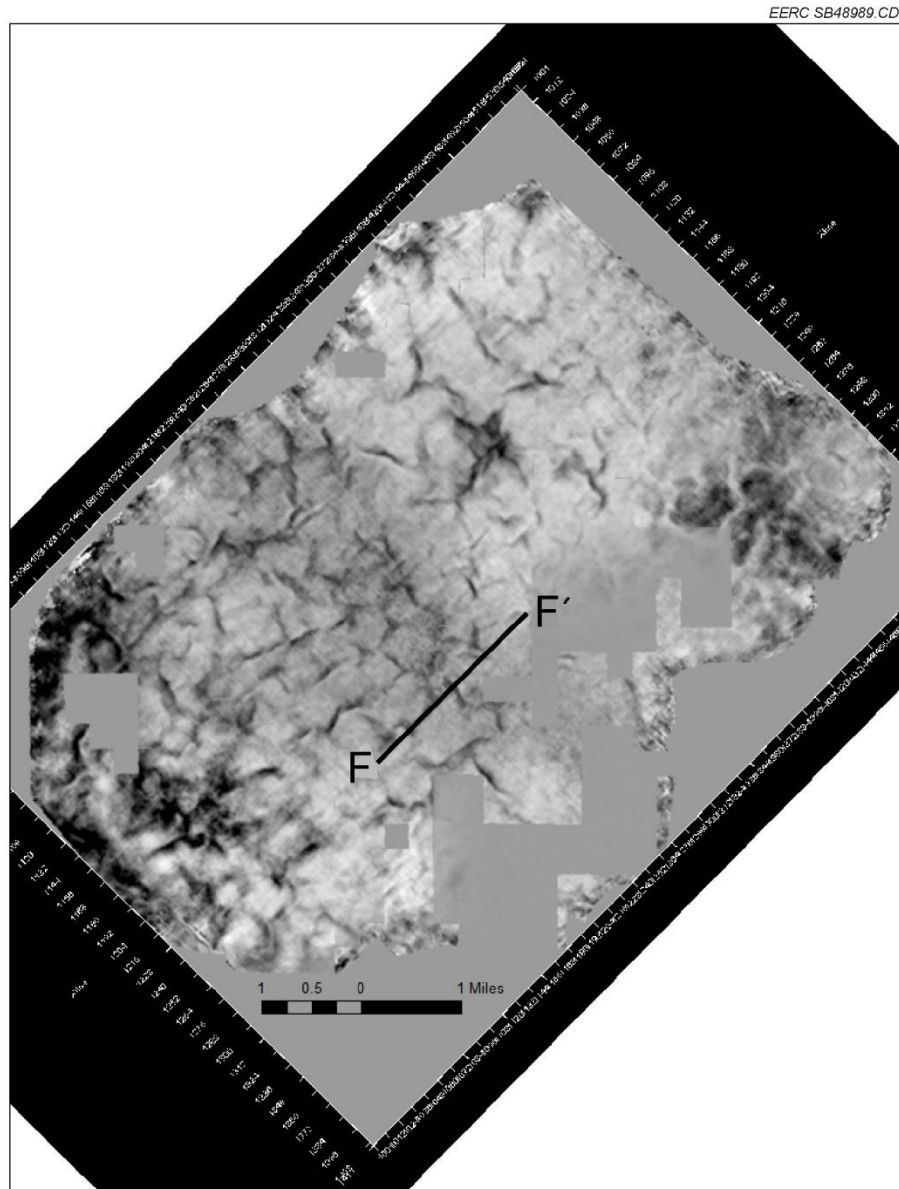


Figure 54. Seismic survey slice through the Belle Fourche Formation in the Bell Creek Field at 1048 msec or approximately 4285' depth. Data volume flattened on Horizon 1 to remove regional dip. F-F' marks cross-section location seen in Figure 55.



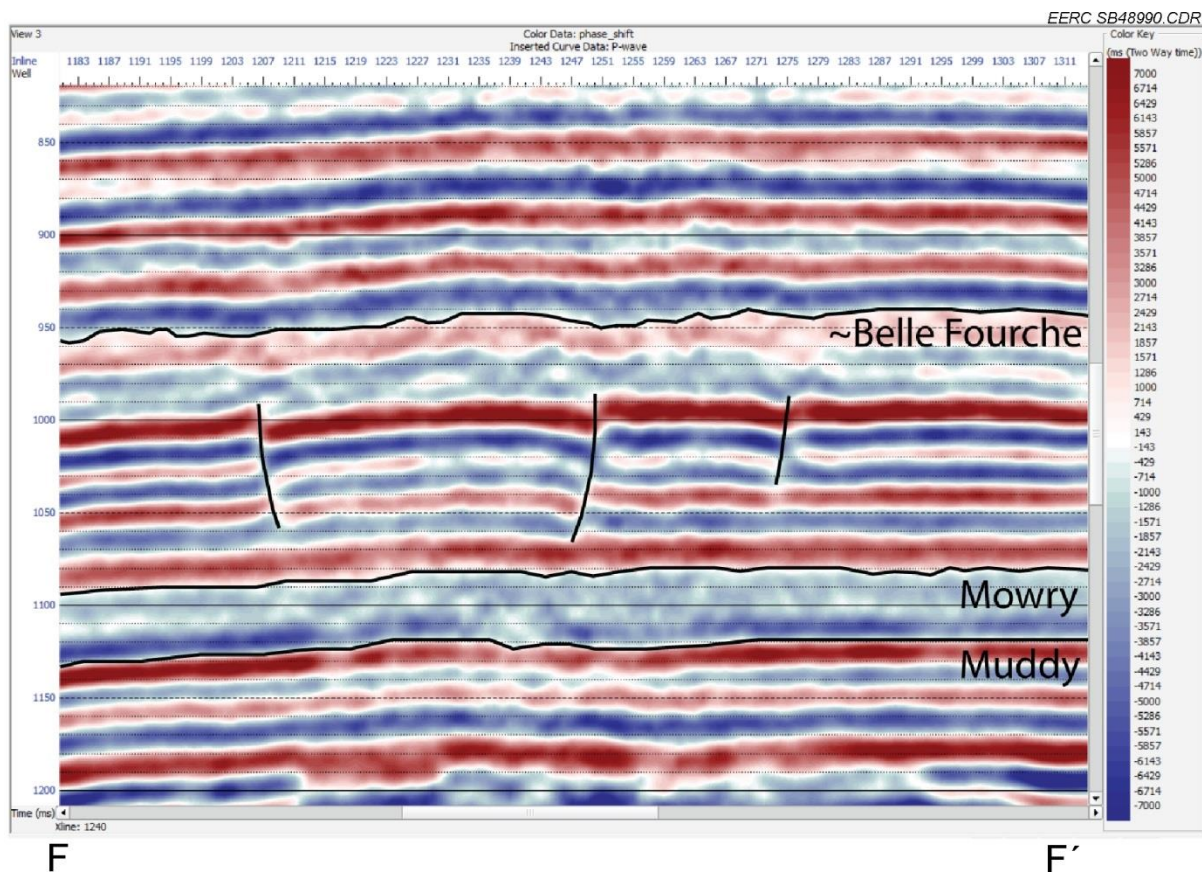


Figure 55. Cross-Section F-F' of PFS in the Belle Fourche Formation at Bell Creek. Faults are normal with ~27 feet of displacement. The faults do not appear to extend through the Mowry and Muddy Formations.

Polygonal fault systems (PFS) are networks of small (tens of meters up to 100 m of displacement), extensional (normal) faults that formed with randomly oriented strikes (Watterson and Walsh, 2000; Cartwright, 2011). In map view, these systems appear as nonuniform polygons bounded by the fault planes. The largest polygons produced by these systems are on the order of several thousand meters in length (Watterson and Walsh, 2000; Sonnenberg and Underwood, 2012). PFS are known from over 100 sedimentary basins worldwide and have typically been discovered by 2-D and 3-D seismic surveys (Cartwright, 2011). They generally form in fine-grained (clay size) sedimentary units deposited where regional dip was less than about 1 degree. Increase in regional dip results in less random strike of occurring faults and, as a result, lower chance of networks forming (Watterson and Walsh, 2000). PFS faults generally intersect at angles greater than 10 degrees (Berndt and others, 2012) and should not be confused with other types of geometric features such as columnar jointing in igneous rocks, desiccation cracks (from subaerial exposure), or permafrost “patterned ground” (Berndt and others, 2012).

PFS are not tectonic in origin but rather the result of soft-sediment deformation early in the burial history (Watterson and Walsh, 2000; Cartwright, 2011; Sonnenberg and Underwood, 2012). Vertically oriented faults are the result of greater vertical stress than horizontal stress on the faulted



unit (Sonnenberg and Underwood, 2012). Multiple causes have been suggested and are covered in more detail by Cartwright (2011) and Berndt and others (2012). Recent consensus is that PFS are caused by compaction dewatering of the soon-to-be-faulted or underlying unit, the process of which created planes of weakness along which faults preferentially developed (Cartwright, 2011; Berndt and others, 2012). Other processes related to dewatering cannot be entirely ruled out.

Knechtel and Patterson (1962) cataloged 27 units of bentonite in the Belle Fourche and 21 units in the Mowry in nearby Crook County, Wyoming. Dewatering of several thicker units near the bottom of the Belle Fourche and the 2-foot-thick Clay Spur bentonite at the top of the Mowry presents a possible cause for the faulting and a reason for why they do not appear to extend downward into the Mowry shale.

Faults can act as conduits to subsurface fluid flow and, as such, are important to recognize during site characterization for oil, gas, or CO<sub>2</sub> storage. Because PFS typically present in fine-grained sediments that are normally considered impermeable cap rocks, the need for characterization of the faulted strata (and over- and underlying strata) becomes even more important (Chen and others, 2011; Berndt and others, 2012).

### **Basement Faulting**

Weimer and others (1988) note that the Bell Creek Field is on a structural and paleotopographic high that was created by recurrent movement on northeast-trending basement lineaments. Working with 2-D seismic sections, Weimer and others identified basement faults along a southwest–northeast line that corresponded with the edges of the paleo-high on the Cretaceous formations. 3-D seismic data provide a higher-quality image for fault resolution, so as a matter of interest, an attempt to identify basement faulting is shown below.

All 554 traces of the southwest–northeast-trending Crossline 1177 are plotted for times from 0 to ~2700 ms (Figure 56). For reference, the Muddy is marked and can be seen near the middle of the section. Deeper in the section below 2 seconds, a long oblique fault plane appears to be imaged, and a vertical fault trace is marked where vertical offset is noticeable. Not all visible faulting is marked. It is not known if these are the controlling basement faults. The redactions to the data make it difficult to follow the faults through the survey. More investigation may be warranted with an unredacted data set.

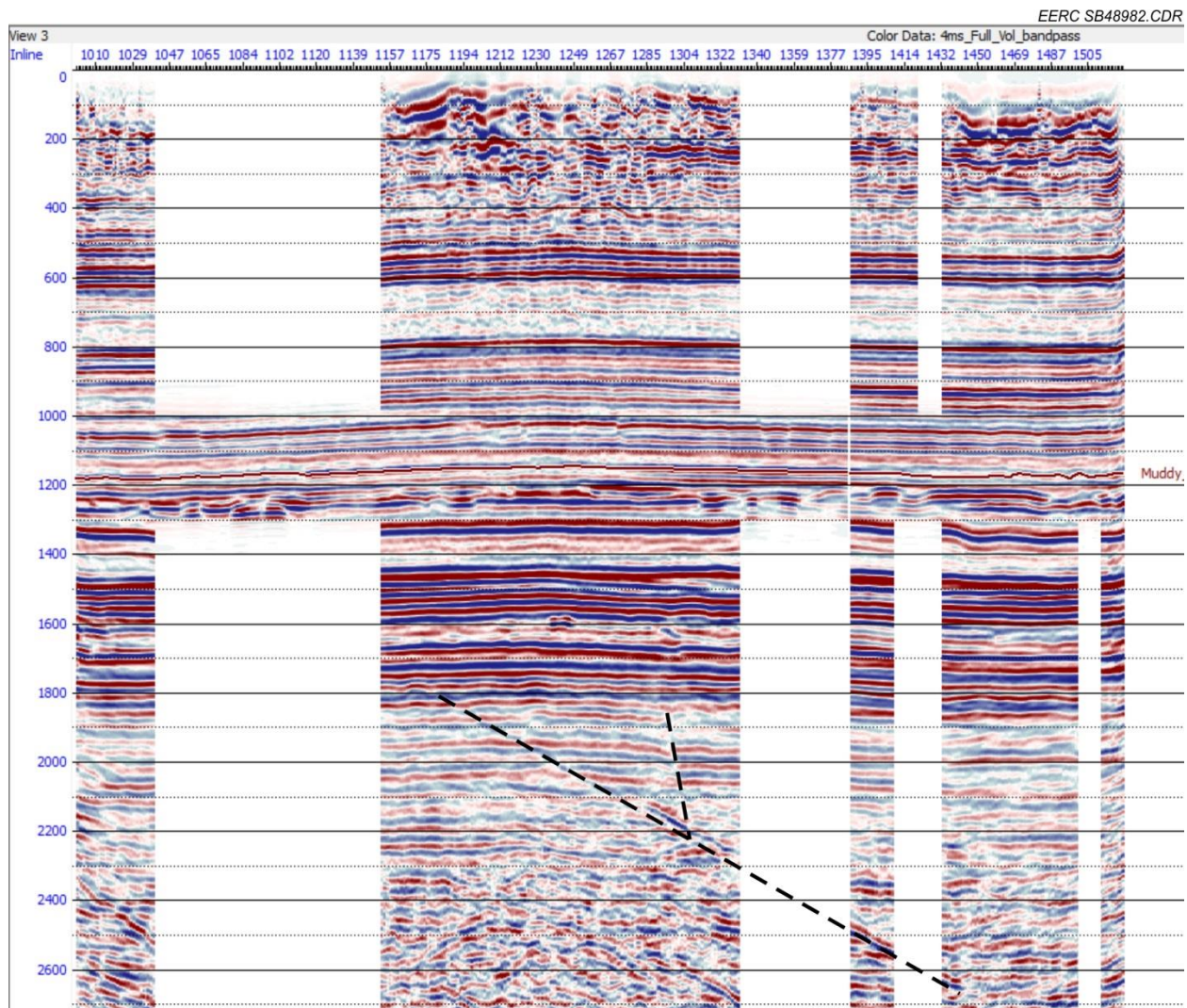


Figure 56. Indications of basement faulting visible on southwest–northeast Crossline 1177 may be part of the paleostructure referred to by Weimer and others (1988) and the cause of the topographic high seen at the reservoir level. The field operator does not have rights to the redacted data.

## FUTURE WORK

### **Integrate Seismic with the Petrel Geocellular Reservoir Model**

To provide a more complete model of the reservoir, the 3-D surface seismic and elements of the 3-D VSPs will be integrated with the Petrel geocellular reservoir model. The seismic data will be depth-converted and tied to the model data. One use would be for seismic trace data attributes to constrain or guide model computations with the well log data that are currently used, for example, to guide computations to spatially honor geobody boundaries, such as the fluvial channel in the north or the incised valley in the south.



To illustrate, a display from the current reservoir model is shown in Figure 57. The display shows the spatial distribution of sand in feet of thickness with effective porosity greater than 18.5% and shale content less than 55% in the layers below the Springen Ranch and above the Rozet; effectively, this is a map of where the clean sand is located. Clean sand is predominantly in the north phases, with a good amount in Phases 1 and 2. There is less in Phase 8 south of Phase 1. The general character of the fluvial channel and incised valleys is present. However, the statistical nature of the model calculations has put sand where the seismic shows the fluvial channel because wells are not present to constrain the result. Sand would not be expected there based on the seismic analysis of the feature.

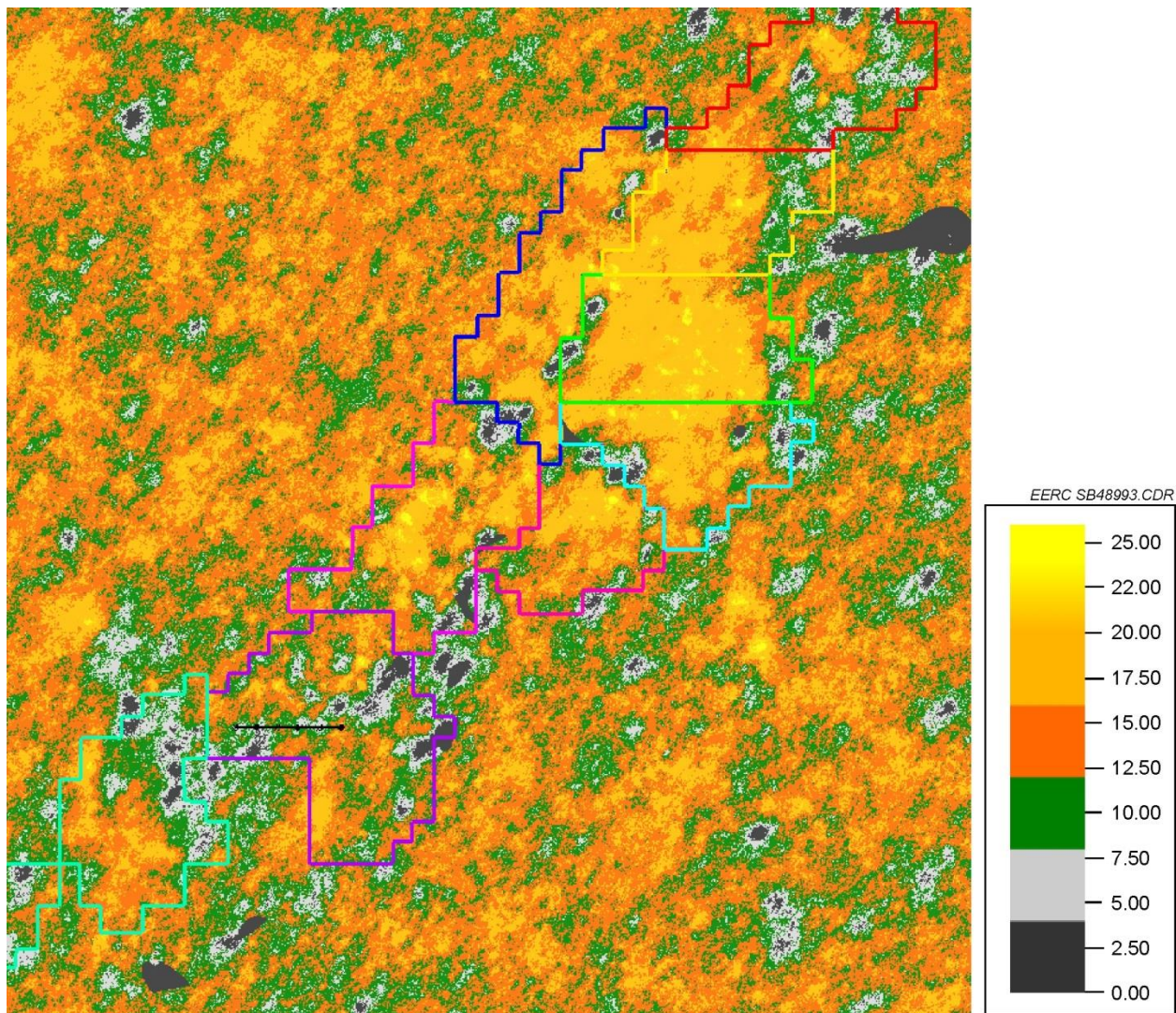


Figure 57. Display from the current reservoir model showing the spatial distribution of clean sand in feet of thickness. Effective porosity is  $> 18.5\%$ , shale content  $< 55\%$ , within Bell Creek sand and Coastal Plain layers.



As noted elsewhere, clean sand is predominant where the seismic amplitudes are low, and the overlay of the seismic amplitude map on the reservoir model demonstrates that relationship especially well in the northeast part of the field (Figure 58). The smaller amount of clean sand corresponding to the southern incised valley is also apparent, and the seismic data could be used to improve its distribution on the model.

Phase 8 in the southern area where clean sand is not predominant corresponds with an area of high amplitude on the map, lending support that fine-grained material in the sand correlates with high amplitude. This conclusion is also supported in Phases 1 and 2 just south of the northern incised valley where the Bell Creek sand tends to be thinner with a fining upward character.

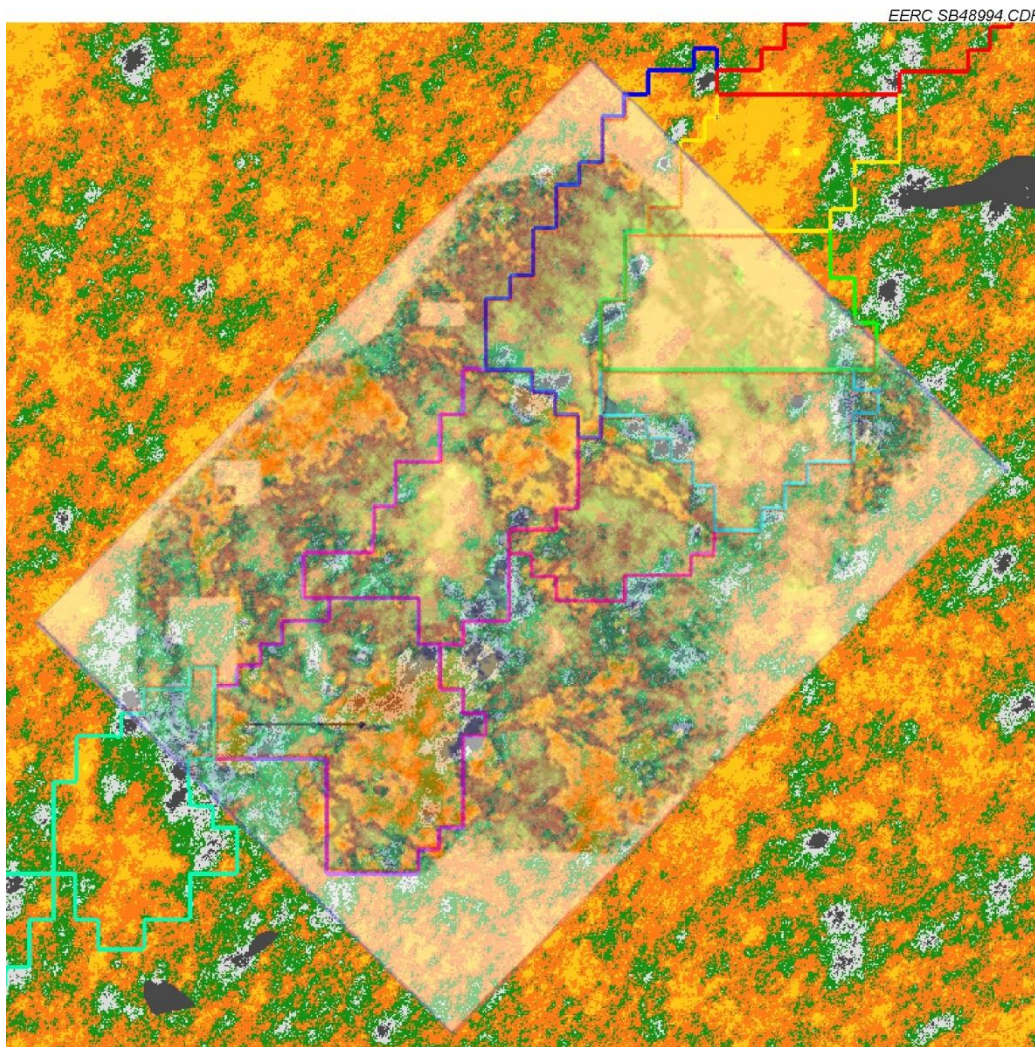


Figure 58. Seismic amplitude map overlaid on the reservoir model showing clean sand. Clean sand is predominant where the seismic amplitudes are low. Seismic amplitude or other attributes may provide an additional constraint for model computations.



### 3-D VSP Integration

In May 2013, as part of the deep monitoring program at Bell Creek, a baseline 3-D VSP incorporating two borehole arrays was acquired (Figure 59). Monitor Well 05-06 OW in the Phase 1 area was equipped with a 60-level removable 3-component geophone array. Monitor Well 04-03 OW near the Phase 1–Phase 2 boundary with its 50-level permanent 3-component geophone array was also used. Data from 930 vibrator shot points were acquired and processed. Delivery of the processed data was in November 2013. Interpretation work analogous with the 3-D surface survey, including well ties, horizon picking, and mapping, was not completed at the time this report was finalized (Figure 60).

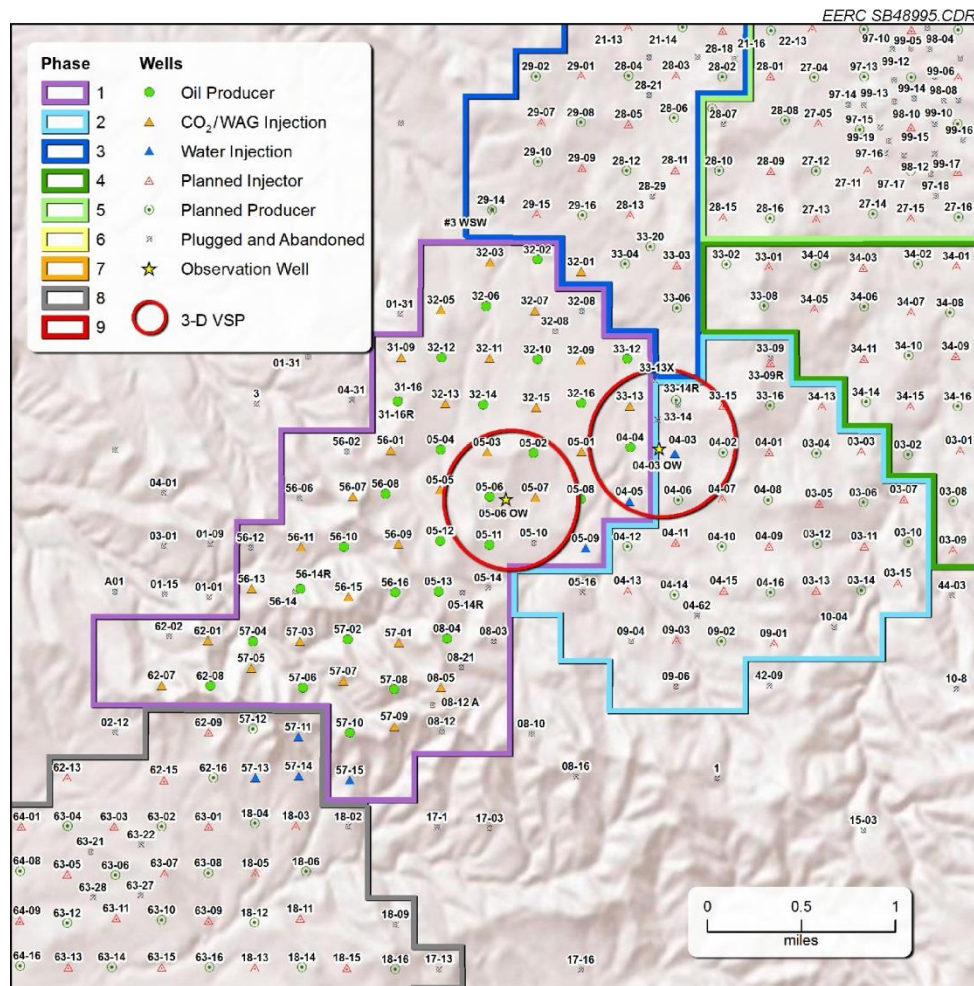


Figure 59. Location map and notional coverage of baseline 3-D VSPs acquired in May 2013. The area of coverage at the Muddy Formation is within the two outlined circles.

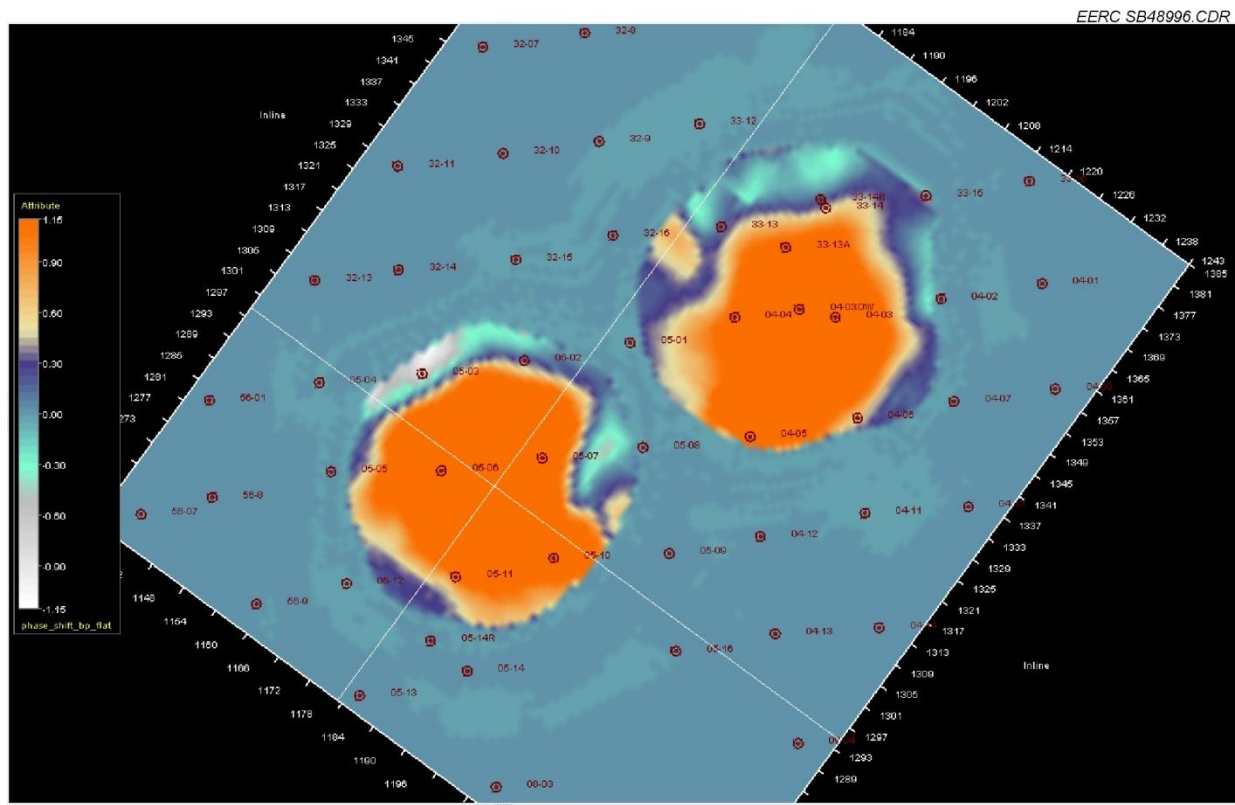


Figure 60. Time slice display from the 3-D VSPs at reservoir level showing well locations. Future work includes integration of the VSP data with the surface 3-D data.

### Computation of Geomechanical Properties

As part of characterization for CO<sub>2</sub> storage, experimentation is being done using the 3-D seismic traces to guide calculation of Poisson's ratio (PR) and Young's modulus for the reservoir zone and above and for the entire surface-to-reservoir geologic section. Figure 61 is an example of PR computed over a portion of the reservoir area. The well trace overlaying is the PR computed using an array sonic logging tool to provide comparison. Geomechanical properties will be used to construct a 3-D mechanical earth model so that geomechanical responses due to injection operations can be modeled in the reservoir and overlying strata.

### 4-D Time-Lapse VSP and 4-D Time-Lapse Surface 3-D

A repeat of the baseline 3-D VSP was started on March 1, 2014. This time-lapse survey will be used to verify the progress of CO<sub>2</sub> that has been injected into the reservoir in the area covered by the repeat survey. If the time-lapse data verifies that sufficient CO<sub>2</sub> has been injected to be imaged by seismic methods, a repeat of the 3-D surface survey will be planned and acquired. Fluid substitution modeling performed by Denbury has shown that modest to heavy concentrations of injected CO<sub>2</sub> will induce a detectable amplitude reduction that will likely be visible on difference displays at the current resolution and bandwidth.

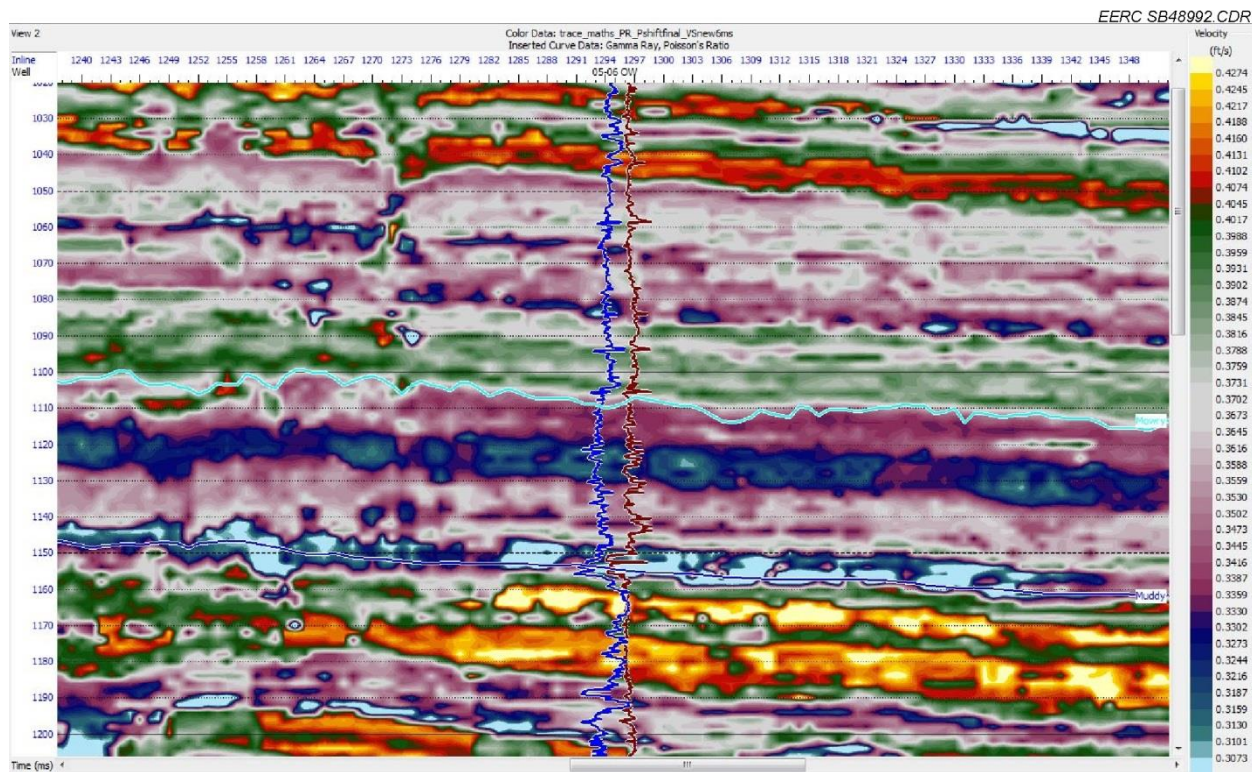


Figure 61. An example cross section of PR computed over a portion of the reservoir area. The blue well trace overlay is the PR computed using an array sonic logging tool to provide comparison.

## CONCLUSIONS

The 3-D surface seismic survey was acquired to serve several purposes for characterization and MVA of the Bell Creek project. Most MVA purposes involve tracking the distribution and movement of CO<sub>2</sub>, which will require pairing this baseline survey with future surveys. To date, this baseline survey has been used to enhance the characterization with several key results which include the following:

- On the migrated, stacked data set as-received, the bandwidth is 10–48 Hz which limits vertical resolution at the reservoir level to about 60 feet. The reflection from the reservoir originates from the impedance contrasts at the top of the Springen Ranch and the top of the Skull Creek Formations. The Bell Creek sand, which makes up the reservoir, is a subset of this interval, and its vertical thickness is not directly resolvable. However, the amplitude of the reflection appears to be related to the character of the sand within: thick and clean sands having a low amplitude and thin or shale impacted sands having a higher amplitude. More work is needed to calibrate this relationship.
- The structural interpretation of the field has been aided. Color contour maps of key horizons, including the reservoir reflector, provide a detailed visualization of structure. Polygonal faulting in the Belle Fourche and lower Mowry has been identified and appears



to be limited to these formations. Basement faulting contributing to or controlling the paleo-high of the reservoir over the field has been identified. The facies change that creates the updip trap for the field does not appear to be discernible on the seismic data.

- Some lateral heterogeneities and flow boundaries within the field can be identified and mapped directly with the seismic. These include two systems of incised erosional valleys and an erosional channel of apparent fluvial nature. The erosional valleys were apparently cut during a significant drop in sea level after the deposition of the marine facies of Bell Creek sand. As the sea level subsequently transgressed, the cut valleys filled with water and supported a low-energy environment in which coals and bentonitic mud shales were deposited on the erosional surface before being further filled with shales and fine-grained material. The northern valley acts as a flow boundary between Phases 1 and 3 and between Phases 2 and 4. The fluvial channel feature was cut later after sea level had risen further and material of a more deltaic nature was being deposited on top of the Bell Creek marine sand. The fluvial channel feature itself is shale-filled and acts as a barrier between Phases 3 and 5 and between Phases 1 and 2.

Different facies are identified with the flow boundaries and can be mapped. The erosional valleys have characteristic deposits of thick layers of valley fill that start with coals and bentonites. The fluvial channel is filled with fine-grained material in place of the eroded sand. The 3-D seismic maps provide a visualization of the spatial distribution and boundaries of these features, and the facies within that can be used to guide computations for the geologic modeling. This will improve the spatial accuracy of the model.

## **BIBLIOGRAPHY**

- Berndt, C., Jacobs, C., Evans, A., Gay, A., and Elliott, G., 2012, Km-scale polygonal sea-bed depressions in the Hatton Basin, NE Atlantic Ocean—constraints on the origin of polygonal faulting: *Marine Geology*, p. 1–23.
- Cartwright, J., 2011, Diagenetically induced shear failure of fine-grained sediments and the development of polygonal fault systems: *Marine and Petroleum Geology*, v. 28, no. 9, p. 1593–1610, doi: 10.1016/j.marpetgeo.2011.06.004.
- Chen, D., Wu, S., Wang, X., and Lv, F., 2011, Seismic expression of polygonal faults and its impact on fluid flow migration for gas hydrates formation in deep water of the South China Sea: *Journal of Geological Research*, v. 2011, p. 1–7, doi: 10.1155/2011/384785.
- Kallweit, R.S., and Wood, L.C., 1982, The limits of resolution of zero-phase wavelets, *Geophysics*, v. 47, p. 1035–1046.
- Knechtel, M.M., and Patterson, S.H., 1962, Bentonite deposits of the northern Black Hills district, Wyoming, Montana, and South Dakota: *Contributions to Economic Geology, U.S. Geological Survey Bulletin 1082-M*.



- Molnar, P., 1990, Geologic reservoir study of the Bell Creek Field, Carter and Powder River Counties, Montana: Unpublished, courtesy of Denbury Onshore LLC.
- Plummer, P., and Gostin, V., 1981, Shrinkage cracks—desiccation or syneresis?: *Journal of Sedimentary Research*, v. 51, no. 4, p. 1147–1156.
- Rebne, C.A., 1985, A seismic stratigraphic study of the Muddy Formation, Bell Creek Field, Montana [M.Sc. Thesis]: Colorado School of Mines, Golden, Colorado, p. 97.
- Saini, D., Braunberger, J., Pu, H., Bailey, T.P., Ge, J., Crotty, C.M., Liu, G., Hamling, J.A., Sorensen, J.A., Gorecki, C.D., Steadman, E.N., and Harju, J.A., 2012, Bell Creek Field test site—simulation report: Plains CO<sub>2</sub> Reduction (PCOR) Partnership Phase III Task 9 Deliverable D66 for U.S. Department of Energy National Energy Technology Laboratory Cooperative Agreement No. DE-FC26-05NT42592, Grand Forks, North Dakota, Energy & Environmental Research Center, January.
- Sheriff, R.E., 2002, *Encyclopedic dictionary of applied geophysics* (Geophysical references no. 13).
- Slack, P.B., 1981, Paleotectonics and hydrocarbon accumulation, Powder River Basin, Wyoming: *AAPG Bulletin*, v. 65, no. 4, p. 730–743.
- Sonnenberg, S., and Underwood, D., 2012, Polygonal fault systems—a new structural style for the Niobrara Formation, Denver Basin, CO: *Search and Discovery*, p. 50624.
- Sutherland, R.B., 2011, Bell Creek petrophysical analysis notes: Unpublished, courtesy of Denbury Onshore LLC.
- Torey, A.W., 1970, A simple theory of seismic diffractions: *Geophysics*, v. 35, no. 5.
- Watterson, J., and Walsh, J., 2000, Geometry and origin of a polygonal fault system: *Journal of the Geological Society of London*, v. 157, no. 1995, p. 151–162.
- Weimer, R.J., Rebne, C.A., and Davis, T.L., 1988, Geologic and seismic models, Muddy Sandstone, Lower Cretaceous, Bell Creek – Rocky Point Area, Powder River Basin, Montana and Wyoming: Wyoming Geological Association 39th Field Conference Guidebook, p. 161–177.

# **APPENDIX A**

## **DATA-PROCESSING DETAILS**

## DATA-PROCESSING DETAILS

### SEISMIC DATA PROCESSING

The 3-D surface seismic data was processed by Geotrace, Inc., during the fall and winter of 2011 and 2012. A summary of the processing can be found in the SEG-Y format data file headers. The processing sequence was as follows, with a brief explanation of each step:

- Reformat
  - Convert field data to internal format for processing.
- Geometry definition and QC
  - Assign x, y, and z values to each record trace associated with each shot to allow sorting by shot, receiver, offset, and common midpoint. Identify and edit defective traces.
- Noise attenuation/FK filter
  - Transform data to the frequency–wavenumber domain and zero-out coherent noise based on apparent velocity – commonly used to remove most ground roll noise.
- Apply spherical divergence spreading correction;  $t = 1.75$ 
  - A time-variant, approximate correction for the geometrical decay of energy as the wavefront propagates away from the source.
- Surface consistent gain
  - A time-invariant trace amplitude correction incorporating source, receiver, offset, and common midpoint factors.
- Surface consistent deconvolution: 200-ms spiking operator with 1% white noise
  - A deconvolution operator to flatten the spectrum of the data. White noise prevents zero division. Incorporates source, receiver, offset, and common midpoint factors.
- Noise attenuation/wavelet transform filter
  - A filtering technique to remove strong linear noise, such as ground roll, by computing a filter based on time-variant spectra.
- Delay time refraction statics: one layer, datum elevation 3700 ft; correction velocity 6500 ft/s
  - A model of the near-surface layer is computed using first break times from the traces, allowing the data to be corrected for elevation differences and time-shifted to the seismic reference datum.
- Initial velocity analysis
  - Gathers are corrected for normal moveout with a range of constant velocities. The velocity at a given time resulting in the greatest coherence is saved.

- Surface consistent residual statics
  - After correcting trace gathers for normal moveout using the new velocities, small static shifts that increase event coherence among trace gathers are computed incorporating source and receiver components.
- Second velocity analysis every 1 square mile
  - As before, after application of residual statics.
- Surface consistent residual statics (second pass)
  - As before, after application of refined velocities.
- Ray trace prestack time migration velocity analysis every 0.5 square mile
  - Migrated gathers are used to perform a velocity analysis specifically for the migration process.
- Ray trace prestack time migration
  - The processed gathers, with the migration velocities applied, are migrated using a Kirchhoff algorithm. This imaging process repositions amplitudes from their apparent reflected location to their actual geometric location in space.
- CMP stack
  - The nominal 24 traces in each migrated gather are summed together to create a single common midpoint trace centered in each 82.5-ft  $\times$  82.5-ft surface bin.
- Bandpass filter: 8/12-out Hz
  - A 10 Hz low-cut filter, with corner frequencies of 8 and 12 Hz, removes frequencies lower than 10 Hz. No high frequencies are removed.
- 1000-ms AGC
  - A trace-by-trace amplitude scaling process using a 1000-msec moving window.

Processed data was output to data files in SEG-Y format for transfer to the client.

### **Processing Statistics**

Prestack traces	4,224,912
Stacked traces	174,630
Record length	4.2 sec
Sample interval	1 msec
Nominal fold	24
Bin size	82.5 ft $\times$ 82.5 ft
No. of inlines	554
No. of crosslines	411
Seismic datum	3700 ft ASL
Datum velocity	6500 ft/s



The data were acquired and processed with reference to the NAD 1927 State Plane Montana South FIPS 2503, units in U.S. feet. Corner points of the 3-D surface are denoted:

<u>Inline</u>	<u>Crossline</u>	<u>X-Coordinate</u>	<u>Y-Coordinate</u>
1001	1001	3,101,363.2	417,849.7
1001	1411	3,126,781.6	395,533.0
1554	1411	3,156,882.0	429,816.8
1554	1001	3,131,463.6	452,133.5

## **APPENDIX B**

### **WELL TIE AND CORRELATION PROCESS**

## WELL TIE AND CORRELATION PROCESS

Tying logs to seismic is often described as both an art and a science. The tie is made between a synthetic seismogram generated from the sonic log and seismic traces located near the well. Ambiguity exists because the physical volumes of rock measured by the sonic and seismic are not exactly the same. The sonic log is a high-resolution, high-frequency, point-to-point measurement influenced by the borehole environment, with depth measured precisely from the kelly bushing (KB) elevation. The seismic is an indirect, lower-resolution surface measurement of reflection-time amplitude sampling a much larger volume of rock and measured in two-way travel time hung from a seismic reference datum that will not coincide with the KB elevation except by chance (see Figure B-1).

A correlation screen is shown in Figure B-2. Plotted on the left are the gamma ray, density, and sonic logs. The blue synthetic seismic trace is computed from the sonic log and repeated 5 times. The red seismic trace is the seismic trace from the well location repeated 5 times. The black traces are the seismic traces near the well, the red trace showing the well location. Above the blue and red traces is the wavelet extracted from data near the well and applied to the synthetic, so it will match the character of the seismic. No corrections have been made for depth or phase.

EERC SB48907.CDR

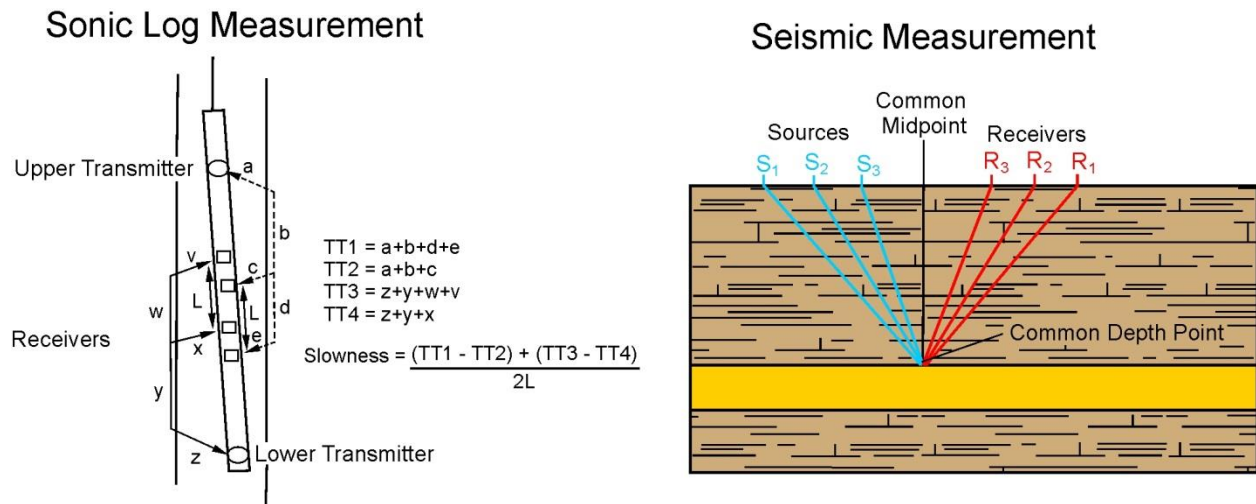


Figure B-1. Seismic and well logs measure geology differently: well logs are physical measurements of the geologic formations at a specific location and depth at a scale close to point measurements. Surface seismic is a remote measurement that samples the rock broadly, and the reflection displayed at any given point is the summation of multiple reflection paths; therefore, their responses may be different but are correlatable.

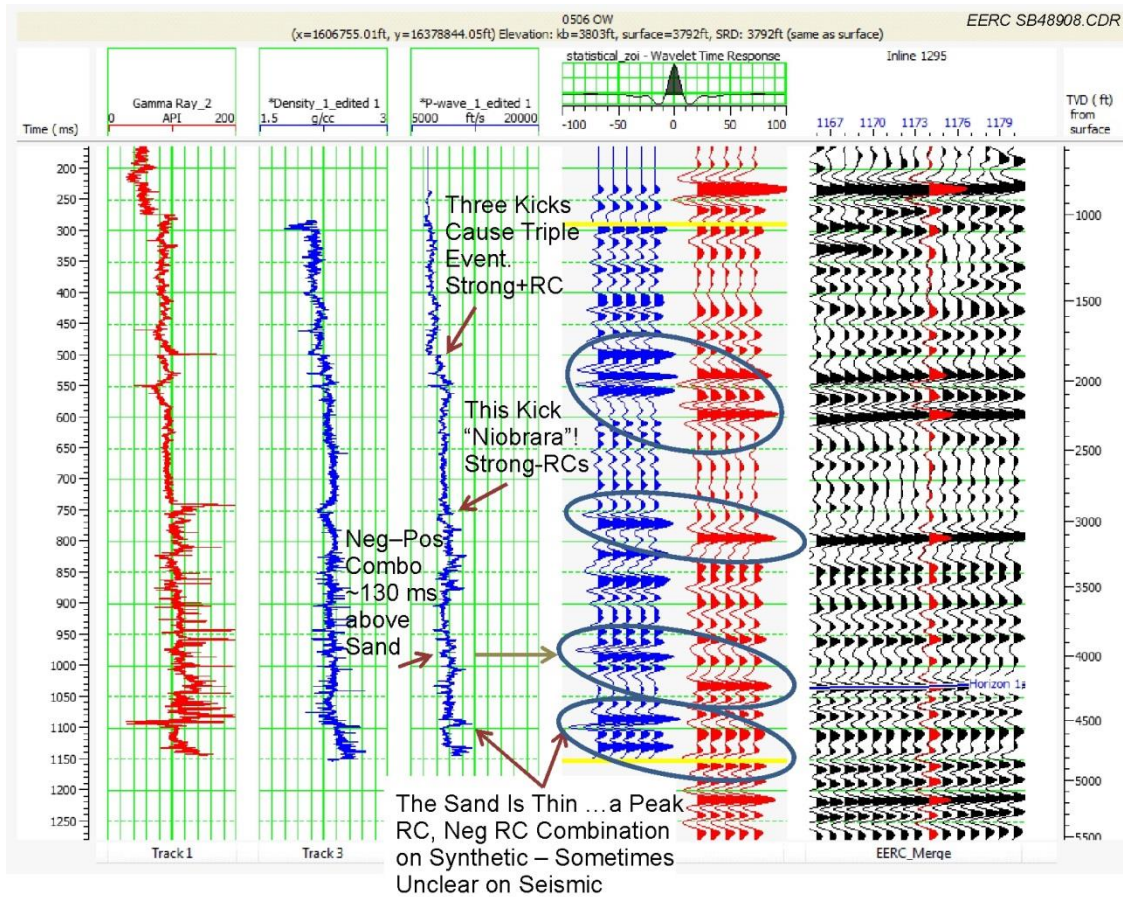


Figure B-2. Correlation screen with gamma ray, density, and sonic logs. Blue synthetic computed from sonic. Red seismic trace nearest the well. The wavelet on the synthetic data is shown above traces. No corrections have been made for depth or phase. Four frequently seen correlation events are shown. RC stands for reflection coefficient, a measure of impedance contrast.

Four strongly correlatable events are circled. The top event is associated with a large increase in sonic velocity in the neighborhood of the Shannon sand. The second is associated with the strong Niobrara reflection. The third event is correlated with a strong reflector above the reservoir between the Belle Fourche and Mowry Formations, and the bottom is the reflection from the Muddy Formation. These events are visible and correlatable in the six wells that have sonic logs that run from the reservoir to casing shoe. The correlation process will shift the well logs down in terms of two-way time by roughly 25 ms for data above the Niobrara to about 50 ms at the reservoir time. The initial 25 ms is a static shift to move the upper events to the seismic reference datum. The additional 25-ms dynamic stretch better aligns events at depth. The need for the dynamic stretch is attributed to the finer sampling of the sonic tool and borehole effects which do not affect the seismic measurement.



An important factor in the tying process is the polarity and phase of the correlation. In other words, is an increase in acoustic impedance represented on the seismic by a peak or a trough? This is critical for identifying the Bell Creek reservoir as it is a thin bed and has a higher acoustic impedance than the encasing shales.

The phase of the synthetic can be rotated arbitrarily to match the phase on the seismic data. The default shown in Figure B-2 is a zero-phase condition in which an increase in impedance is indicated by a peak on the synthetic, and a decrease by a trough. This is visible on the top correlation event at 500 ms. Both sonic and density logs increase which corresponds to an increase in acoustic impedance, and this effect is indicated by a peak on the synthetic. The phase on the seismic data can be different.

The tie resulting in the maximum computed correlation coefficient occurred with the wavelet reversed. It has the opposite polarity from the zero degree default with an additional 28 degree phase “lean” (Figure B-3). Note that the wavelet displayed above the synthetic traces has a changed appearance that reflects this phase condition. This polarity relationship indicates that an increase in impedance results in a trough or negative deflection on the seismic trace. The lean value varies some from well to well. What is important is the fact that the wavelet is reversed from the default state. In this case, the Muddy reflector is represented by a trough–peak combination on the section.

There are inevitable imperfections in synthetic-to-seismic ties. An obvious one on Figure B-3 is the Niobrara at 800 ms. The reflections appear to be off-depth, but a static shift to tie them would cause all others below to untie. To reposition the event by adjusting the sonic log, the equivalent of locally stretching the synthetic seismogram, is not justifiable based on the log appearances. The cause is unknown but may be attributed to the different scale of measurements between logs and seismic as described above. Events below the Niobrara tie very well, and the relationships shown are verified on other wells.

Getting the phase relationship correct for the Muddy Formation reflection is necessary as most wells in the field have either a sonic or density log run only over 400 feet covering the zone of interest to the top of the Mowry. This is not a sufficient interval to generate an unambiguous synthetic for deducing a well tie as shown in Figure B-4. The only reflector to correlate is the Muddy Formation, and one needs to know the proper polarity relationship a priori to make the correct tie. The phase applied to the synthetic is the 152 degrees computed from the previous example. If the polarity relationship was chosen incorrectly, e.g., reversed, ties would be significantly off-depth.

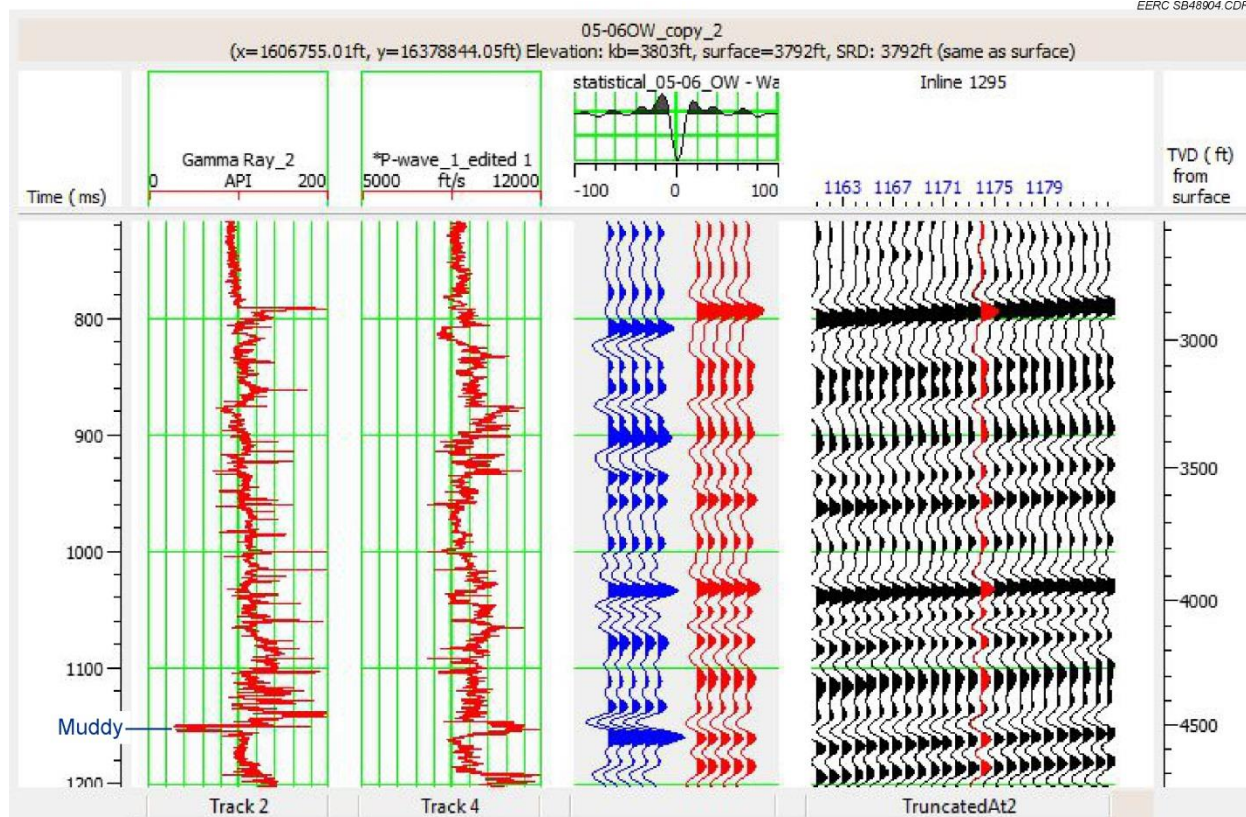


Figure B-3. A strong synthetic-to-seismic tie with a correlation coefficient of 0.52 is shown. The phase of the wavelet is 152 degrees. This phase relationship means an increase in impedance results in a trough or negative deflection on the seismic trace. The Muddy reflector is the large event at 1150 ms or 4500 feet and is represented by a trough–peak combination on the seismic section.

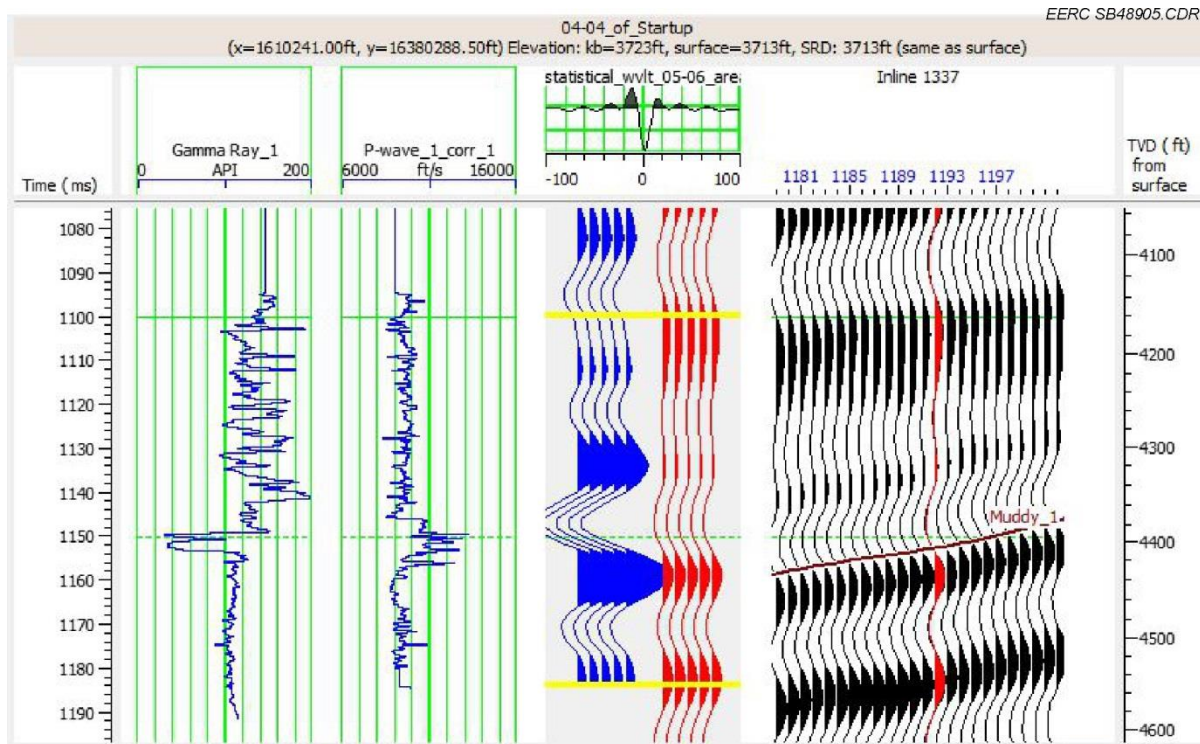


Figure B-4. Sonic log and GR (gamma ray) were often only run over the zone of interest to the top of the Mowry. The only reflector to correlate is the Muddy Formation. If the phase relationship was chosen incorrectly, ties would be off-depth. Events above the top of the log on the synthetic are artifacts and not real.

## **APPENDIX C**

# **DATA BANDWIDTH AND TEMPORAL RESOLUTION**



## DATA BANDWIDTH AND TEMPORAL RESOLUTION

The geologic target zone of interest at Bell Creek is the Muddy Formation and especially the Bell Creek sandstone, the Bell Creek sand, within it that makes up the reservoir. The Muddy Formation is about 4500 feet in depth and varies from 70 to 90 feet in thickness. The Bell Creek sand varies in thickness but is typically between 20 and 30 feet. To resolve formations of this thickness requires both an acoustic impedance contrast at the layer boundaries great enough to generate an interpretable reflection and a frequency bandwidth sufficient to produce a wavelet, with a duration short enough to avoid interference from the lower interface reflection.

The concept of how frequency bandwidth impacts time domain resolution is shown in Figure C-1. The bottom panel has three frequency bands; 8–40, 8–70, and 8–100 Hz. The top panel shows the time domain wavelets associated with each frequency band. As bandwidth increases, the wavelets become progressively thinner and able to resolve thinner geologic beds.

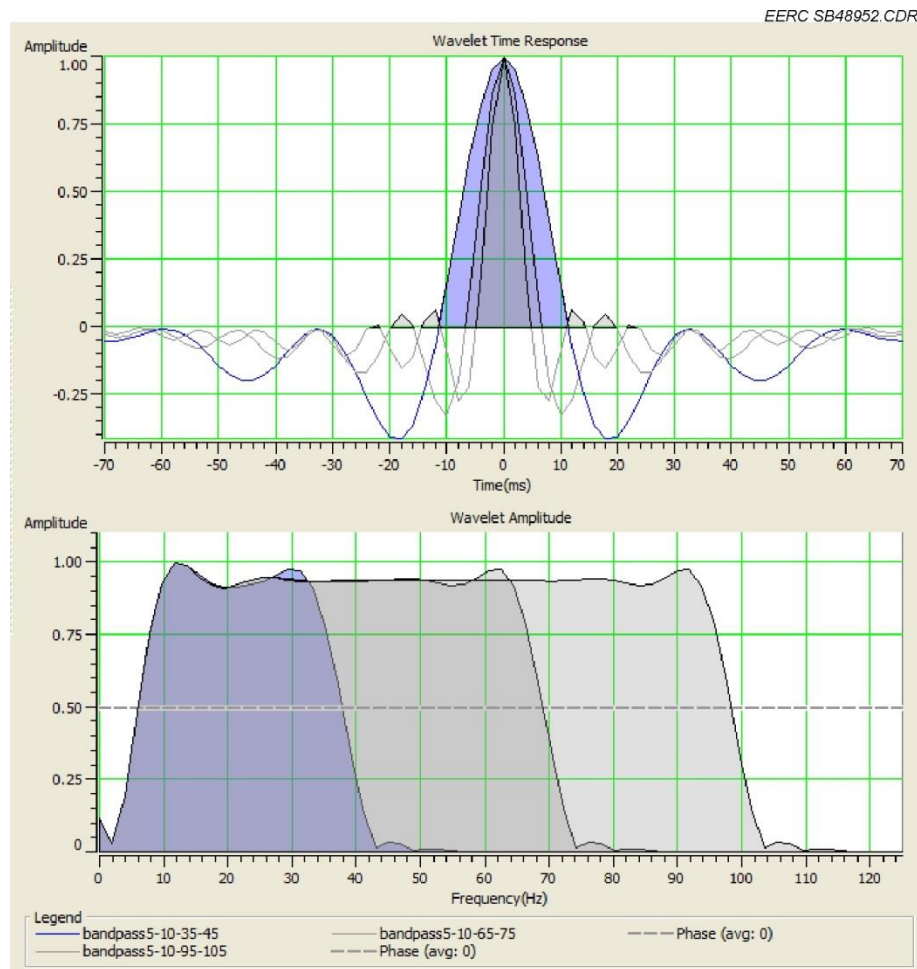


Figure C-1. Time domain wavelets and their corresponding frequency spectra. The broad blue-shaded wavelet has the narrowest bandwidth, 8–40 Hz, and a poor ability to resolve thin beds. The broadest frequency bandwidth, 8–100 Hz, has the sharpest wavelet.

The bandwidth of the data on the surface seismic can be seen in Figure C-2. An amplitude spectrum computed over a data window in time and space that includes the zone of interest in the neighborhood of the 05-06 OW monitor well in Phase 1 is shown. The range of frequencies that are above level extend from 10 to about 48 Hz, with a large peak at 38 Hz. The data have a low-cut filter applied which explains the rolloff at 10 Hz. There is no high cut applied, but frequencies drop steeply to the noise level at 48 Hz as if there were, which is a curious result given that the data window is not deep and the source sweep extended above 80 Hz.

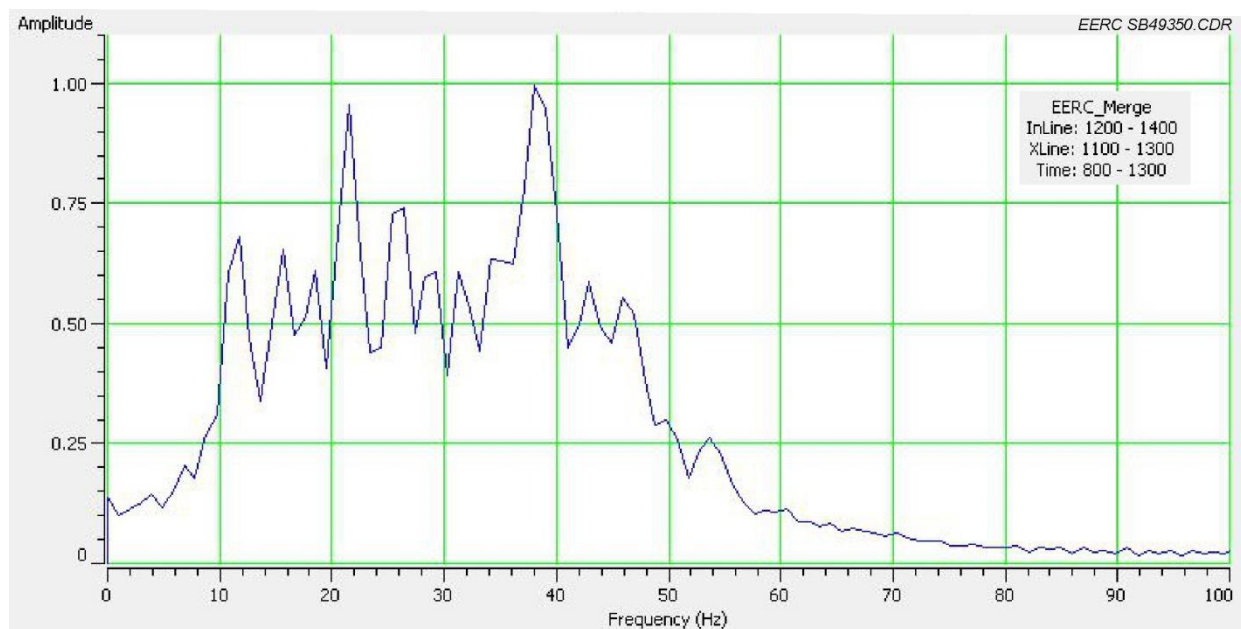


Figure C-2. Amplitude spectrum computed over 40,293 traces in the central area of Phase 1 in a 500-msec window centered on the zone of interest. Bandwidth is clearly 10–48 Hz.

Analysis of prestack gathers shows that the zone of interest is in a time window strongly impacted by normal movement (NMO) stretch, an artifact that occurs on far offset traces after stacking velocities are applied and which is most pronounced on shallow data. Summing stretched data into the stack has the effect of reducing bandwidth. Experimentation showed that a slightly improved broader bandwidth on the stack was achievable by using a more conservative mute to better remove stretch, together with balancing trace amplitudes before stacking. Figure C-3 shows gathers before and after application of a conservative mute. Interpretation efforts to date have used the initially supplied stacked data.

The Society of Exploration Geophysicists (SEG) defines an embedded wavelet as the time-domain reflection shape from a single positive reflector at normal incidence. The wavelet can be extracted from the data and represents the impulse response of the amplitude spectrum.

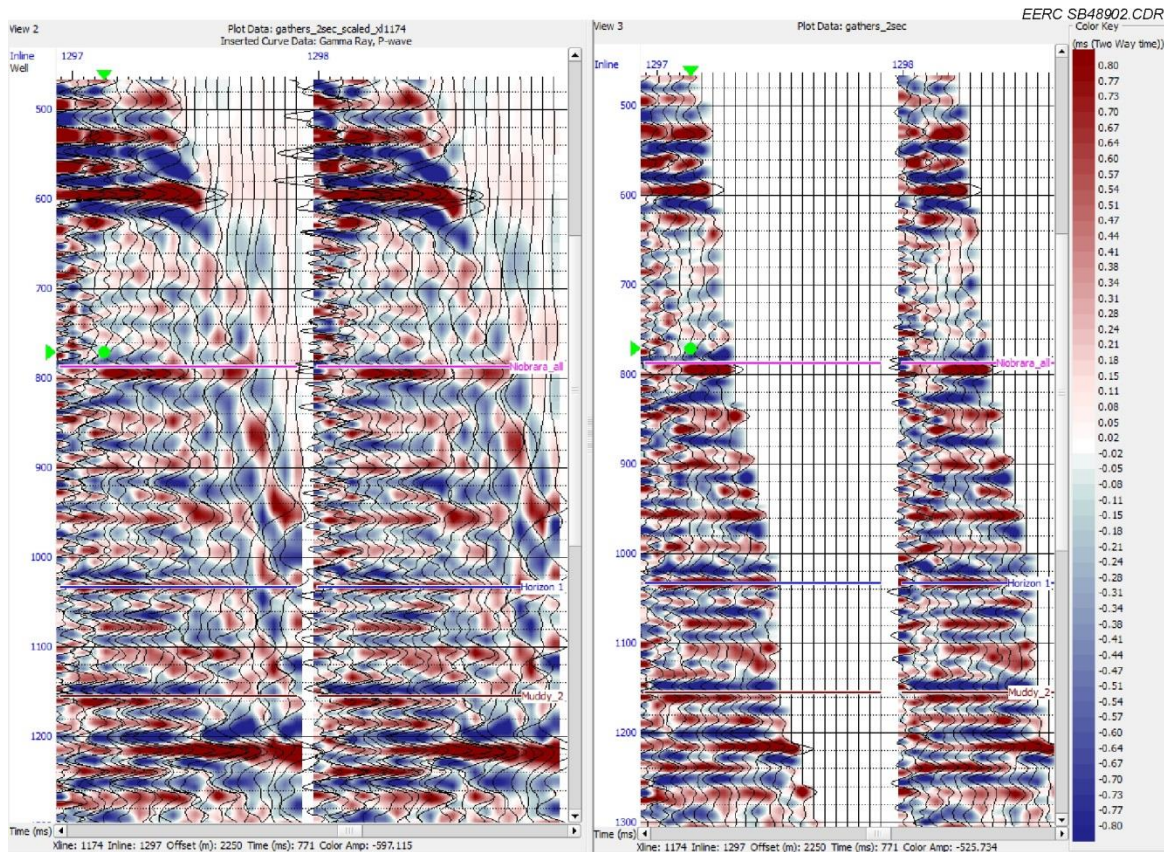


Figure C-3. Gathers before and after muting far offsets to remove NMO stretch. The zone of interest is within the mute zone. Failure to sufficiently mute stretched data will lower the bandwidth on the stack and negatively impact resolution.

A wavelet derived from the amplitude spectrum of the data is shown in the top panel of Figure C-4. Phase information is lost in the process, so it is displayed as zero phase. If the layered earth is represented by a series of reflection coefficient impulses determined by the density and velocity changes of the physical layers, this wavelet convolved with that series of reflection coefficients over the same time window would reproduce the seismic data in that window (with a phase adjustment).

The wavelet has a time thickness which determines the limit of its ability to resolve a thin bed such as the Muddy Formation and especially the Bell Creek sand within the Muddy. The wavelet extracted from the data has a resolution limit of 11 ms. To illustrate how resolution is limited, Figure C-5 shows the extracted wavelet and a reversed version in gray separated by 5 ms to represent the impulse responses overlaying a simplistic model of a bed 5 ms thick. The waveform in blue is a superposition of the two waveforms. Note that the peak-to-peak interval of the superposition is 11 ms not the actual value of 5 ms. The superposition is what would be seen on the seismic section. For bed thickness intervals less than 11 ms, the peak-to-peak interval would remain about 11 ms; only the amplitude would change. Thickness intervals greater than 11 ms will be resolved accurately in theory. As a practical matter, resolution at the theoretical limit on real data is not always possible.

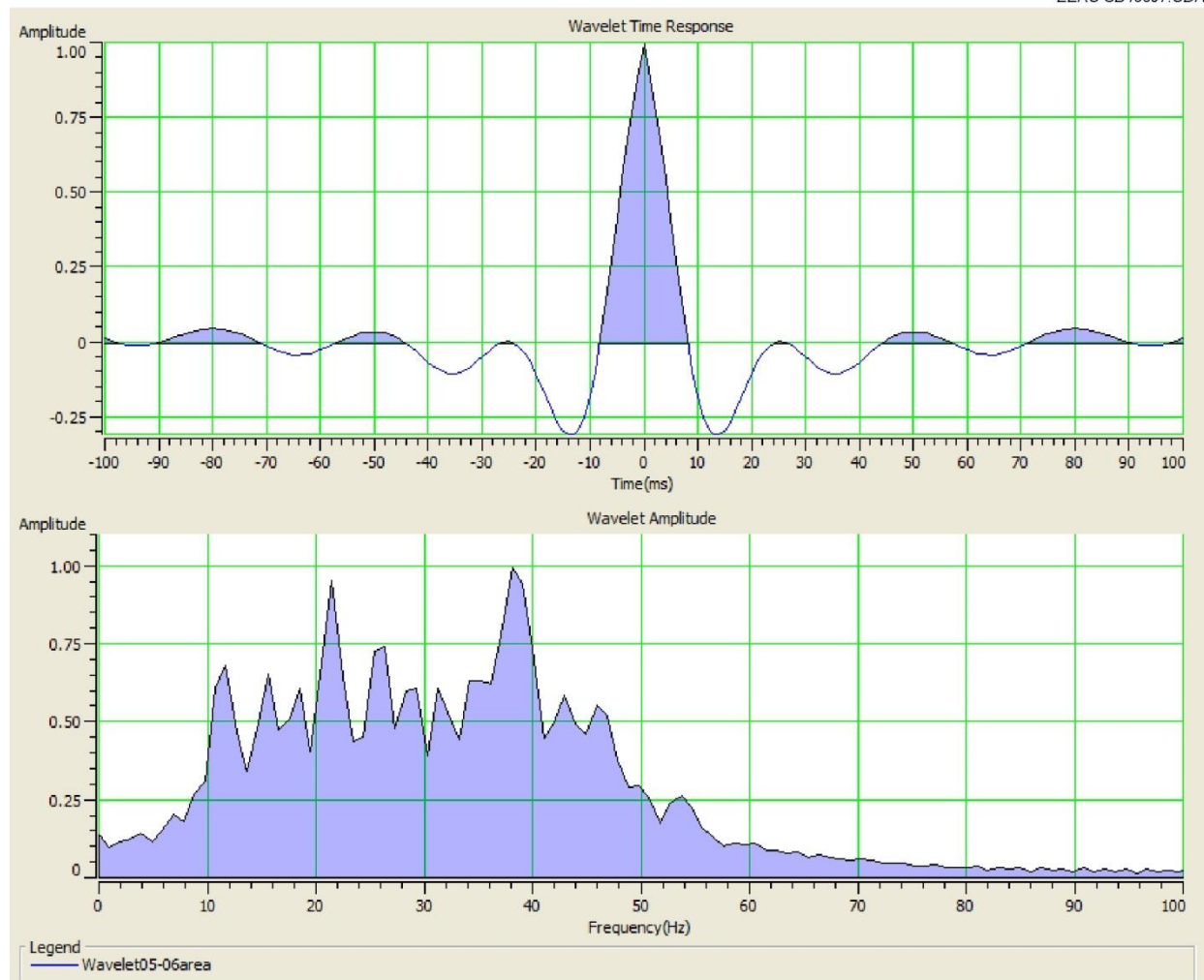


Figure C-4. The wavelet (upper panel) embedded in the data derived from the amplitude spectrum (lower panel). Tuning thickness for this wavelet is 14 ms. Maximum resolution is 11 ms. Any bed with a two-way time thickness less than 11 ms will not be resolvable.



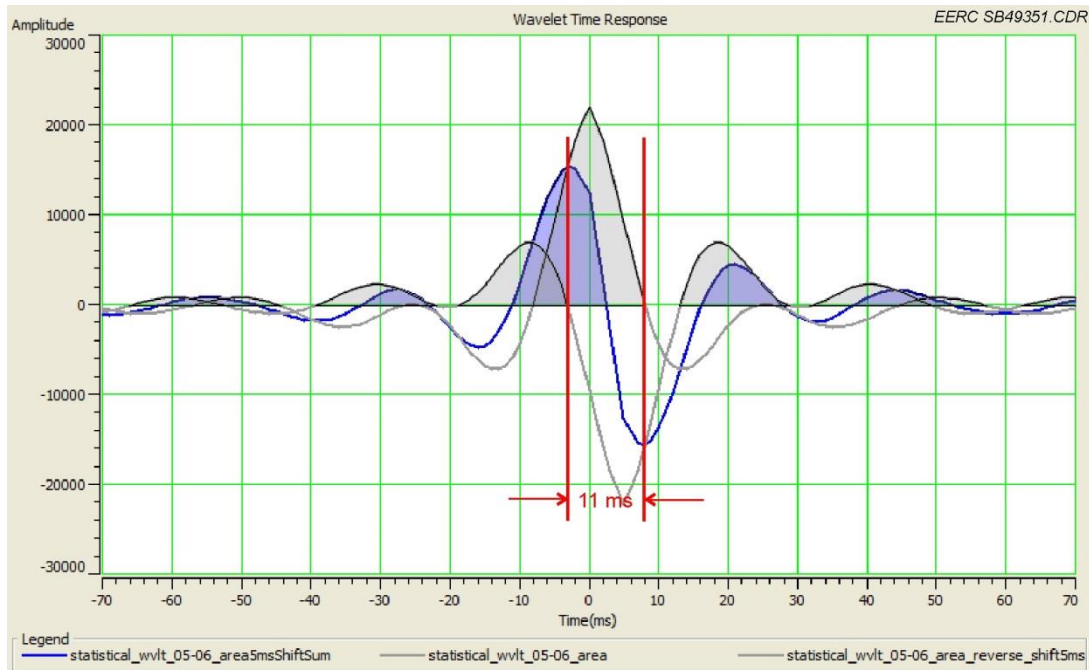


Figure C-5. Demonstration of the limit of resolution of the embedded wavelet. Two wavelets in gray are shown 5 ms apart and reversed from each other to represent the impulse responses on a bed 5 ms thick. The blue wavelet is the superposition of the other two. The peak-to-peak interval on the blue wavelet is 11 ms even though the two gray wavelets are only 5 ms apart. The peak-to-peak interval would remain at ~11 ms for any wavelet interval less than 11 ms. Only the amplitude will vary.

The tuning thickness for the wavelet is 14 ms. That is the interval in which the overlapping waveforms add constructively to sum to the highest possible amplitude. Figure C-6 shows the result at the tuning thickness. The vertical scales for both Figures C-4 and C-6 are the same to allow direct comparison.

The vertical scale for both wells and geologic models is depth, not time. The physical measurement made by surface seismic is the amplitude of sonic wave reflections which have traveled to subsurface layers and back-measured in two-way travel time (twt). That is the vertical scale on a seismic section. Two-way travel time is related to depth by the velocity field:  $\text{Depth} = \text{Velocity} \times \text{twt}/2$ . If the 11-ms resolution limit described above occurred in a homogeneous layer that had an interval velocity of 10,800 ft/s, which is about the average Muddy velocity, the resolution limit in terms of feet would be  $(10,800 \text{ ft/s} \times 0.011 \text{ s})/2 = 59.4$  feet thick.

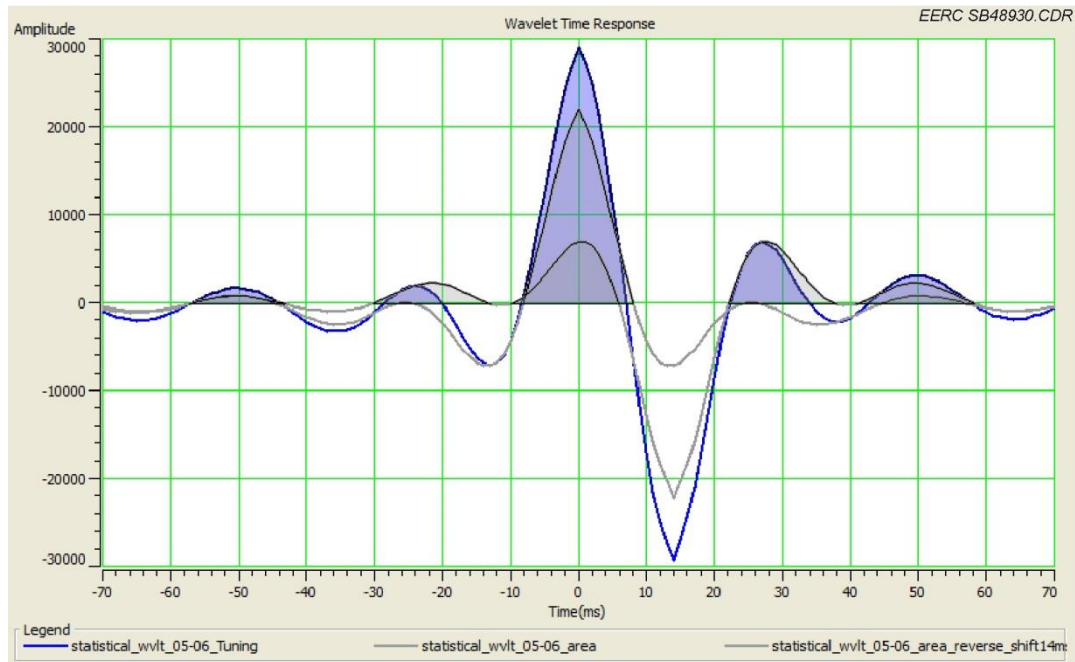


Figure C-6. Demonstration of the tuning thickness of the embedded wavelet. Two wavelets in gray are shown 14 ms apart and reversed from each other to represent the impulse responses on a bed 14 ms thick. The blue wavelet represents the superposition of the other two. The 14-ms interval results in the maximum amplitude as the wavelets sum constructively.

The same calculation for the tuning thickness in feet would be  $(10,800 \text{ ft/s} \times 0.014 \text{ s})/2 = 75.6$  feet thick. An interval of this thickness could be expected to produce the maximum amplitude reflection, again assuming a homogeneous layer. For the actual, inhomogeneous case, contributions from lithologic changes within the layer will contribute to the actual amplitude.

To generate a reflection, there must be an acoustic impedance contrast. Acoustic impedance is defined as the product of velocity and density. The acoustic impedance can be easily calculated at a well using the sonic p-wave velocity and the bulk density log. Using Well 05-06 OW, Figure C-7 shows the computed impedance log in the center. The gamma ray log is plotted on the left to provide lithology identification, and the seismic data within the depth window are plotted on the right, the red waveform indicating the well location. Lithologic tops have been marked with the naming convention used in the EERC's geologic model.

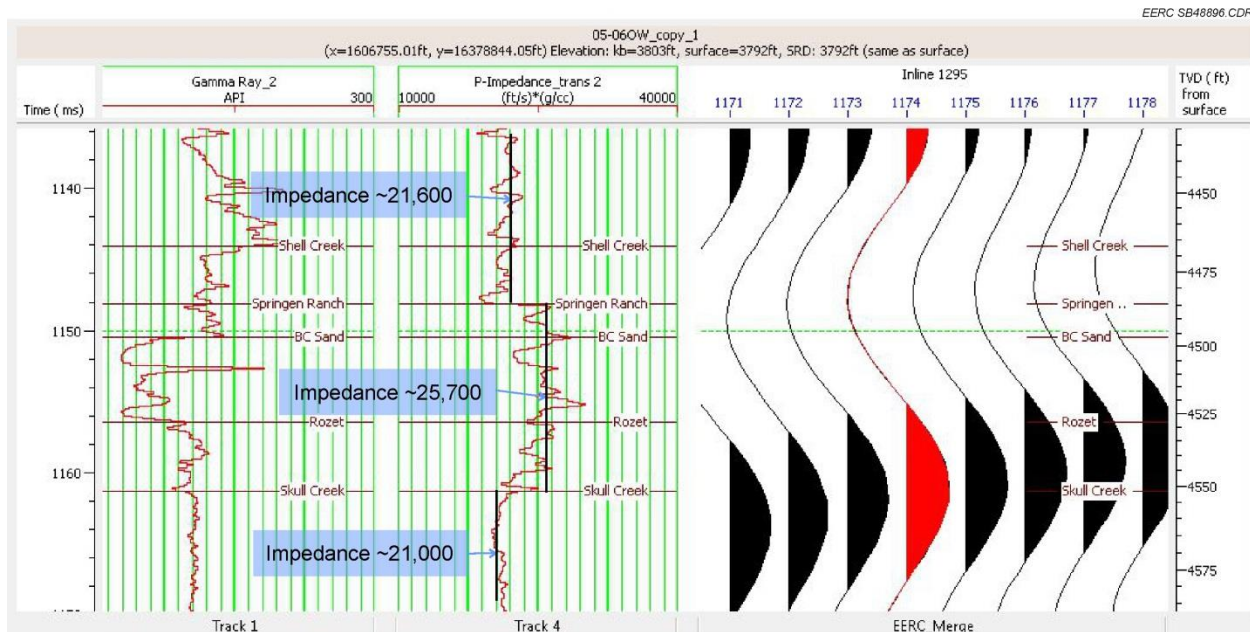


Figure C-7. The P-wave acoustic impedance curve (sonic velocity  $\times$  density) demonstrates that significant impedance changes occur at the Springen Ranch and Skull Creek boundaries which give rise to the Muddy Formation reflection. Bell Creek sand boundaries exhibit impedance contrasts of less magnitude and are below the resolution of the wavelet. Note that the twt through the impedance contrast is 12 to 13 msec. This is near the limit of resolution of the embedded wavelet.

The acoustic impedance log varies at the resolution level of the well logs, but the eye can detect three different average levels within the window that relate to the lithology. From the top of the Springen Ranch through the Rozet, the impedance value is more than 20% greater than the Shell Creek and Mowry above and that of the Skull Creek below. This impedance contrast gives rise to the waveform shown. The polarity of the seismic data is such that an increase in impedance is represented by a trough or negative deflection. A decrease is represented by a peak or positive deflection. The zone of increased impedance in 05-06 OW is 65 feet thick and occurs over a depth range of 4485 to 4550 feet (right vertical axis). This corresponds to a twt interval of 13–14 ms from 1148 to 1162 ms (left vertical axis) which is close to the limit of vertical resolution and tuning as determined above. The relationship of the seismic reflection to the well logs and geology is clearly displayed.

The Bell Creek sand within this interval totals about 30 feet which puts it below the vertical limit of resolution. Also, the impedance contrast between it and the Springen Ranch above and the Rozet below, although notable, does not appear as dramatic as that of the Springen Ranch and Skull Creek interfaces in this well at this location but could cause interference effects that impact the reflection amplitude. The interval is clearly not homogeneous.

Mapping the sand thickness directly may not be possible with the seismic data in its current state. The time thickness of the sand is shown as 6 ms, so roughly twice the current bandwidth would be needed to resolve it directly. The source bandwidth used comes close to what is needed,

although attenuation of high frequencies appeared to be a challenge in the field. If high frequencies were preserved on the field data, a data-processing effort that specifically sought to preserve bandwidth in the zone of interest may result in additional vertical resolution.

Another representation of well logs and geology juxtaposed with the seismic is in Figure C-8. The logs from left to right are the gamma ray, resistivity, and sonic p-wave velocity from the 05-06 OW well. As before, the seismic data are on the right, with the red waveform indicating the well location. The phase of the seismic data has been rotated 90 degrees so that instead of the thin-bed trough–peak combination, the Muddy is represented by a centered peak. Geologic units are labeled. The peak is between the Springen Ranch and the Skull Creek tops.

The ability to resolve different geologic features as seen on the logs within the peak is not something that can be done directly. The peak does have attributes that may be exploited to glean information, such as amplitude. The reflection is a composite response of the geologic characteristics occurring within it, and they may influence whether the amplitude is high or low in an area. The power of this attribute is seen when mapping and while interpreting along section lines.

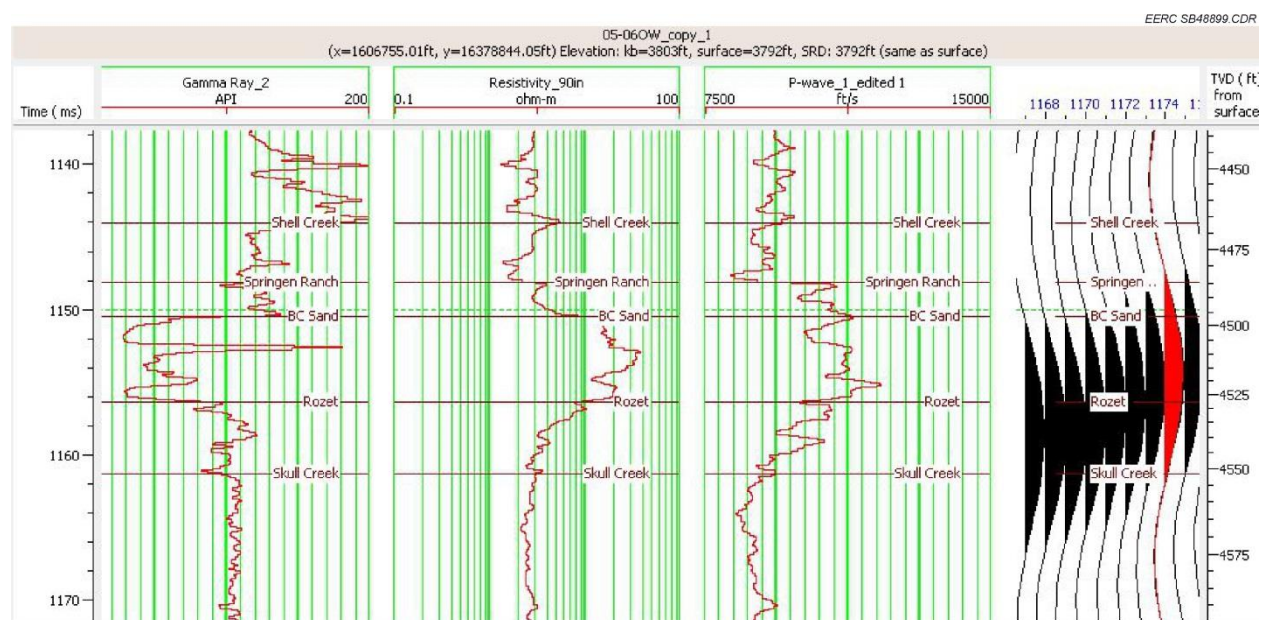


Figure C-8. The relationship between the well logs, formation tops, and seismic reflection from the reservoir zone is shown. The seismic data have been phase-shifted +90 degrees to convert the trough–peak, thin-bed response to a centered peak. The red-filled peak represents the well location. The reflection encompasses a “greater-Muddy” which includes the Springen Ranch through Skull Creek Formations. The vertical limits of the clean, 30-foot-thick Bell Creek sand are not discernible.



## Lateral Resolution

Spatially, the seismic data traces are 82.5 feet apart in both the x and y directions. This is a significantly finer sampling interval than the current quarter-mile well spacing. Even though the trace data lack the fine resolution of well logs, the ability to track events away from and between wells is very powerful.

Lateral resolution issues with seismic data occur because of depth, velocities, and significant structure. Assuming a gentle dip, as energy propagates outward from the source in a roughly hemispherical manner, the energy reflected back from a horizon at depth comes from a circular area called the Fresnel zone. The relevant formulas are in Figure C-9. Rebne (1985) used an average velocity of 7600 ft/s and calculated the size of the Fresnel zone on the Muddy Formation in the Bell Creek area to be about 760 feet in diameter. This value is relevant only to unmigrated stacked data. Modern 3-D prestack migration methods, such as applied to the Bell Creek data, combined with the relatively shallow target, gentle structure, and well-behaved velocities of the area, collapse the energy to a focus with dimensions well within the bin size limits. Using Rebne's parameters which assume a dominant frequency of 30 Hz, the collapsed value would be 63 feet. Substituting the upper frequency of 48 Hz from the analysis above lowers the value to 40 feet.

### Fresnel Zone Equations

#### Pre-Migration

$$F_d = V_{avg} \sqrt{T/F}$$

#### Post-Migration

$$F_d = \lambda/4 = V_{avg}/4 F$$

Where:

$F_d$  = Fresnel Diameter

$V_{avg}$  = Average Velocity

$T$  = Time

$F$  = Frequency of Pulse

$\lambda$  = Wavelength

EERC SB48906.CDR

Figure C-9. Fresnel zone diameter formulas for pre- and postmigration.

## REFERENCE

Rebne, C.A., 1985, A seismic stratigraphic study of the Muddy Formation, Bell Creek field, Montana [M.Sc. Thesis]: Colorado School of Mines, Golden, Colorado, p. 97.